

DOCTORAL THESIS

2013

MODELLING APPROACHES FOR ANALYSING PERSISTENT
ACTIVITY IN THE PREFRONTAL CORTEX

ATHANASIA PAPOUTSI

DEPARTMENT OF BIOLOGY

UNIVERSITY OF CRETE

And

INSTITUTE OF MOLECULAR BIOLOGY AND BIOTECHONOLOGY

FOUNDATION FOR RESEARCH AND TECHNOLOGY

ACKNOWLEDGEMENTS

My PhD was a long journey and would have been an even longer one, if I didn't have the support of many people throughout these years. The most self-evident support came from my supervisor, Yiota Poirazi, who not only financed my PhD studies and guided my research throughout all these years, but most importantly, truly believed in my skills and continuously provided moral support. If not for that, this thesis would have not been completed.

I would also like to thank the other members of my PhD committee, Prof. George Chalepakis for his confidence in me and Prof. Idan Segev for always finding time to give more than valuable feedback. It was a great honor being able to discuss my PhD issues with an expert on the field. I would also like to thank the other members of my 7 member PhD committee, for taking the time to read and evaluate my PhD thesis.

In this journey I was not alone, I always had the guidance, support and more than just good-willing patience of my colleague George Kastellakis. Without our everyday conversations, these 4 years would have been a little bit blue.

Many other people contributed in this study with different ways: I would like to thank Dr. Kyriaki Sidiropoulou for her valuable insights at the beginning of my PhD studies and Dr. Vassilis Cutsuridis for his critical thinking. Furthermore, I appreciate and commend the systematic work of Maria Psarrou, whose study set the foundations of the final part of my PhD.

When I started my PhD three people were there to show me the secret pathways: Eleftheria Tzamali, Maria Manioudaki and Anastasis Oulas. Our laughter but also our conversations showed me how to make every day working life a pleasure and I am more than thankful for that. I would also like to thank all the other members of Poirazi's lab, and especially George, Nestoras, Pavlos, Panayiotis and Stefanos, the boy-band of science always giving a new and unexpected meaning to strange questions.

Finally, my courage and persistence was always driven by my life-time friends: the Athens gang Efi, Angelina, Natassa, Stavros and Vivi, and the Heraklion gang Betty, Vassilis, Sissy, Christina, Voula, Rena and Maria. And of course Stelios who was always

there to help me keep my balance. And last (but not least), I would have never learned to stand on my own two feet had it not been for the unconditional love of my family: every trouble is really small when Eti, Stathis and Yiannis are looking out for you.

During my Master studies that lead to the present PhD I was funded by "*Maria-Michail Manassaki Scholarship*" (October 2006- September 2008). During my PhD, my work was funded by several grants of Dr. Poirazi including: the FP-7 grant: HP-SEE "High-Performance Computing Infrastructure for South East Europe's Research Communities", the NSRF grant: "Synergasia" and the ERC grant: "dEMORY".

Contents

1	INTRODUCTION	1.
1.1	THE PREFRONTAL CORTEX	1.
1.1.1	WORKING MEMORY FUNCTION OF THE PREFRONTAL CORTEX	2.
1.1.2	ANATOMY OF THE PREFRONTAL CORTEX	4.
1.2	MICROCIRCUITS	8.
1.2.1	MICROCIRCUITS OF PYRAMIDAL NEURONS	8.
1.2.2	INHIBITORY NEURONS DO NOT FORM MICROCIRCUITS	11.
1.2.3	MODELLING NETWORKS	12.
1.3	MORPHOLOGY OF PFC PYRAMIDAL NEURONS	14.
1.4	INTEGRATIVE PROPERTIES OF PYRAMIDAL NEURONS	16.
1.4.1	PASSIVE PROPERTIES	16.
1.4.2	ACTIVE PROPERTIES	17.
1.4.3	DENDRITIC INTEGRATION	18.
1.4.4	DENDRITIC NONLINEARITIES AND PREFRONTAL CORTEX FUNCTION	20.
1.4.5	INTRINSIC PROPERTIES AND PREFRONTAL CORTEX FUNCTION	21.
1.5	THE ROLE OF MORPHOLOGY IN SHAPING DENDRITIC INTEGRATION	23.
2	MOTIVATION	25.
3	METHODOLOGY	26.
3.1	PYRAMIDAL NEURON MODEL	26.
3.1.1	SIMPLIFIED PYRAMIDAL NEURON MODELS	26.
3.1.2	PYRAMIDAL NEURON MODELS WITH DETAILED MORPHOLOGY	28.
3.2	INTERNEURON MODEL	28.
3.3	SYNAPTIC PROPERTIES	28.
3.4	MICROCIRCUIT	31.
3.5	STIMULI	32.
3.6	BACKGROUND NOISE	33.
4	PFC MICROCIRCUITS AS TUNABLE MODULES	34.

4.1	PREAMBLE	34.
4.2	MATERIALS AND METHODS	35.
4.3	RESULTS	36.
4.3.1	INDUCTION OF PERSISTENT ACTIVITY	36.
4.3.2	STIMULUS EFFECTS ON PERSISTENT ACTIVITY	36.
4.3.3	EXCITATION-INHIBITION BALANCE AND DADP EFFECTS ON PERSISTENT ACTIVITY INDUCTION	40.
4.3.4	INTRINSIC MECHANISMS INVOLVED IN THE INITIATION OF PERSISTENT ACTIVITY	41.
4.4	DISCUSSION	46.
4.4.1	MINIMAL ANATOMICAL SUBSTRATE OF PERSISTENT ACTIVITY	46.
4.4.2	PAIRING EXCITATION TO INHIBITION	47.
4.4.3	(NO) STIMULUS CODING	48.
4.4.4	ROLE OF INTRINSIC MECHANISMS	48.
5	<u>DENDRITIC NONLINEARITIES REDUCE SIZE REQUIREMENTS AND MEDIATE ON AND OFF STATES OF PERSISTENT ACTIVITY IN A PFC MICROCIRCUIT MODEL</u>	52.
5.1	PREAMBLE	52.
5.2	MATERIALS AND METHODS	54.
5.3	RESULTS	55.
5.3.1	NETWORK SIZE VS. NETWORK CONNECTIVITY	55.
5.3.2	NETWORK SIZE VS. NMDA SPIKES	56.
5.3.3	NMDA IS CRITICAL FOR SMALL BUT NOT LARGE SCALE NETWORKS	58.
5.3.4	PERSISTENT ACTIVITY TERMINATION IS STRENGTH, TIME AND DADP DEPENDENT	60.
5.3.5	PREDICTING STATE TRANSITIONS	61.
5.4	DISCUSSION	66.
5.4.1	NMDA SPIKES <i>VERSUS</i> NETWORK PROPERTIES	66.
5.4.2	MECHANISMS UNDERLYING PERSISTENT ACTIVITY TERMINATION: NEW ROLES FOR OLD PLAYERS	67.
5.4.3	PREDICTIVE FEATURES OF UPCOMING STATE TRANSITIONS	68.
6	<u>ROLE OF DENDRITIC MORPHOLOGY IN NEURONAL FUNCTION</u>	69.
6.1	PREAMBLE	69.
6.2	MATERIALS AND METHODS	71.
6.2.1	PYRAMIDAL NEURON MODELS	71.
6.2.2	CHARACTERIZATION OF DENDRITIC INTEGRATION MODE	73.

6.2.3	CLASSIFICATION OF DENDRITES USING THEIR MORPHOLOGICAL/PASSIVE FEATURES	73.
6.2.4	NEURONAL INPUT-OUTPUT GAIN FUNCTION	75.
6.2.5	THE PFC MICROCIRCUIT MODEL	75.
6.3	RESULTS	77.
6.3.1	MORPHOLOGY OF THE BASAL DENDRITES SHAPES DENDRITIC INTEGRATION	77.
6.3.2	MORPHOLOGY OF THE BASAL DENDRITES SHAPES NEURONAL FUNCTION	87.
6.4	DISCUSSION	93.
7	CONCLUSIONS	96.
8	FUTURE DIRECTIONS	102.
9	REFERENCES	104.
10	APPENDIX	120.

Abbreviations

ADHD:	Attention deficit hyper-activity disorder
PFC:	Prefrontal Cortex
MD:	Mediodorsal nucleus
VA:	Ventral anterior nuclei
L5:	Layer 5
L2/3:	Layer 2/3
FS:	Fast spiking
PV:	Parvalbumin
UDS:	Up and Down states
EPSP:	Excitatory postsynaptic potential
NMDA:	N-methyl-D-aspartate
AMPA:	α -Amino-3-hydroxy-5-methyl-4-isoxazolepropionic acid
GABA:	γ -Aminobutyric acid
TRPC:	Transient receptor potential channels
CAN:	Calcium-activated non selective cation current
VGCC:	Voltage-gated calcium channels
dADP:	delayed Afterdepolarization
sAHP:	Slow after-hyperpolarization
fAHP:	Fast after-hyperpolarization
ISI:	Inter-Spike-Interval
SVM:	Support Vector Machine

List of Figures

FIGURE 1.1.1 PHINEAS GAGE	2.
FIGURE 1.1.2 THE CLASSICAL DELAYED-MATCH-TO SAMPLE TASK.....	3.
FIGURE 1.1.3 EXITATORY LOOPS BETWEEN THE PREFOTNAL AND THE THALAMUS.	5.
FIGURE 1.1.4 LONG –RANGE CONNECTIONS OF THE PFC.	6.
FIGURE 1.2.1 MICRO CIRCUITS IN THE PFC.	10.
FIGURE 1.3.1 MORPHOLOGY OF PFC PYRAMIDAL NEURONS.....	15.
FIGURE 1.4.1 COMPLEX INTEGRATION MEDIATED BY DENDRITIC SPIKES.	19.
FIGURE 3.1.1 VALIDATION OF PFC PYRAMIDAL NEURON.....	27.
FIGURE 3.3.1 SYNAPTIC VALIDATION.....	29.
FIGURE 3.4.1 THE L5 PFC MICRO CIRCUIT.....	31.
FIGURE 4.3.1 PERSISTENT ACTIVITY INDUCTION.....	36.
FIGURE 4.3.2 STIMULUS DURATION MODULATES PERSISTENT ACTIVITY INITIATION.	37.
FIGURE 4.3.3 ISIS AS A FUNCTION OF STIMULUS.....	38.
FIGURE 4.3.4 ISIS AS A FUNCTION OF STIMULUS AND DADP ACTIVATED.	39.
FIGURE 4.3.5 MICRO CIRCUITS DOES NOT SUPORT GRADED PERSTENT ACTIVITY.....	40.
FIGURE 4.3.6 SYNAPTIC AND INTRINSIC CONDUCTANCES GATE AND MODULATE THE PERSISTENT EXCITABLE STATES.....	41.
FIGURE 4.3.7 INTRINSIC CONDUCTANCES MODULATE PERSISTENT ACTIVITY INDUCTION.	43.
FIGURE 4.3.8 LOCATION SPECIFIC MODULATION OF PERSISTENT ACTIVITY.	44.
FIGURE 5.3.1 SYNAPTIC DRIVE UNDERLIES PERSISTENT ACTIVITY INDUCTION.....	55.
FIGURE 5.3.2 NMDA SPIKES UNDERLIE PERSISTENT ACTIVITY INDUCTION.....	57.
FIGURE 5.3.3 DEPOLARIZING PLATEAU UNDERLIES PERSISTENT ACTIVITY ONLY IN THE PRESENCE OF NMDA RECEPTORS.	59.
FIGURE 5.3.4 STABILITY OF PERSISTENT ACTIVITY DEPENDS ON THE ACTIVATION OF THE DADP CURRENT.	61.
FIGURE 5.3.5 PREDICTING STATE TRANSITIONS.	62.
FIGURE 5.3.6 TOTAL SPIKING ACTIVITY DISCIMINATES STATE TRANSITIONS.	63.
FIGURE 5.3.7 SYNAPTIC CURRENTS AS PREDICTIVE FEATURES.	64.
FIGURE 5.3.8 DEPOLARING PLATEAU DISCRIMINATES STATE TRANSITIONS.....	65.
FIGURE 6.2.1 MODIFICATIONS DURING EXPERIMENTS.	72.
FIGURE 6.3.1 ‘GENERIC’ MORPHOLOGY.....	77.
FIGURE 6.3.2 INTEGRATION MODE OF BASAL DENDRITES.....	78.
FIGURE 6.3.3 HISTOGRAMS OF THE MORPHOLOGICAL FEATURES.	79.
FIGURE 6.3.4 DISTANCE AND DIAMETER DISCRIMINATE INTEGRATION MODES.	80.
FIGURE 6.3.5 SOMATIC AND DENDRITIC EPSP PROPERTIES.....	81.
FIGURE 6.3.6 NMDA SPIKES UNDERLIE SIG INTEGRATION.	82.
FIGURE 6.3.7 MORPHOLOGY SHAPES INTEGRATION MODE.	83.
FIGURE 6.3.8 NMDA IS REQUIRED FOR SIG INTEGRATION.....	83.
FIGURE 6.3.9 MORPHOLOGY OF THE 9 CASE NEURONS.....	84.

FIGURE 6.3.10 INDICATIVE EXAMPLES OF ALTERED INTEGRATION MODE.	85.
FIGURE 6.3.11 DENDRITIC GAIN IS SHAPED BY INTRINSIC PROPERTIES.	87.
FIGURE 6.3.12 SIG AND SUB DENDRITES HAVE DIFFERENT SPIKING PROPERTIES.	88.
FIGURE 6.3.13 DETAILED MICROCIRCUIT.	89.
FIGURE 6.3.14 SIG DENDRITES FASCILITATE PERSISTENT ACTIVITY INDUCTION.	90.
FIGURE 6.3.15 PROPERTIES OF PERSISTENT ACTIVITY ARE DENDRITIC-SPECIFIC.	91.
FIGURE 6.3.16 HIGLY RANDOM SPIKING ACCTIVITY.	92.

List of tables

10.1.1	STRUCTURE OF MODEL CELLS WITH SIMPLIFIED MORPHOLOGY.....	120
10.1.2	PASSIVE PROPERTIES OF SIMPLIFIED PYRAMIDAL CELLS AND INTERNEURONS.....	120
10.1.3	ACTIVE IONIC PROPERTIES OF SIMPLIFIED PYRAMIDAL NEURONS.....	120
10.1.4	DISTRIBUTIONS OF ACTIVE AND PASSIVE CONDUCTANCES OF THE PYRAMIDAL NEURONS WITH DETAILED MORPHOLOGY.....	121
10.1.5	ACTIVE IONIC PROPERTIES OF INHIBITORY INTERNEURONS.....	123
10.1.6	SYNAPTIC PARAMETERS.....	123
10.1.7	SUMMARY OF SYNAPTIC CONNECTIONS IN THE MICROCIRCUIT.....	124
10.1.8	MEAN \pm STD OF THE MORPHOLOGICAL FEATURES BETWEEN SIG AND SUB.....	124
10.1.9	CLASSIFICATION RESULTS OF THE MORPHOLOGICAL FEATURES.....	125
10.1.10	MEAN \pm STD DEVIATION OF THE PREDICTIVE MORPHOLOGICAL FEATURES BETWEEN SIG AND SUB DENDRITES FROM THE 9 CASE NEURONS.....	125

Abstract

Working memory refers to the temporary storage of information and is strongly associated with the prefrontal cortex (PFC). Persistent activity of cortical neurons, namely the activity that persists beyond the stimulus presentation, is considered the cellular correlate of working memory. Although past studies suggested that this type of activity is characteristic of large scale networks, recent experimental evidence imply that small, tightly interconnected clusters of neurons in the cortex may support similar functionalities. In addition, very little is known about the biophysical mechanisms giving rise to persistent activity in small-sized microcircuits in the PFC. In this work, we developed biophysically detailed microcircuit models of morphologically simplified or detailed layer 5 PFC neurons that incorporated connectivity constraints and were validated against a multitude of experimental data. We used this microcircuit model to study the mechanisms that support persistent activity in a realistic framework. Our results show that PFC microcircuits can serve as tunable modules for persistent activity induction. We show that the underlying mechanisms are different when investigated in large-scaled compared to small-scaled networks: in microcircuits, persistent activity strongly depends on dendritic non-linearities and is shaped by the morphological properties of the basal dendrites, providing a link between dendritic morphology and neuronal function. Overall, this study zooms out from dendrites to cell assemblies and suggests a tight interaction between dendritic non-linearities, morphology and network properties that may facilitate the short-term memory function of the PFC. Our model generates a number of experimentally testable predictions that may lead to a better understanding of the physiological and pathological function of prefrontal cortex.

Περίληψη

Η μνήμη εργασίας είναι η προσωρινή αποθήκευση και επεξεργασία αισθητηριακής πληροφορίας και σχετίζεται κυρίως με αυξημένη νευρική δραστηριότητα στον προμετωπιαίο φλοιό. Τόσο οι πυραμιδικοί νευρώνες, όσο και οι ενδονευρώνες του προμετωπιαίου φλοιού παρουσιάζουν παραμένουσα δραστηριότητα, δηλαδή δραστηριότητα η οποία παραμένει μετά την απομάκρυνση ενός αισθητηριακού ερεθίσματος. Αν και προηγούμενες έρευνες υποστηρίζουν ότι η παραμένουσα δραστηριότητα είναι χαρακτηριστικό δικτύων μεγάλης κλίμακας, πρόσφατα πειραματικά δεδομένα έδειξαν ότι ο φλοιός εμφανίζει χαρακτηριστική μικρο-αρχιτεκτονική, όπου μικρός αριθμός νευρώνων δημιουργεί ανεξάρτητα αθροίσματα (μικροκυκλώματα) ικανά να υποστηρίξουν διάφορες λειτουργίες. Αν και είναι πειραματικά επιβεβαιωμένη η ύπαρξη αυτών των μικροκυκλωμάτων στον προμετωπιαίο φλοιό, μέχρι τώρα δεν έχει μελετηθεί η λειτουργία τους στην παραμένουσα δραστηριότητα. Στην παρούσα εργασία αναπτύξαμε λεπτομερή βιοφυσικά μοντέλα των αθροισμάτων με απλοποιημένη ή λεπτομερή μορφολογία της στιβάδας 5 του προμετωπιαίου φλοιού, των οποίων οι ιδιότητες (συνδεσμολογία / ηλεκτροφυσιολογικές ιδιότητες) βασίστηκαν εκτενώς σε πειραματικά δεδομένα, με σκοπό να μελετήσουμε την παραμένουσα δραστηριότητα σε ένα βιολογικά ρεαλιστικό πλαίσιο. Τα αποτελέσματά μας δείχνουν ότι τα μικροκυκλώματα του προμετωπιαίου φλοιού μπορούν να υποστηρίξουν παραμένουσα δραστηριότητα με διαφορετικές ιδιότητες. Οι μηχανισμοί που συμμετέχουν σε αυτή την δραστηριότητα είναι διαφορετικοί στα μεγάλης-κλίμακας σε σχέση με τα μικροκυκλώματα: στα μικροκυκλώματα, η παραμένουσα δραστηριότητα εξαρτάται από τη μη-γραμμική ολοκλήρωση των συναπτικών ερεθισμάτων σε δενδρίτες με περίπλοκη μορφολογία. Συνολικά, η μελέτη αυτή προτείνει ότι η στενή αλληλεπίδραση μεταξύ της μορφολογίας, της συναπτικής ολοκλήρωσης και των μικροκυκλωμάτων είναι αναγκαία για τη λειτουργία του προμετωπιαίου φλοιού στη μνήμη εργασίας. Το μοντέλο μας παράγει μια σειρά από πειραματικά ελέγξιμες προβλέψεις που μπορεί να οδηγήσουν σε καλύτερη κατανόηση της φυσιολογικής αλλά και της παθολογικής λειτουργίας του προμετωπιαίου φλοιού.

Brief Overview

This PhD thesis investigates the role of biophysically constrained layer 5 microcircuits in prefrontal cortex function. It is organized in 8 Sections and is based on work that is in preparation, submitted, or published. The first Section is the Introduction and zooms in from the behavioral studies and gross anatomy, to the microarchitecture, to single-neuron and dendritic properties of the prefrontal cortex. Given the background literature, in Section 2 we provide the motivation of our research and the open questions tangled in this study. In Section 3 we present our model microcircuit that served as the basis for the subsequent studies. Section 4 presents the first Results of this work, and verifies that prefrontal cortex microcircuits act as modules able to generate persistent activity. These results are published in Papoutsi et al. *Frontiers in Neural Circuits* 2013. Section 5 investigates how dendritic integration and microcircuit function are linked. This work is submitted and currently under review. In Section 6, we advance our study one step further by investigating how dendritic morphology drives microcircuit function. This work is currently under preparation to be submitted. In Section 7 we bring together our results to provide basic insights on how dendritic morphology-dendritic integration and microarchitecture organization form the basic framework for studying functional properties. Extensions of our basic ideas are presented in Section 8.

Apart from journal publications, this work has been presented in numerous conferences, including CNS 2009, SFN 2009, AREADNE 2010, FENS 2012 and CNS 2013 and resulted in one review article (*Coding and Decoding with Dendrites*, *Journal of Physiology Paris*, 2013) and one book chapter (*Memory Beyond Synaptic Plasticity: The Role of Intrinsic Neuronal Excitability*, *Memory Mechanisms in Health and Disease*, World Scientific Pub Co Inc., 2012).

1 Introduction

1.1 The Prefrontal Cortex

The prefrontal cortex (PFC) is one of the association regions of the neocortex occupying the anterior part of the frontal lobe, in front of motor and premotor areas. By receiving input related to both the external environment and the internal state of the animal, activity in PFC is correlated with complex cognitive processes, including working memory, decision making, rule learning, formation of concepts and social behavior. PFC function is also of major importance to a number of clinical syndromes like schizophrenia, attention deficit hyper-activity disorder (ADHD), stress and drug addiction (Arnsten, 2009; Miller, 2000; Russell et al., 2000).

Attention was drawn to the function of the PFC when a railway construction foreman, Phineas Gage (1823–1860), suffered from an accident in which an iron bar was driven through his head, destroying much of his brain's left frontal lobe (Ratiu et al., 2004) (Figure 1.1.1). Although Phineas Gage accident occurred more than a century ago, its influence is still apparent in modern neuroscience and philosophy of mind, regarding the localized or distributed nature of cerebral functions. After the accident, the behavior and personality of Phineas Gage was changed dramatically as he was unable to follow conventional social rules and make long-term plans (Harlow, 1868). Although exaggerations and lack of true facts transformed Phineas story over

the years to a scientific myth, other cases of prefrontal dysfunction have shown that humans with prefrontal cortex damage are socially disinhibited, unable to ignore irrelevant stimuli, have emotional impairments, difficulty in planning and impaired working memory (Squire et al., 2012).



*Figure 1.1.1 Phineas Gage
Portrait of Phineas Gage showing him holding the iron bar (Wilgus and Wilgus, 2009).*

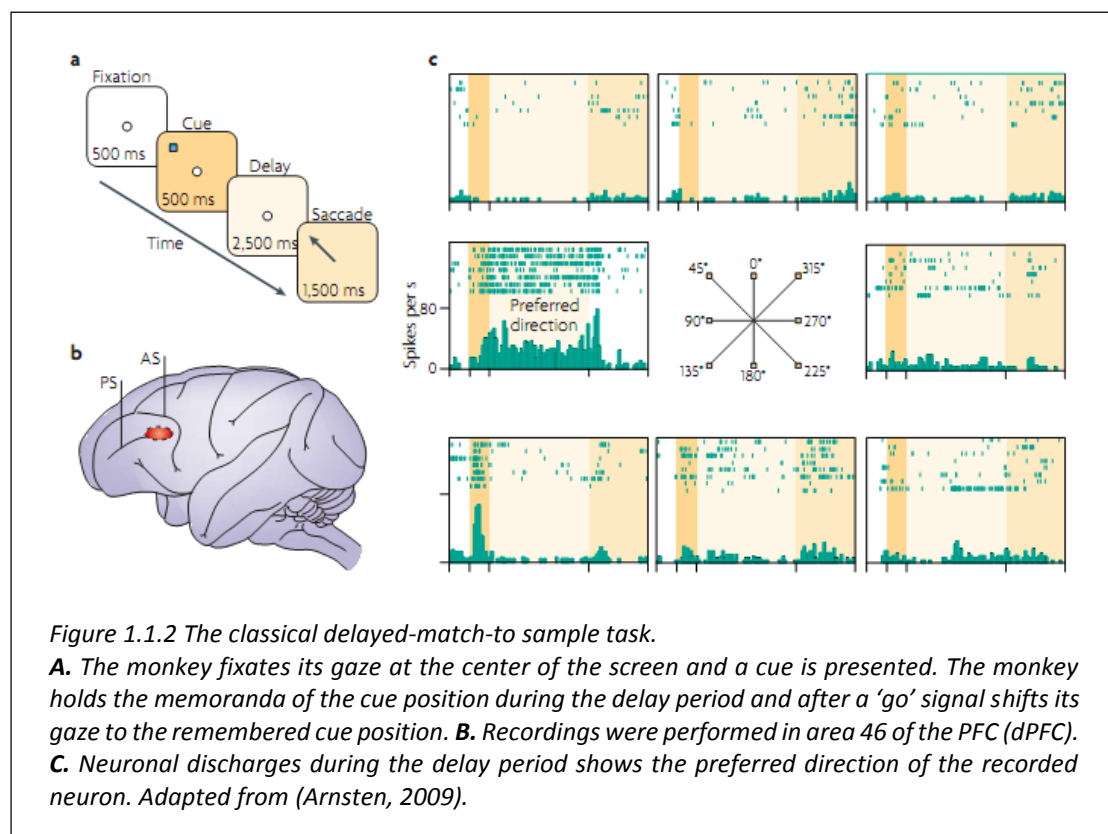
1.1.1 Working Memory Function of the Prefrontal Cortex

Memory, the ability to retain, store and recall information is the most fundamental cognitive function in everyday life. Among the various memory systems, working memory is the type of short term memory with a special role in shaping behaviour, since it is involved in the ‘on-line’ monitoring and manipulation of information or actions. A classical experimental procedure used to evaluate working memory is the delayed match to sample task. During this task a transient cue is presented and after a delay period (during which the individual holds the cue features in mind) the individual is asked to execute a specific action (for example, locate the cue) (Goldman-Rakic, 1995) (Figure 1.1.2A).

In vivo experiments conducted in the 70’s identified prefrontal cortex as the “residence” of working memory. Neuronal activity of both pyramidal neurons and interneurons that persists after termination of a stimulus presentation has been primarily recorded in PFC from both primates (Fuster and Alexander, 1971; Kubota and Niki, 1971) and rodents (Jung et al., 1998), suggesting that these neurons provide

the necessary neural processing to establish behavioral continuity over time (Figure 1.1.2B).

Since it was first recorded, persistent neuronal activity has been correlated with a wide range of cognitive functions. The most classic approach attributes persistent activity to the ‘on-line’ maintenance of stimulus information (sensory integration) (Goldman-Rakic, 1995). According to this approach, working memory is the short-term retention of either continuous (e.g. spatial location or frequency) or discrete (e.g. faces, objects) information (Figure 1.1.2C). Nevertheless, other studies reject the static stimulus representation hypothesis and suggest that sustained spiking activity is dynamical in nature and, apart from maintenance, it also involves manipulation of goal-related stimuli. In this view, persistent activity has been involved in the association of stimuli or tasks separated in time (temporal summation) (Fuster et al., 2000; Histed et al., 2009) and the monitoring of sensory information processed by providing ‘top-down’ bias in other brain areas (Chamod and Petrides, 2007). In addition, persistent activity has also been implicated in decision making (Curtis and Lee, 2010), attention (Gazzaley and Nobre, 2012), representation of abstract rules (Miller et al., 2002) and cognitive inhibition (Aron et al., 2004). In analogy to primates,



behavioral studies and *in vivo* recordings have also established the role of PFC in rodents in various functions, such as holding on-line in memory items (e.g. spatial location in a maze), attention, decision making and rule-learning (Seamans et al., 2008).

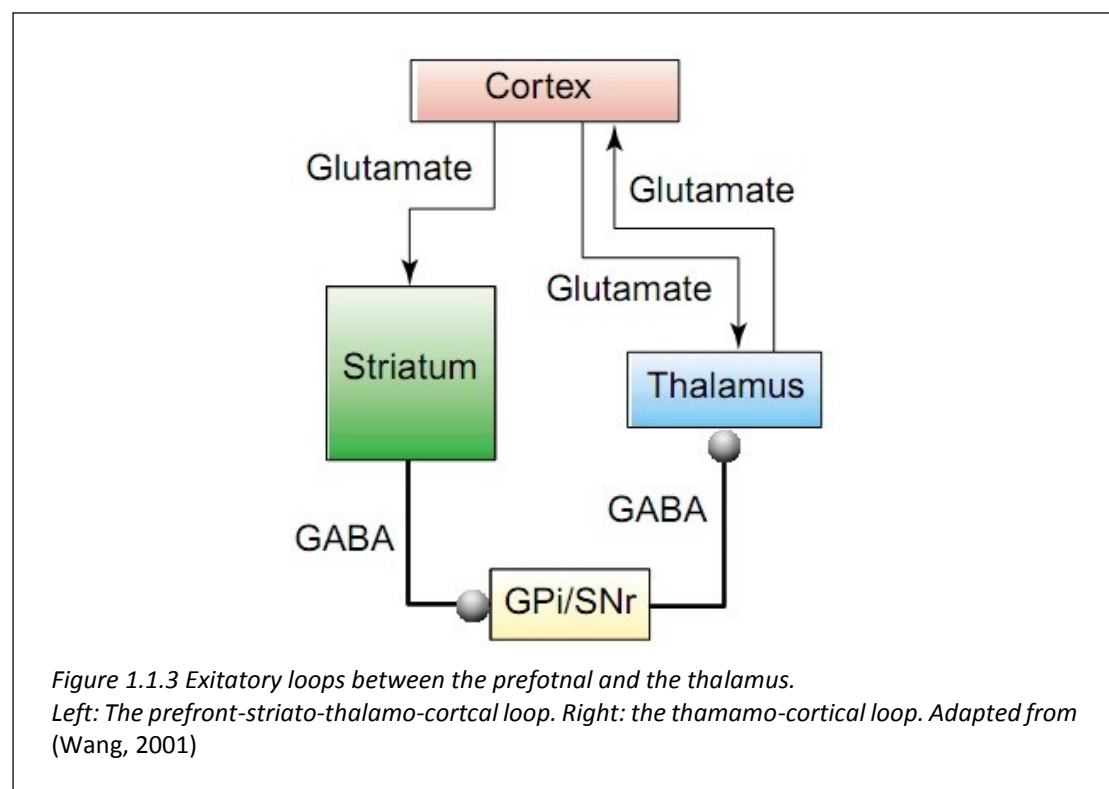
Prolonged spiking activity that outlasts stimulus presentation is not unique to the prefrontal cortex. It has also been reported in other cortical areas, such as the posterior parietal and the inferotemporal cortex (Constantinidis and Steinmetz, 1996; Miller et al., 1996), as well as in subcortical areas, such as the thalamic mediodorsal nucleus (MD) (Watanabe and Funahashi, 2004). Nevertheless, the capacity of PFC neurons to sustain activity displays some unique properties not observed in these regions. The most important feature of persistent activity observed in the PFC is its stability to noise and resistance to distractors (Asaad et al., 2000; Miller, 2000; Shafi et al., 2007). It is expected that a memory system, able to maintain its activity for several seconds, must be robust during this time period to random noise, as well as to distracting stimuli. In addition, activity of PFC neurons is highly adaptive to task aspects, indicating its dynamic nature in shaping goal-directed behaviour (Seamans et al., 2008).

1.1.2 Anatomy of the Prefrontal Cortex

The PFC areas process information about the external environment through connections with sensory, cortical and subcortical regions, and internal information through connections with the limbic system and midbrain structures (Squire et al., 2012). The PFC in primates encompasses a heterogeneous set of areas, such as dorsolateral (dPFC) and orbitofrontal prefrontal, with distinct cytoarchitectonic properties regarding the distribution and density of the various neuronal subtypes and the density of glia (Dombrowski et al., 2001). Although the PFC of humans is much larger compared to other animals, its architectonic organization is in great part similar to that of other primates (Petrides, 2005).

PFC neurons have characteristic organization with the thalamus. The PFC is reciprocally connected with the thalamus via two pathways. First, PFC projects to the striatum (caudate and putamen) and to the nucleus accumbens of the basal ganglia, that inhibit activity in the globus pallidus and substantia nigra and thus disinhibits

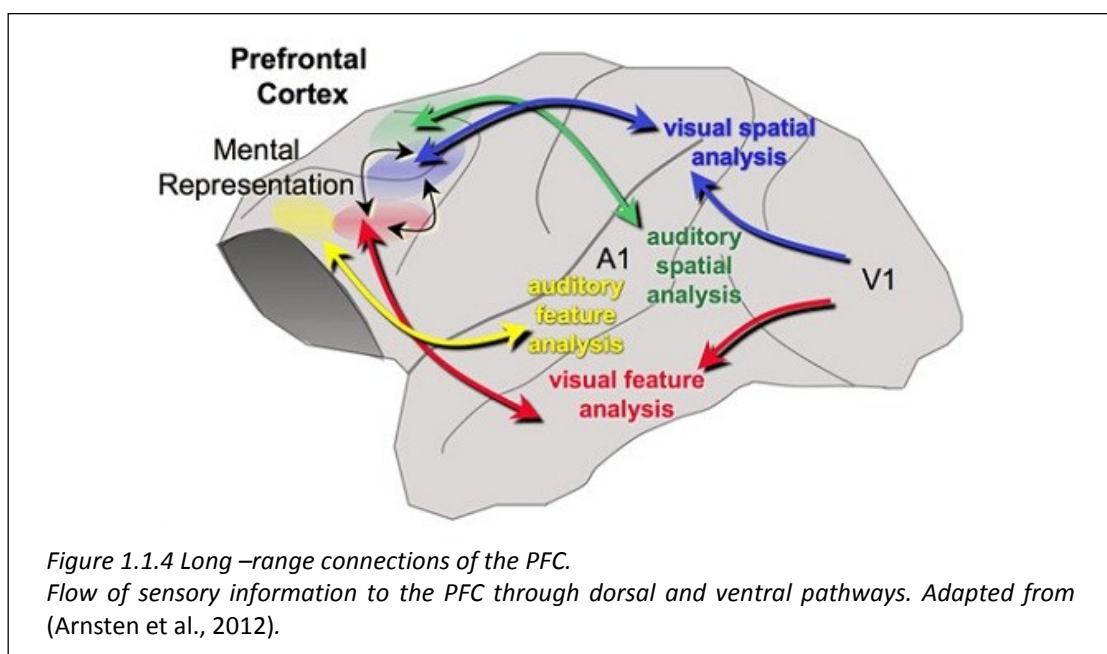
thalamic nuclei (Figure 1.1.3). PFC receives information through the thalamic mediodorsal and ventral anterior nuclei (VA) of the thalamus (prefronto-striato-thalamo-cortical loops). Although basal ganglia receive information from most cortical areas, they selectively project via the thalamus to the frontal cortex (including also premotor and motor areas). As in PFC, sustained activity during the delay period of working memory tasks in the caudate nucleus reflects combined visual information and reward expectation (Constantinidis et al., 2004).



The second pathway involves direct, reciprocal connections with thalamic nuclei (thalamo-cortical loop) (Figure 1.1.3). Prefrontal cortices receive and send direct projections to the MD and VA (Constantinidis et al., 2004). The connecting pathways between VA and PFC are classified as ‘drivers’, which secure efficient synaptic transmission, and ‘modulators’, which evoke small responses on postsynaptic neurons, forming parallel reciprocal circuits. The thalamo-cortical network is further regulated by the prefrontal projections to the thalamic reticular nucleus, which sends inhibitory projections back to the MD. This connection implies a central role of the PFC in the control of information flow from sensory-related thalamic nuclei (MD) to the cortex (Barbas and Zikopoulos, 2007; Zikopoulos and Barbas, 2007). In rodents, the

thalamo-cortical loop displays well-organized properties: Thalamo-cortical projections innervate the apical dendrites of L2/3 and L5 PFC neurons and the cortico-thalamic projection to MD arises from neurons in layers 5/6. Some of the thalamo-cortical axon terminals from MD make directly synaptic connections with dendrites of cortico-thalamic projection neurons in PFC, suggesting strong reciprocity in the thalamo-cortical loop. In contrast to primates, PFC interneurons in rodents receive direct excitation from MD. This raises the possibility that local inhibitory neurons in the prefrontal cortex may restrain persistent activity through feed-forward inhibition (Kuroda et al., 1998).

Apart from the thalamus, PFC is also connected in a topographically specific manner with most other cortices, including sensory and association areas, such as the parietal cortex, and areas associated with cognition, memory and emotions. In particular, the various prefrontal areas in primates of both hemispheres are interconnected through the corpus callosum and are also densely interconnected locally (Squire et al., 2012). In addition, PFC receives information from both the ventral (object recognition) and dorsal (spatial recognition) pathways in primates (Figure 1.1.4). Neurons with memory-related receptive responses have been reported in the inferior temporal and posterior parietal regions (areas LIP and 7a), which are the end edges of the ventral and dorsal visual pathways (Arnsten, 2013). *In vivo* recordings have shown that similar percentages of neurons display persistent activity in the dPFC



and the posterior parietal and inferotemporal cortex. Nevertheless, persistent discharges of inferotemporal and parietal neurons are interrupted by irrelevant, distracting stimuli presented in the context of a delayed-matching-to-sample task (Miller, 2000). The PFC also receives directly sensory information from cortices representing early stages in visual, auditory and somatosensory gustatory and olfactory processing (Constantinidis and Wang 2004).

PFC is also connected with areas of the limbic system. Dorsal PFC receives input from cingulate areas that are associated with attention, error detection and goal-directed behavior. The orbitofrontal PFC displays robust connections with the amygdala, a key structure related to emotions. Orbitofrontal cortex is also connected with memory-related regions, including the perirhinal region, the entorhinal cortex, the parahippocampal cortex and the hippocampus (Barbas, 2000). PFC is connected with the neuromodulatory systems of the brain stem, midbrain and basal forebrain, such as ventral tegmental area (VTA, dopamine), the raphe nuclei (serotonin), locus coeruleus (norepinephrine) and cholinergic systems (Barbas, 2000). In the rat, the projections from MD and dopaminergic fibers from VTA to PFC overlap, suggesting that the dopamine modulates the recurrent loop between MD and PFC (Kuroda et al., 1998).

Projections of the PFC to motor areas mediate its function in motor control. Although not directly connected with the motor cortex, targets of the projections of the PFC include premotor areas (including the frontal eye fields), the supplementary motor area and brain stem oculomotor systems, such as the superior colliculus that controls eye movement. PFC also projects to the cerebellum (via the pontine nuclei), a brain region that shapes the coordination and timing of movements. Orbitofrontal cortex projects also to autonomic nuclei of the hypothalamus, and thus influences autonomous responses.

Overall, PFC is a key region supporting diverse cognitive functions in both primates and rodents, as it is evident from its afferent and efferent connections. How PFC neurons integrate this wide range of inputs in the cellular and micro-architectural level and how this integration is shaped by neuromodulators are questions essential to understanding prefrontal function and require shifting our level of analysis from the macroscopic to the microscopic level.

1.2 Microcircuits

“(…), the term ‘microcircuit’ is used to denote a minimal number of interacting neurons that can collectively produce a functional output, such as locomotor central pattern generators, hippocampal circuits producing gamma and theta rhythms, and circuits in the neocortex and cerebellum” (Grillner et al., 2005, TINS Microcircuits Special Feature).

1.2.1 Microcircuits of Pyramidal Neurons

Investigations of how structure relates to function require detailed descriptions of the synaptic properties of its basic elements. Pyramidal cells are the most abundant neurons in the cerebral cortex and their function is closely associated with higher cognitive and emotional processes. Connections of pyramidal neurons with neighboring cells, cells in different layers and cells in different regions, are a dominant feature of the cortical circuit. Anatomical studies during the 90’s focusing on the local circuitry calculated that a single L5 pyramidal neuron innervates approximately 50 other neighboring L5 pyramidal neurons (within a distance of 300 μ m) via 4 to 8 synaptic contacts (Markram, 1997). The connectivity diagram between L5 pyramidal neurons depends on their distance: neighboring pairs innervate each other at their basal dendritic compartments and evoke somatic EPSPs with large amplitude, whereas neurons that are more distally are primarily connected through weak synapses at the apical dendrites. Ultimately these studies revealed that the organization of the neocortex is not random but governed by segregated local and distal pathways (Feldmeyer and Sakmann, 2000; Markram, 1997; Thomson and Deuchars, 1997).

Although very insightful for the connectivity diagram, these studies were primarily based on random sampling of pairs that could allow for a variety of statistical errors. Recent advances in neuroanatomical methods, in parallel with the development of computational tools for the acquisition and analysis of large amount of data, have allowed the dense mapping of connections in the cortex (Feldt et al., 2011; Seung, 2009). *In vitro* studies of the connectivity diagram have shown that locally pyramidal neurons are not randomly connected but form clusters of few neurons (up to 20) that are dispersed in space (Cossart et al., 2003; Perin et al., 2011),

also termed 'assemblies', 'ensembles' or 'microcircuits'. Within a cluster of neurons, bidirectional connections are over-represented and stronger (Song et al., 2005). The adjacent neurons (both pyramidal and interneurons) that are connected to each other, also share common inputs (Yoshimura and Callaway, 2005; Yoshimura et al., 2005).

In vivo data also favor the idea of topological specificity of connections between adjacent excitatory neurons (Kozloski J et al., 2001). This specificity of connections has been proposed to be formed early in development (Yu et al., 2009, 2012) and enhanced with learning (Komiyama et al., 2010) or experience (Ko et al., 2013). There seems to be a bias towards reciprocal connections in these assemblies, as functional similarity (e.g. preferred orientation in the visual cortex) is strongly reflected in the rate of reciprocal than unidirectional connections between neurons with similar orientations preferences (Ko et al., 2011). These findings pinpoint to a modular architecture of cortical neuronal microcircuits that has also been documented in other brain regions (Grillner S et al., 2005).

The functional role of these neuronal assemblies in cognitive processes remains a mystery. At first glance, the existence of highly specific synaptic connections inside a cluster of neurons ensures that similar physiological properties are shared by a neuronal assembly (Dombeck et al., 2009). Recent findings suggest that these assemblies may serve as computational modules in various processes, including receptive field formation (Ko et al., 2013) and the generation of Up-and-Down states both *in vitro* (Cossart R et al., 2003) and *in vivo* (Yassin et al., 2010). Microcircuits that support Up-and-Down states are also functionally compartmentalized between layers: L5 rather than L2/3 microcircuits have been reported *in vivo* to initiate the Up states (Beltramo et al., 2013). Note that adjacent microcircuits (even within a 50 μm range) can display heterogeneous responses, such as whisker selectivity (Sato et al., 2007), allowing adjacent neurons to convey information independently. On the other hand, since clusters of neurons are dispersed in space, overlapping clusters may interact and to mediate other, higher-order functions.

Although the above studies involved investigations of the microcircuits in primary sensory areas (visual, motor and barrel cortices), there is evidence that the same functional clusters of neurons are also formed in the prefrontal cortex. In the PFC, L5 neurons form discrete sub-networks, among which pyramidal neurons with complex morphology are hyper-reciprocally connected (and with higher probability than primary sensory areas) through facilitating synapses (Wang et al., 2006). As in sensory cortices, L5 PFC neurons receiving common input from a L2/3 pyramidal neuron, belong to the same subtype (have the same firing pattern) and are connected with high probability (Otsuka and Kawaguchi, 2008). The same rule applies to their projection sites: L5 PFC pyramidal neurons with the same projection site are reciprocally connected with higher probability compared to other pyramidal neurons with different projection sites (Morishima and Kawaguchi, 2006) (Figure 1.2.1). Reciprocal connections also display higher somatic EPSCs amplitudes (Morishima et al., 2011).

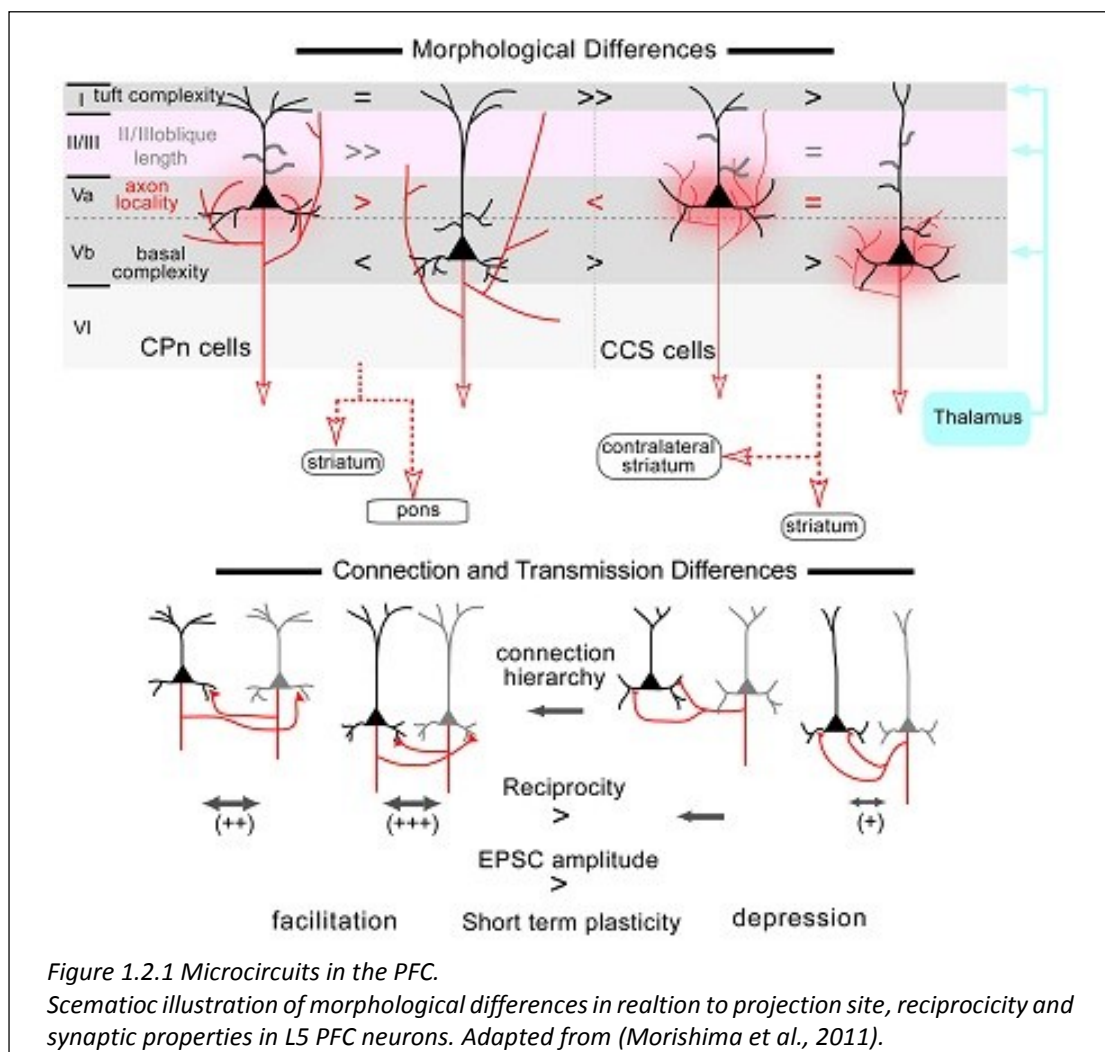


Figure 1.2.1 Microcircuits in the PFC. Schematic illustration of morphological differences in relation to projection site, reciprocity and synaptic properties in L5 PFC neurons. Adapted from (Morishima et al., 2011).

Thus, PFC microcircuits are characterized by strong reciprocal connections and specificity in both their input and their projection sites, forming independent modules with homogenous physiological properties. Looking at the functional level, *in vivo* data propose that working memory is mediated by sequential recruitment of such assemblies in the PFC (Fujisawa et al., 2008). PFC assemblies have also been reported to mediate rule learning from trial-to-trial basis (Durstewitz et al., 2010) and also encode rule-learning related memory (Ferrari et al., 2013; Peyrache et al., 2009).

Taken together, recent technological advances in neuroanatomy and in probing the activity of neurons *in vivo* have established that neurons form highly specific reciprocal sub-networks with enhanced synaptic strengths in a pool of sparse connections with moderate synaptic strengths (Song et al., 2005). The role of these independent clusters in mediating specific functions remains an open issue.

1.2.2 Inhibitory Neurons do not Form Microcircuits

Sparse and highly selective connectivity is an organizing principle of pyramidal neurons, but not of inhibitory neurons that receive more dense and broad connections from pyramidal neurons (Hofer et al., 2011). Specificity of connections in the inhibitory population arises primarily through diversity in phenotype, site of postsynaptic targets, efficacy of inhibitory control and distribution pattern in the cortex among the different classes of inhibitory neurons (Markram et al., 2004). Among the various types, PV (parvalbumin) interneurons are the most prevalent in the lateral prefrontal areas in monkeys in contrast to limbic areas (Dombrowski et al., 2001) and are found preferentially in the middle-deep layers (Barbas and Zikopoulos, 2007; Grobin et al., 2003). PV interneurons are fast-spiking (FS) basket cells (innervation of the soma and the proximal dendrites) with typical characteristics the absence of spike frequency adaptation and the spike duration of less than 0.5 msec. Axon arborization of FS interneurons displays significant horizontal spread. PV interneurons are particularly sensitive to reductions in excitatory transmission through NMDA receptors and inhibitory transmission from this subtype is impaired in schizophrenia (Homayoun and Moghaddam, 2007; Lewis and González-Burgos, 2006; Wang and Gao, 2009). FS interneurons have also been shown to fire persistently during the delay-period in working memory tasks (Rao et al., 1999). Thus, impaired recruitment of FS neurons in

working memory circuits could disrupt feedback inhibition to the pyramidal network resulting in pathological phenotypes (González-Burgos et al., 2005).

Taken together, although the microcircuitry formed by the wide range of interneuronal subtypes seems to exert fine control of excitatory transmission, fast-spiking basket cells have a special role in both normal and pathological functions of the PFC.

1.2.3 Modelling networks

When analyzing network properties, one can focus on different abstraction levels: the macroscopic level, which concerns networks formed between different brain areas, the mesoscopic level, which refers to circuits formed between the layers of a given area and the microscopic level, where networks are formed between individual, close-by neurons. Note that in the first two cases, what is actually studied is a network of networks (Kumar et al., 2013) and in the third case what is actually studied are the microcircuits described in the above sections. Consequently, two complementary modelling strategies can be used to represent the different levels: the ‘top-down’ and the ‘bottom-up’. ‘Top-down’ approaches use abstract models to cast general principles of the system under study into a minimal model, describing its essential properties with as few parameters as possible. ‘Bottom-up’ simulations start from biophysically realistic models that simulate details of the system under study and enable investigation of its properties. These models can also incorporate lower scales of analysis of the microcircuit properties, such as dendritic compartmentalization, by incorporating morphologically realistic models of neurons (De Schutter et al., 2005). Thus far, bridging together the two computational approaches has been prohibited due to lack of computational resources. Only recently advances in parallel computing have allowed the simulation of full-scale models of an entire brain area (Schneider et al., 2012).

1.2.3.1 Top-Down Modelling Studies of the PFC

The features of PFC persistent activity have been investigated mostly using a top-down approach, by constructing attractor-based models of abstract or conductance-based large-scale networks of point neurons, in an effort to reproduce

the *in vivo* characteristics of persistent activity (Brody et al., 2003; Constantinidis and Wang, 2004). These studies have greatly contributed to linking sustained activity with different types of working memory (Compte, 2006), have uncovered the importance of the slow currents (such as NMDA and other regenerative currents) in the stability of persistent activity (Tegnér et al., 2002; Wang, 1999) and have identified the significance of excitation-inhibition balance in maintaining persistent states (Fellous and Sejnowski, 2003).

Although these models are able to reproduce the *in vivo* characteristics of persistent activity, such as stimulus coding, they are phenomenological and, in great part, neglect the differential expression of synaptic and ionic mechanisms along the somato-dendritic compartments of neurons. The latter allows for functional compartmentalization and enables neurons to perform difficult computations relevant to their neuronal function (Papoutsi et al., 2013; Segev and London, 2000). In addition, the underlying anatomical micro-architecture is considered to participate in the observed electrophysiological output and biophysical properties are also differentially expressed between different cell-types. Hence, incorporation of these models in a more realistic and plausible framework will also generate more biologically- relevant predictions (Fisher et al., 2013). Towards this direction, recent models have advanced in adding different kinetics between the excitatory-to-excitatory and excitatory-to-inhibitory synapses, as observed experimentally, and have generated experimentally testable predictions for working memory disorders (Lim and Goldman, 2013).

1.2.3.2 Bottom-Up Modelling Studies of the PFC

Interestingly, the functional role of L5 PFC microcircuits has not been extensively investigated thus far. Thus, it remains unknown whether L5 PFC microcircuits can indeed support persistent firing, how their properties may be influenced by changes in their intrinsic and/or synaptic mechanisms and whether they can express stimulus-specific coding, such as the one seen in large scale networks (Romo et al., 1999). The present study tangles these issues using a compartmental modelling approach.

Compartmental models allow neuroscientists to perform *in silico* experiments in reconstructions of neurons in order to investigate their electrical behavior under various conditions. In contrast to simplified integrate and fire neuronal models, detailed compartmental models explicitly consider all the complexity of the cell structure: in such models, the dendrites, the soma and the axon of a neuron are divided in a number of cylinders that closely resemble the anatomical structure of the cell. Neuronal morphology can be very precisely replicated in digital form from microscope images using specialized tracing programs, such as NeuroLucida. The simulated form of a neuron consists of a network of connected electrically conductive cylinders. Each compartment, dendritic, somatic or axonic, is represented by an equivalent electrical circuit which includes the membrane capacitance, membrane resistance and axial resistance and the various electrically conducting ionic mechanisms that are found in neurons. Cable theory and the Hodgkin-Huxley model of ionic kinetics provide the theoretical foundation for computing neuronal activity patterns. This flexible framework allows the simulation of all known ionic/synaptic mechanisms that are found in neuronal membranes across the brain.

Modern compartmental models can include thousands of electrical compartments, each one simulating tens of different ionic mechanisms. The calibration of the parameters of these mechanisms in each compartment requires a careful examination of the relevant literature, experimental evidence, as well as the intuition of the experimenter. When validated, a well-constructed model can be a powerful tool, as it can simulate the electrical behavior of neurons in ways or conditions that may not be possible experimentally. For example, synaptic stimulation can be precisely delivered at specific points in order to investigate the temporal aspects and the fine structure of dendrites (Sterratt et al., 2011).

1.3 Morphology of PFC Pyramidal Neurons

Neocortical pyramidal cells are multipolar neurons with a triangular soma, an axon and dendrites which are organized in two distinct and elaborate dendritic trees. The apical tree consists of a main thick apical dendrite (apical trunk) -which descends from the apex of the cell body and may bifurcate into two apical dendritic tufts- and several oblique dendrites that branch out from the trunk. The basal tree consists of

numerous dendrites the majority of which arises directly from the base of the soma. Pyramidal neurons display high heterogeneity in their size, branching complexity, and number of spines across different species (Elston et al., 2011), cortical areas (Elston, 2003) and layers (Spruston, 2008). The intense interest in investigating their anatomy resulted in a series of new experimental and computational techniques for labeling, visualization, tracing and reconstructing their morphological properties and simulating their function (Parekh and Ascoli, 2013).

Dendritic trees of PFC pyramidal neurons are more complex and possess more dendritic spines than primary sensory areas (Amatrudo et al., 2012; Elston, 2003). PFC pyramidal neurons display high variability in their morphological and electrophysiological features, with the L5 pyramidal neurons being the most distinct type (van Aerde and Feldmeyer, 2013). Although L5 PFC pyramidal neurons form a morphologically distinct group compared to pyramidal neurons in other layers and areas, they also display high morphological heterogeneity (Elston et al., 2011; Tsiola et al., 2003). When investigating their electrophysiological profile, synaptic properties

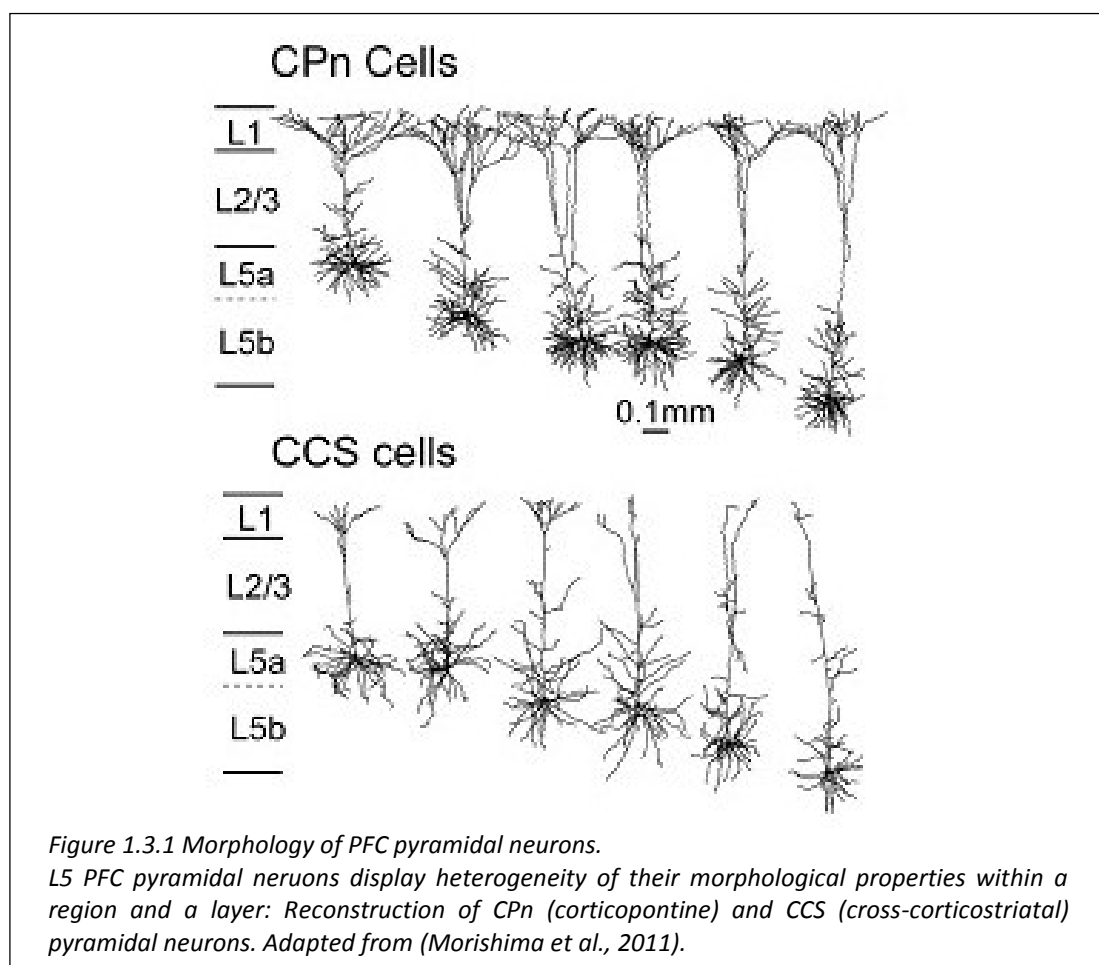


Figure 1.3.1 Morphology of PFC pyramidal neurons. L5 PFC pyramidal neurons display heterogeneity of their morphological properties within a region and a layer: Reconstruction of CPn (corticopontine) and CCS (cross-corticostriatal) pyramidal neurons. Adapted from (Morishima et al., 2011).

and axonal projections, they can be further categorized in various subclasses that are also morphologically distinct. The main subtypes are: Type I (corticopontine, CPn) that project to the pons (CPn), are bursty and have a thick tufted apical dendrite and Type II (commisural, COM) that project to the contralateral cortex, are regular spiking and have smaller somata and apical dendrites without or with very small apical tuft (Dembrow et al., 2010; Molnár and Cheung, 2006). Basal trees of CPn PFC neurons are also more elaborate (have more branch points) than those of COM neurons (Morishima et al., 2011) (Figure 1.3.1).

Therefore, dendritic complexity is correlated with species, region, layer and microcircuit identity. The obvious question that arises is how this morphological complexity relates to their function.

1.4 Integrative Properties of Pyramidal Neurons

For several decades -and despite their morphological diversity-, dendritic trees were considered simply passive devices that transmit signals towards the soma. Accordingly, neurons were thought to act as nodes that summate synaptic excitation and inhibition. When a certain threshold is reached by the additive combination of synaptic input, an action potential is generated in the axon hillock (McCulloch and Pitts, 1943). However, it soon became apparent that the passive properties together with the complex geometry of dendrites allow neurons to integrate their inputs in a non-linear manner and thus structure must be taken into account when investigating function.

1.4.1 Passive Properties

Passive properties of dendritic branches shape both the amplitude and duration of electrical signals. As predicted by Wilfrid Rall back in 1967, when a post-synaptic potential propagates through a passive dendrite to its integration site (soma or axon), its amplitude is attenuated in a distance-dependent manner, with the dendrite acting as a low-pass filter (Rall, 1967). Distal dendrites are thinner compared to proximal ones and consequently the synaptic potentials travelling towards the soma are reduced in amplitude (Jaffe and Carnevale, 1999; Rinzel and Rall, 1974; Zador et al., 1995). On the other hand, the large input resistance of distal thin

dendrites results in larger local EPSPs (Agmon-Snir and Segev, 1993; Jaffe and Carnevale, 1999; Rinzel and Rall, 1974). Attenuation is also asymmetric: reduction of the peak amplitude is greater when moving towards the soma than the opposite direction (Segev and London, 2000).

Due to their anatomical properties, summation of multiple excitatory synaptic inputs in passive dendrites depends on the degree of their spatial and temporal isolation, so that when they are clustered or synchronous they summate sublinearly as a consequence of the reduction in the ionic driving force or decrease in the dendritic input resistance. Passive dendrites have also been shown to support complex computations, such as direction selectivity (proximal-to-distal versus distal-to-proximal) and, more generally, linear non-separable functions (Cazé et al., 2013; Rall, 1967).

1.4.2 Active Properties

Although passive properties alone alter the computational processing of neurons, numerous technological advances in experimental techniques that allowed access to isolated dendritic compartments have added multiple new players in the dendritic integration game: an array of voltage-and/or ligand-dependent (active) conductances that greatly influence local responses. The discovery of voltage-dependent ion channels with different densities and biophysical properties along the axo-somato-dendritic axis shows that not only the soma, but the dendrites as well, have an active role in shaping neuronal excitability. Dendritic branches are enriched with a variety of voltage-dependent channels, whose conductance and distribution differs among neuronal types and dendritic branches (e.g. apical *versus* basal dendrites). Thus, the output of the neuron is not only shaped by the morphological and passive properties of the dendritic tree, but also by the expression profile and kinetics of its active conductances (Spruston, 2008).

The toolkit of active dendritic mechanisms includes various channel types, such as voltage-gated Na^+ , Ca^{++} , K^+ , h (hyperpolarization-activated cation) channels and NMDA receptors. In general, Na^+ and Ca^{2+} channels are considered as boosters of postsynaptic potentials, whereas both K^+ and h channels are more likely to dampen dendritic excitability and contribute to the control of action potential frequency or act

as pacemaker currents respectively (Larkum and Nevian, 2008; Migliore and Shepherd, 2002; Spruston, 2008). On the other hand, inward active currents can amplify inputs, thus contributing to 'dendritic democracy' (Spruston, 2008). Importantly, various ionic conductances in the dendrites, such as sodium (Stuart and Sakmann, 1994), calcium (Yuste et al., 1994), NMDA (Larkum et al., 2009; Schiller et al., 2000) or a combination of the above (Ariav et al., 2003; Wei et al., 2001) initiate dendritic spikes, which allow for supra-linear summation of synaptic inputs (Losonczy and Magee, 2006; Poirazi et al., 2003a; Polsky et al., 2009), coincidence detection (Larkum et al., 1999) and LTP induction (Magee and Johnston, 1997; Remy and Spruston, 2007).

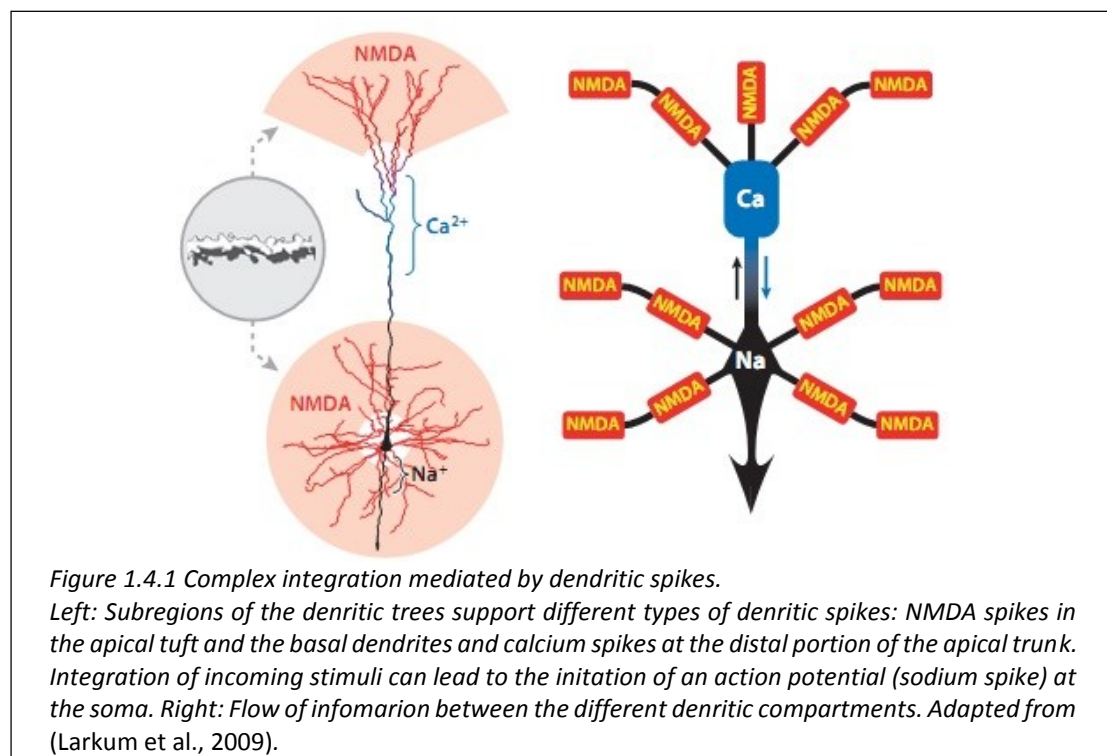
In particular, NMDA receptors, when sufficiently activated, can lead to the generation of dendritic regenerative events termed NMDA spikes (Major et al., 2013). Those spikes are characterized by larger local amplitude and duration, compared to the briefer Na⁺ spikes, but smaller amplitude compared to Ca²⁺ spikes. NMDA spikes are highly localized events, confined to thin dendritic branches. NMDA spike generation is facilitated by previous depolarization and thus make act as coincident detectors (Major et al., 2013). For these reasons, NMDA spikes are considered an attractive dendritic mechanism for the detection of incoming signals that arrive at close temporal and/or spatial proximity (Ariav et al., 2003; Losonczy and Magee, 2006).

1.4.3 Dendritic Integration

The various active properties of dendrites expand the computational capabilities of pyramidal neurons and add spatio-temporal specificity to their functional output (Oviedo and Reyes, 2005; Silver, 2010). In pyramidal neurons, synaptic inputs are integrated linearly when they are located on different dendritic branches and sigmoidally when located within the same dendrite (Losonczy and Magee, 2006; Poirazi et al., 2003a, 2003b; Polsky et al., 2004), but they could also be integrated sublinearly, depending on the spatial distribution of incoming signals (Oviedo and Reyes, 2012). Supralinear responses are supported by the generation of dendritic spikes, such as NMDA spikes, when provided with appropriate synaptic input (Branco and Häusser, 2011; Larkum et al., 2009; Major et al., 2008; Nevian et al., 2007;

Wei et al., 2001). Linear responses are also supported, as a result of competitive active conductances, such as the NMDA and the I_A conductances (Cash and Yuste, 1999).

The combination of a complex dendritic morphology with a location-specific distribution of ionic mechanisms results in the formation of distinct dendritic subunits which can integrate inputs in a quasi-independent manner (Losonczy and Magee, 2006; Poirazi et al., 2003a, 2003b; Polsky et al., 2004) (Figure 1.4.1). This compartmentalization of information processing endows neurons with a second processing layer that boosts the computational capacity of the neuron by at least an order of magnitude compared to that of a thresholding point neuron (Poirazi and Mel, 2001). Recent experimental evidence shows that the distribution of synapses along both the somato-dendritic axis as well as along the oblique branches in CA1 neurons favors this two-layer integration model (Katz *et al.*, 2009). At a smaller scale, single dendrites of layer 2/3 and layer 5 pyramidal neurons exhibit non uniform synaptic integration modes along their length. Synaptic inputs in the distal end of the dendrite summate sigmoidally with a low threshold for dendritic spike generation, while inputs to the proximal end of the same dendrite summate linearly and exhibit a higher threshold for dendritic spikes (Branco and Häusser, 2011; Major et al., 2008). Overall,



these findings show that dendritic arithmetic obeys complex rules that are often not only brain region but also branch-type specific.

The importance of dendritic integration with respect to neuronal function has recently been the subject of intense investigation (Major et al., 2013; Papoutsi et al., 2013; Spruston, 2008). Several studies have hinged on the computational advantages of nonlinear dendrites, including a significant enhancement of the processing power (Pissadaki et al., 2010; Poirazi et al., 2003b) and the dynamic range (Gollo et al., 2009) of individual neurons along with much larger storage capacity (Poirazi and Mel, 2001). Recent *in vivo* studies are beginning to shed light on the functional implications of both supralinear (Lavzin et al., 2012; Murayama et al., 2009; Sivyer and Williams, 2013; Smith et al., 2013; Xu et al., 2012) and sublinear (Longordo et al., 2013) dendritic integration in shaping the behavior of awake animals.

1.4.4 Dendritic nonlinearities and prefrontal cortex function

The PFC function has been shown to be particularly dependent on NMDA receptors (Compte, 2006; Wang, 1999; Wang et al., 2008). Apart from the increased complexity of the basal dendritic tree (Amatrudo et al., 2012), dendrites of PFC pyramidal neurons also have distinct NMDA receptor properties with enriched NR2B subunits and slower kinetics compared to sensory areas (Myme et al., 2003; Wang et al., 2008). In fact, the expression of mRNAs for NMDA subunits is higher in the PFC than in other regions of the human neocortex (Lewis and González-Burgos, 2006).

How exactly do NMDA receptors contribute to PFC function? Computational studies have traditionally considered NMDA current as a slow mechanism that provides stability to persistent activity in large scale networks (Wang, 1999). This view has recently been challenged as oversimplified, involving asymmetric contributions of NMDA receptors in excitatory *versus* inhibitory pathways (Lim and Goldman, 2013). Considering that the majority of the excitatory glutamatergic inputs in layer 5 pyramidal neurons is received by their basal, oblique and apical tuft dendrites (Antic *et al.*, 2010) and the slow kinetics of the NMDA receptors in the PFC, it is plausible to expect that regenerative NMDA events take place in thin dendrites of PFC neurons. Indeed, NMDA spikes are triggered in the basal dendrites of PFC neurons through the recruitment of extrasynaptic receptors (Chalifoux and Carter, 2011; Oikonomou et al.,

2012). Generation of NMDA spikes is important for the induction and maintenance of the periodical sustained firing *in vitro*, known as Up and Down states (UDS) in the PFC (Milojkovic et al., 2007; Oikonomou et al., 2012; Shu et al., 2003; Woodward and Pava, 2009). In addition, recent evidence shows that persistent activity is abolished when blocking NMDA receptors *in vivo* through the intracellular application of the NMDA-specific blocker MK-801 (Wang et al., 2013). However, whether NMDA spike generation is critical for persistent activity remains unexplored.

1.4.5 Intrinsic properties and prefrontal cortex function

The active membrane ionic mechanisms that are present in L5 PFC pyramidal neurons are:

- 1) The fast, transient (Naf) sodium current that participates in action potential generation and the slow inactivating, persistent (Nap) sodium current that contributes to burst firing (van Drongelen et al., 2006; González-Burgos and Barrionuevo, 2001; Yang et al., 1996).
- 2) Three different types of voltage-gated potassium channels: the delayed rectifier K⁺ currents (Kdr) that are rapidly inactivating and shape action potentials, the dendritic, transiently activated, A-type potassium current and the slow inactivating D-type potassium current (Hammond and Crépel, 1992; Korngreen and Sakmann, 2000; Schaefer et al., 2007).
- 3) Ca⁺⁺-dependent potassium channels that result in the after-hyperpolarization (AHP) (van Aerde et al., 2009).
- 4) The hyperpolarization-activated non-selective inward current (I_h) that has been shown to regulate the excitability of L5 PFC pyramidal neurons (Day et al., 2005).
- 5) The voltage-gated calcium channels (VGCCs), including the low voltage –activated (LVA) T-type calcium channel that mediate a transient calcium current (de la Pena and Geijo-Barrientos, 1996) and the high-voltage activated (HVA) calcium channels, including the long-lasting L-type current, the R-type and the N-type calcium channels (Lorenzon and Foehring, 1995).

Various neuromodulators alter the properties of the above active currents. As mentioned in Section 1.1.2., PFC receives direct dopaminergic afferents from the ventral tegmental area. Dopaminergic innervation of PFC neurons is of special

importance, since it modulates performance in working memory tasks (Durstewitz and Seamans, 2002; Goldman-Rakic et al., 2000) and is associated with neurophysiological disorders, such as schizophrenia (Knable and Weinberger, 1997). Dopamine (DA) acts on G-protein coupled receptors that are divided in D1-like (including D1 and D5 subtypes) and D2-like (including the D2, D3, and D4 subtypes). The effect of DA in the prefrontal cortex is task- and concentration-dependent and, in general, involves altering both the intrinsic and synaptic properties of PFC neurons (Seamans and Yang, 2004). For example, DA via D1 receptors enhances excitability through the modulation of the persistent sodium and L-type calcium channels and the down-regulation of the D-type potassium current (Dong and White, 2003; Gorelova and Yang, 2000; Young and Yang, 2004). Among the effects of DA in synaptic currents, its modulation of NMDA receptors is of special importance: activation of D1 receptors enhances the NMDA current (Chen et al., 2004; Seamans et al., 2001), whereas activation of the D2 receptors suppresses the NMDA current (Zheng et al., 1999). Given the dependence of PFC function on NMDA receptors, it is evident that such modulations must be taken into consideration.

Most importantly, one of the main features of the intrinsic properties of L5 PFC pyramidal neurons is the somatic current that generates a prolonged depolarizing plateau that lasts for several seconds (delayed afterdepolarization-dADP). The dADP supports regenerative events in single pyramidal neurons in the absence of AMPA and NMDA-mediated synaptic activity (Egorov et al., 2002; Sidiropoulou et al., 2009), but following pharmacological or synaptic activation of G_q-coupled receptors, such as mGluRs, mAChR and 5-HT receptors (Constanti and Libri, 1992; Greene et al., 1994; Haj-Dahmane and Andrade, 1998). The dADP is activated following an increase of intracellular calcium, through IP₃-dependent calcium release from the endoplasmic reticulum, as well as activation of voltage-gated calcium channels (Fowler et al., 2007; Hagenston et al., 2008). This calcium influx then activates a calcium-activated non selective cation current (I_{CAN}) mediated by the transient receptor potential channels (TRPCs) (Fowler et al., 2007). Recently it was shown that dADP can also be produced locally in the dendrites following activation of Group I metabotropic receptors (Kalmbach et al., 2013).

The dADP provides a short temporal window (2-3 seconds) during which incoming inputs may reach action potential threshold easier due to the underlying depolarizing envelope, converting subthreshold inputs to suprathreshold responses (Egorov et al., 2002; Sidiropoulou et al., 2009). Sequential dADP-inducing stimuli result in increased firing rate during the sustained activity with each successive stimulus, a phenomenon known as graded persistent activity, and provide a mechanism by which a neuron can 'remember' its activation history (Egorov et al., 2002).

Modeling studies suggest that the underlying mechanism that mediates graded persistent activity involves the interplay between the activation of the dADP and dendrite-specific, non-linear calcium dynamics. Non-linear calcium waves that are generated within dendritic branches propagate from the tip to the root of dendrites with increasing intensities depending on the strength of incoming stimuli and activate the dADP. The outcome is persistent spiking activity that co-varies with the temporal sum of incoming inputs (graded persistent activity) (Fransén et al., 2006; Loewenstein and Sompolinsky, 2003). In addition, dendritic bi-stability and summation of stimuli from multiple dendritic processes normalize the output and stabilize sustained neuronal activity to noisy incoming inputs (Goldman, 2003; Loewenstein and Sompolinsky, 2003). Interestingly, it was recently shown that NMDA spike generation at the basal dendrites serves as a mechanism for the detection of 'preferred' sensory signals, namely signals that will induce persistent activity that depends on dADP activation in a single layer 5 PFC pyramidal neuron (Sidiropoulou and Poirazi, 2012).

Therefore, the interplay between dendritic processing and the intrinsic features of L5 PFC neurons may have a pivotal role in shaping the computations supported by these neurons.

1.5 The role of morphology in shaping dendritic integration

Given the important role of dendritic processing to the functional output, what is missing is a systematic characterization of how distinct anatomical and biophysical features of the basal dendrites determine synaptic integration and shape the function of pyramidal neurons. Electrophysiological characterization with current injection *in vitro* has shown that PFC neurons with a more complex morphology display bursting firing patterns, whereas neurons with simpler morphologies tend to fire tonic spikes

(Yang et al., 1996). A basic issue with experimental studies is that they cannot dissect the role of morphology from the various types of ionic currents that are present in these neurons. Simulations of reconstructed neurons using uniform distributions of the ionic conductances, focusing mainly on the apical dendritic tree, have revealed that differences in morphology alone can account for a variety of different electrophysiological profiles (Krichmar et al., 2002; Mainen and Sejnowski, 1996), burst firing (van Elburg and van Ooyen, 2010), action-potential back propagation efficacy (Vetter et al., 2001), synaptic efficacy (Jaffe and Carnevale, 1999; Komendantov and Ascoli, 2009), coupling between somatic and dendritic action potentials (coincidence detection) (Schaefer et al., 2003) and branch excitability and coupling (Ferrante et al., 2013). To our knowledge, only one study has raised the issue of how morphology alters neuronal computations, yet using artificially constructed morphologies (Stiefel and Sejnowski, 2007). Surprisingly, the morphological diversity and the functional role of synaptic activation of the basal tree has been essentially ignored.

Taken together, dendritic morphology plays a key role in shaping neuronal responses and should be taken into account when investigating dendritic integration properties. Towards this goal, compartmental models can be particularly useful as they can account for morphologically and biophysically realistic neuronal cells and circuits.

2 Motivation

Driven by the vast, yet fragmented, data regarding dendritic biophysics, anatomy and integrative properties, this thesis aims to characterize the role of dendrites in PFC function, and particularly the expression of persistent spiking activity. The methodological approach includes the development and application of biophysically detailed PFC microcircuits consisting of L5 neurons. L5 PFC pyramidal neurons are selected because of their complex morphology, high dependence on NMDA receptors and ability to form hyper-reciprocally connected microcircuits.

The following open questions are tackled in this study:

1. Are L5 PFC microcircuits the minimum structure that supports persistent activity? (Section 4)
2. Do microcircuits also support more complex computations, such as coding of stimulus characteristics? (Section 4)
3. How do intrinsic active conductances along the somato-dendritic axis contribute to the observed phenotype? (Section 4)
4. What are the mechanisms that support the initiation of persistent activity in the microcircuits? Do the same mechanisms apply to both small and large scale networks? (Section 5)
5. What are the mechanisms that contribute to persistent activity robustness? Do these mechanisms also contribute to persistent activity initiation? (Section 5)
6. Does the complex dendritic morphology of L5 PFC pyramidal neurons contribute to the observed phenotype? (Section 6)

Overall, this study spans three levels of analysis, from morphology to dendritic integration to neuronal function and seeks to establish a link between dendritic and the expression of persistent activity, the cellular correlate of working memory, in L5 microcircuits of the PFC.

3 Methodology

The microcircuit model was implemented in the NEURON simulation environment (Hines and Carnevale, 2001).

3.1 Pyramidal neuron model

Two pyramidal neurons models were used in the present study. The first simulated a layer 5 PFC pyramidal neuron model with simplified morphology based on (Durstewitz and Gabriel, 2007; Durstewitz et al., 2000), was extended to incorporate active ionic conductances and validated against experimental data. In the second, different detailed morphologies were incorporated and adapted from (Sidiropoulou and Poirazi, 2012).

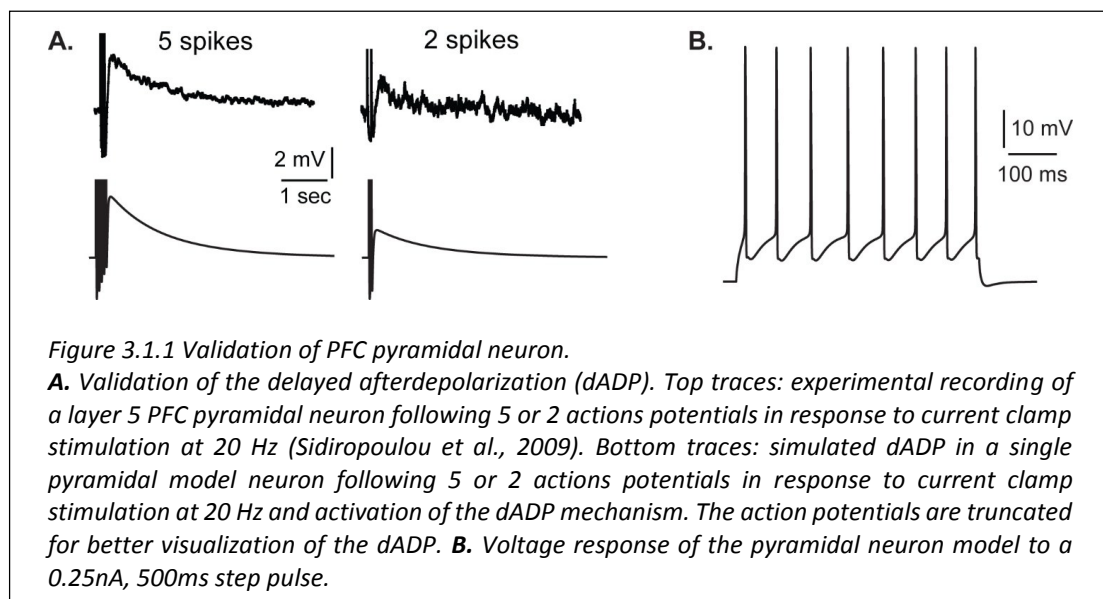
3.1.1 Simplified pyramidal neuron models

The simplified morphology was used in order to dissect the role of intrinsic and synaptic currents from that of a detailed dendritic tree. It consisted of five compartments: a soma, an axon, a basal dendrite, a proximal apical dendrite and a distal apical dendrite. The somatic, proximal and distal apical dendritic compartments included Hodgkin–Huxley-type transient (I_{NaT}) and persistent (I_{NaP}) Na^+ currents, voltage-dependent K^+ currents (I_{Kdr} ; I_A ; I_D), a fast Ca^{++} and voltage-dependent K^+

current, (I_{fAHP}), a slow Ca^{++} -dependent K^+ current (I_{sAHP}), a hyperpolarization-activated non-specific cation current (I_h), a low-voltage activated calcium current (I_{CaT}) and four types of Ca^{++} - and voltage-dependent calcium currents (I_{CaN} ; I_{CaR} ; I_{CaL} , I_{CaT}). The basal dendrite included a transient sodium current, a delayed K^+ rectifier current, a persistent Na^+ current, an A-type K^+ current, a D-type K^+ current, an N-type Ca^{2+} current and an h current. The axon included a sodium (I_{NaF}) current and a delayed rectifier K^+ current (I_{Kdr}).

The calcium-activated non-selective cation (CAN) current (Sidiropoulou and Poirazi, 2012) that results in the generation of the delayed after depolarization (dADP) was activated only in specific cases. The kinetics of the dADP mechanism were fit to the experimental recordings of (Sidiropoulou et al., 2009) as shown in Figure 3.1.1A. Parameters of the dADP mechanism were adjusted so that the dADP was activated following more than 4 spikes and had decay kinetics in the order of a few (~ 3) sec. When activated, its amplitude was within the experimentally reported range (1-6 mV) as per (Sidiropoulou et al., 2009).

Active properties of the neuron model were validated according to the experimental results of (Nasif et al., 2005). Specifically, input resistance R_{IN} was set to $80M\Omega$, the current needed to generate an action potential was $0.23nA$ and the action potential threshold was $-43.5mV$. The pyramidal neuron responded to a depolarizing current pulse ($0.25nA$, $500ms$) with 8 spikes, as shown in Figure 3.1.1B.



The dimensions of the somatic, axonic, and dendritic compartments of the pyramidal model cell are presented in Table 10.1.1. The passive parameters of the model neuron are listed in Table 10.1.2, while the active ionic properties are listed in Table 10.1.3.

3.1.2 Pyramidal neuron models with detailed morphology

The biophysical mechanisms incorporated in the detailed pyramidal model neurons were the same as the simplified model, but their parameters (e.g. conductances, kinetics) were fitted to account for the detailed morphology. Model construction and validation, as well as modeling equations were developed and presented in (Sidiropoulou and Poirazi, 2012). A list of all conductances used for each compartment is shown in Table 10.1.4.

3.2 Interneuron model

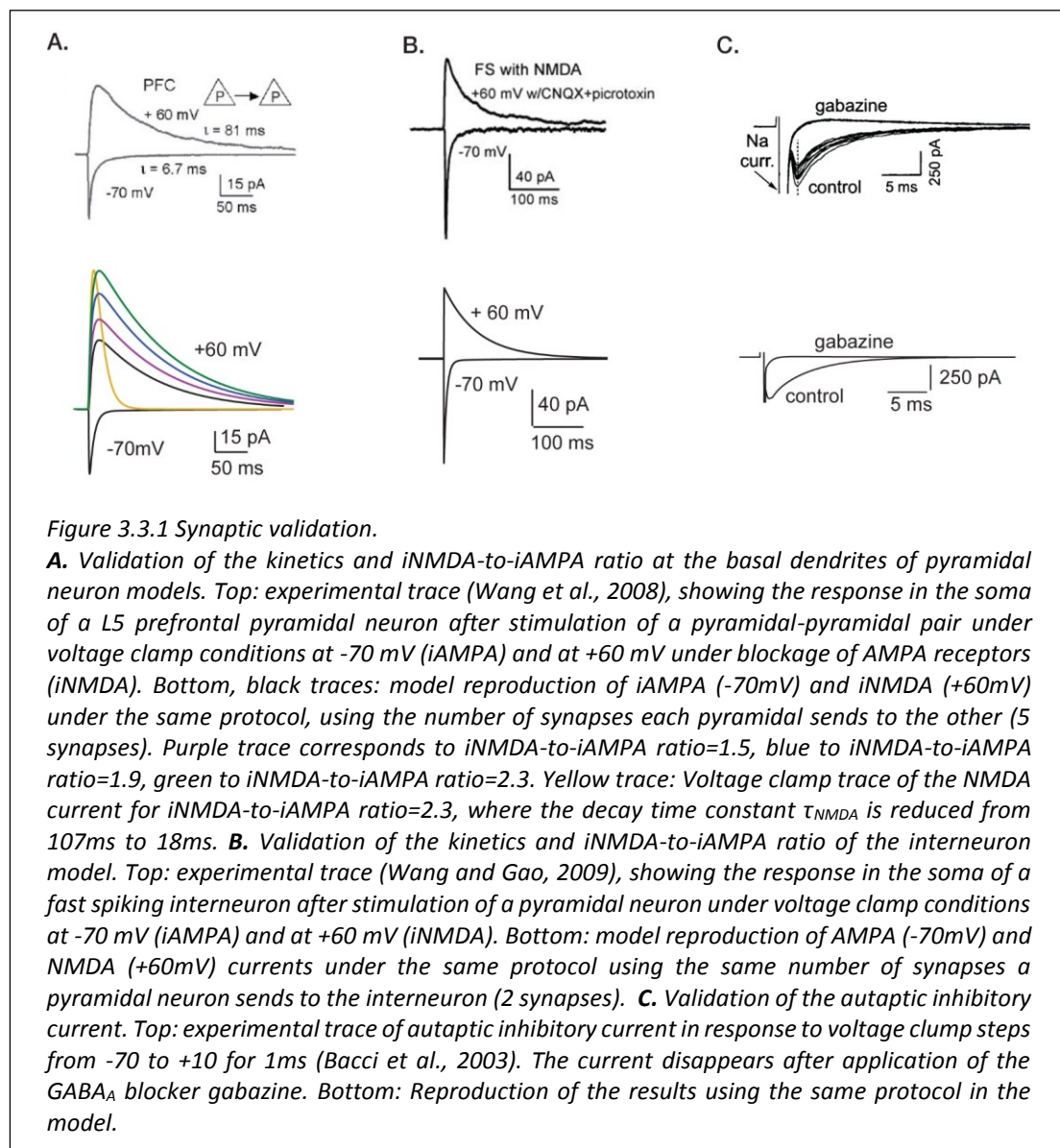
The interneuron model (fast spiking) was adapted from (Durstewitz and Gabriel, 2007) (Model-DB, accession number 82784), with the addition of an axonal compartment and validated against experimental data. The somatic compartment included a fast Na^+ current (I_{Naf}) and two types of K^+ currents (I_{Kdr} ; I_{D}). The axon included a Na^+ current (I_{Naf}) and a delayed rectifier K^+ currents (I_{Kdr}). The resting membrane potential (V_m) was set to -70mV and the input resistance R_{IN} to $207\text{ M}\Omega$ (Cauli et al., 1997; Kawaguchi and Kubota, 1993). The interneuron responded to step pulses of 0.2nA and 0.35nA with a firing frequency of 60 Hz and 90 Hz , respectively in agreement with (Cauli et al., 1997; Kawaguchi and Kubota, 1993; Wang and Gao, 2009).

The dimensions of the somatic and axonic compartments are presented in 9.1.1 Passive and active ionic properties of the interneuron model are listed in 9.1.2 and 9.1.5, respectively.

3.3 Synaptic properties

The AMPA current in the pyramidal cell was tuned to match the experimental data of (Wang et al., 2008): under voltage clamp conditions at -70mV and activation of 5 synapses (simulating the monosynaptic connections between layer 5 pyramidal

neurons), the amplitude and kinetics of the AMPA current fit the experimentally reported values as shown in Figure 3.3.1A. The amplitude and kinetics of the NMDA current in the pyramidal cell were also validated with voltage clamp at +60 mV under conditions of blocked AMPA, Na⁺ and K⁺ currents as per (Wang et al., 2008) and are shown in Figure 3.3.1A (black traces). The baseline value for the iNMDA-to-iAMPA ratio (measured as the ratio of the peak amplitude of the iNMDA and the iAMPA under voltage clamp at +60mV and -70 mV respectively) at the basal dendrite was set to 1.1 as per (Wang et al., 2008). Since the NMDA current in the PFC increases either by dopamine (Seamans et al., 2001; Wang and O'Donnell, 2001) or due to the recruitment of extrasynaptic receptors (Chalifoux and Carter, 2011; Oikonomou et al., 2012), in certain experiments we varied the iNMDA-to-iAMPA ratio (iNMDA increased



while iAMPA remained unaltered) to values of 1.5, 1.9, and 2.3 (i.e. 36%, 72% and 100% increase). All ratios were calculated under voltage clamp conditions and the respective NMDA traces are shown in Figure 3.3.1A (purple, blue and green traces). For another set of experiments we decreased the decay time constant of the NMDA current from $\tau=93\text{ms}$ to $\tau=18\text{ms}$ (Figure 3.3.1A, yellow trace). For the proximal apical dendrite, the iNMDA-to-iAMPA ratio was half of the baseline basal dendrite value, according to (Dodt et al., 1998).

The AMPA and NMDA EPSC kinetics in the interneuron model were validated using data from fast spiking L5 prefrontal cortex interneurons, by holding the membrane potential of the interneuron at -70 mV and +60 mV respectively, as per (Wang and Gao, 2009). The corresponding amplitudes were also validated according to (Wang and Gao, 2009) and the results are shown in Figure 3.3.1B. Finally, for the validation of the interneuron autapses, a three-step voltage clamp was used (-70mV to 10 mV to -70 mV) that resulted in a self-inhibitory current of approximately 350pA (Figure 3.3.1C). It should be noted that only during the validation of this synaptic current, the reversal potential of Cl^- was adjusted from -80 mV to -16 mV, in order to reproduce the experimental set up of (Bacci et al., 2003). During the simulations we assumed physiological reverse potential (-80mV).

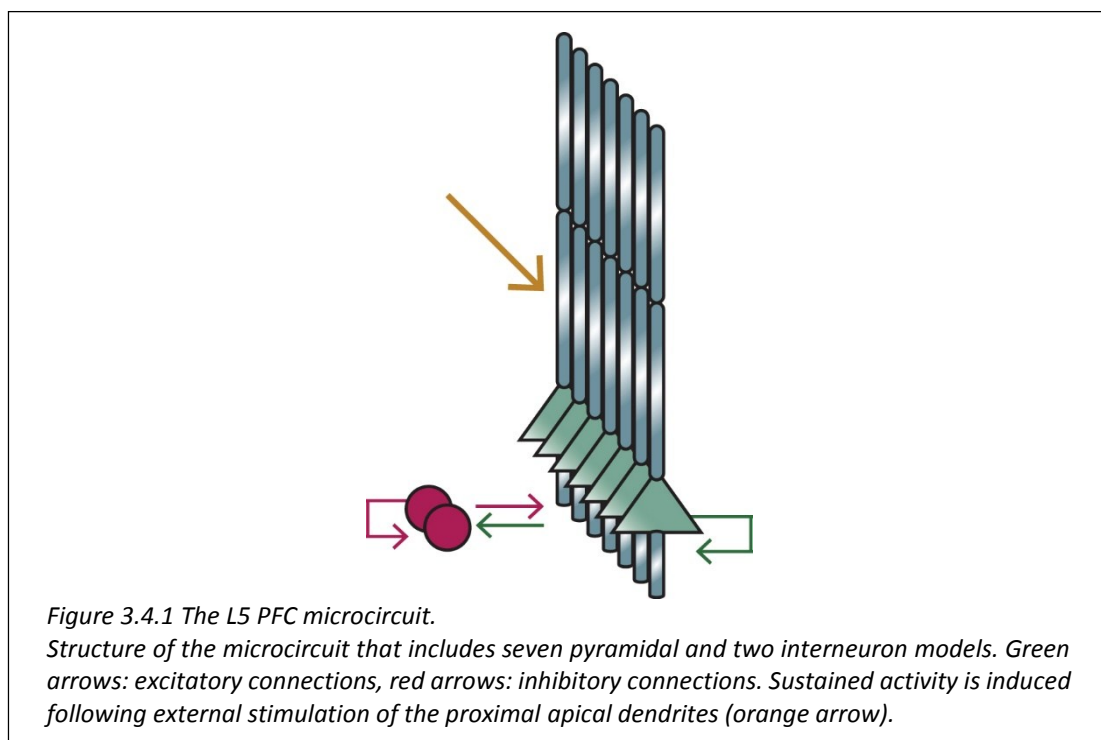
The conductance of the GABA_A mechanism was set so that the amplitude of the mIPSC was 10pA at a holding potential of -65 mV, as per (Woo et al., 2007). Finally, we implemented the slow inhibitory synaptic current (iGABA_B). Physiological data regarding the iGABA_B -to- iGABA_A ratio in layer 5 pyramidal neurons are conflicting. Application of GABA on layer 5 pyramidal neurons was shown to result in a GABA_B response that is 80% of the amplitude of the GABA_A response (Eder et al., 2001), while dual-recordings between an interneuron and a pyramidal neuron resulted in pure GABA_A or GABA_B responses, with the GABA_B responses being elicited in about 20% of the cases (Thomson and Destexhe, 1999). Due to the discrepancy of these findings, the iGABA_B -to- iGABA_A ratio was varied from 0.2 to 0.8. This ratio was measured as the peak amplitude of the GABA_B current over the peak amplitude of the GABA_A current after stimulation that resulted in the saturation of the GABA_B current (40 events at 100Hz), according to (Thomson et al., 1996).

The synaptic waveform parameters and conductances of AMPA, NMDA, GABA_A and GABA_B currents are listed in Table 10.1.6.

3.4 Microcircuit

The microcircuit model (graphically illustrated in Figure 3.4.1), consists of seven pyramidal neurons and two interneurons, as inhibitory neurons in the prefrontal cortex constitute 25%-35% of the neuronal population (Dombrowski et al., 2001). Connectivity properties including the location and number of synaptic contacts, the latencies between pairs of neurons, as well as the electrophysiological properties of their synaptic connections, were based on anatomical and electrophysiological data (see Table 10.1.7 for parameter values). The complete mathematical formalism of the model can be found in the Section 9.2 of the Appendix.

Specifically, the microcircuit incorporates the high reciprocity of connections reported in (Wang et al., 2006). Pyramidal model neurons were interconnected at the basal dendrite through 5 synapses (Markram et al., 1997; Morishima and Kawaguchi, 2006), although this number could increase (Elston, 2003). The latency between pyramidal pairs drawn from a Gaussian distribution with $\mu=1.7\text{ms}$ and $\sigma=0.9$ according to (Morishima and Kawaguchi, 2006; Thomson and Lamy, 2007). Autapses, that have



been observed between axon arbors and basal dendrites of pyramidal cells in the neocortex (Van der Loos et al., 1972), equal one third of the contacts formed between two synaptically coupled pyramidal neurons, with a mean value of 2.3 ± 0.9 according to (Lübke et al., 1996). Based on the above, we used 1 autapse per neuron. In each simulation, the precise location of the connecting synapses varied randomly across the basal dendrite of each neuron. The reasoning behind this manipulation, along with all other sources of noise (membrane fluctuations, conductance delay variability, etc.), was to represent the existence of multiple microcircuits in the PFC whose properties are not identical.

Pyramidal neurons also connect to interneurons by 1-2 synaptic contacts according to (Buhl et al., 1997). The latencies of these connections are drawn from a Gaussian distribution with $\mu=0.6\text{ms}$ and $\sigma=0.2$ as per (Angulo et al., 1999). Inhibitory neurons connect to pyramidal neurons and the number of these contacts is such as to produce a unitary IPSP of amplitude ~ 1 mV, according to (Tamás et al., 1997a). The latencies of these connections are drawn from a Gaussian distribution with $\mu=1.8\text{ms}$ and $\sigma=0.8$ as per (Thomson and Lamy, 2007).

Autaptic innervation in fast-spiking interneurons is accomplished through 12 ± 7 synaptic contacts as reported in (Tamás et al., 1997b). According to a functional study of autaptic inhibitory currents in fast-spiking neurons, a single action potential evokes an autaptic inhibitory current with peak amplitude ~ 350 pA and mean latency of $1.76 \pm 0.07\text{ms}$ (Bacci et al., 2003). Since autapses strongly regulate the spike-timing of the interneurons (Bacci and Huguenard, 2006), 12 synapses producing the autaptic inhibitory current was implemented using the protocol reported in (Bacci et al., 2003; Tamás et al., 1997b).

3.5 Stimuli

Persistent activity in the microcircuit was induced by providing external synaptic stimulation (10 pulses at 20Hz, 90 excitatory synapses) to the proximal dendrites (yellow arrow in Figure 3.4.1) of each pyramidal model neuron (Kuroda et al., 1998). In the prefrontal cortex, when two pyramidal neurons have common input, they have a significant higher probability of being connected (Otsuka and Kawaguchi, 2008). Since neurons within a microcircuit share similar stimulus properties (Petreanu

et al., 2009; Yoshimura et al., 2005), the same initial stimulus was delivered to all pyramidal neurons.

3.6 Background noise

In order to simulate as closely as possible the noise fluctuations in the membrane potential of both pyramidal cells and interneurons that are seen *in vitro*, an artificial current with Poisson characteristics was injected in all neuronal models.

4 PFC microcircuits as tunable modules

4.1 Preamble

Although the experimentally confirmed prevalence of highly-reciprocally connected microcircuits in the PFC (Morishima et al., 2011; Wang et al., 2006), it remains unknown whether these assemblies can support persistent firing, how their properties are influenced by changes in their intrinsic and/or synaptic mechanisms and whether they can express stimulus-specific coding, such as the one seen in large scale networks (Brody et al., 2003). To address these questions, we used the microcircuit model (see Model development) to study whether persistent activity can emerge in small clusters of neurons and characterize the conditions that allow its emergence. In this Section we focused on the mechanisms that could modulate persistent firing, providing new insights on how PFC microcircuits may serve as key players in working memory formation.

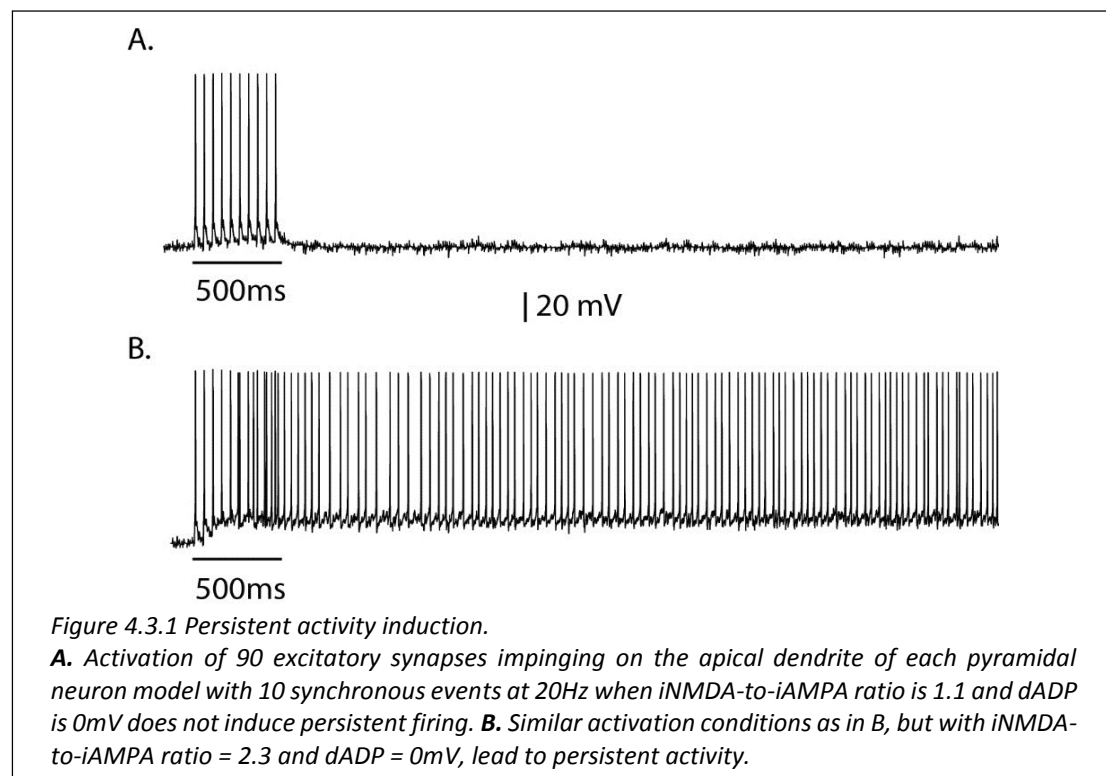
4.2 Materials and Methods

Model microcircuit and stimulation protocol are extensively described in Section 3: Model Development. For the analysis of spike trains, we used single-neuron Inter-Spike-Intervals (ISIs) and the Synchronization index. Single neuron distribution of ISIs was estimated for each pyramidal neuron under each condition used. In addition, in order to evaluate the synchronization or de-synchronization of pyramidal neurons during persistent activity, we also estimated the Synchronization index. For this measurement we obtained the spike trains simultaneously from the pyramidal neuron population and then we calculated the time intervals between successive spikes occurring in any of the participating pyramidal neurons. If there are no phase lags between the spike trains (neurons fire synchronously) the synchronization index will have values of zero. In general, small values of synchronization index indicate synchronicity, whereas large values indicate asynchronous spiking activity (for details of the method see (Kreuz et al., 2011)). ISI distributions were compared using either the pair-wise Mann-Whitney or the Kruskal-Wallis non-parametric statistical test. Comparisons with p values <0.05 were deemed statistically significant.

4.3 Results

4.3.1 Induction of persistent activity

Our first goal was to test whether the microcircuit model could generate persistent activity in response to a realistic stimulus. We found that under conditions of control NMDA currents (iNMDA-to-iAMPA ratio=1.1) and dADP = 0mV, activation of 90 excitatory synapses impinging on the apical dendrite of each pyramidal neuron model (with 10 synchronous events at 20Hz) lead to transient stimulus response (Figure 4.3.1A). When we increased the iNMDA-to-iAMPA ratio to 2.3 and kept dADP deactivated, persistent activity emerged with a probability of 0.86 (Figure 4.3.1B). Persistent activity in the microcircuit model was an all-or-none phenomenon: if induced, it lasted for the whole duration of the simulation, namely 5 seconds.

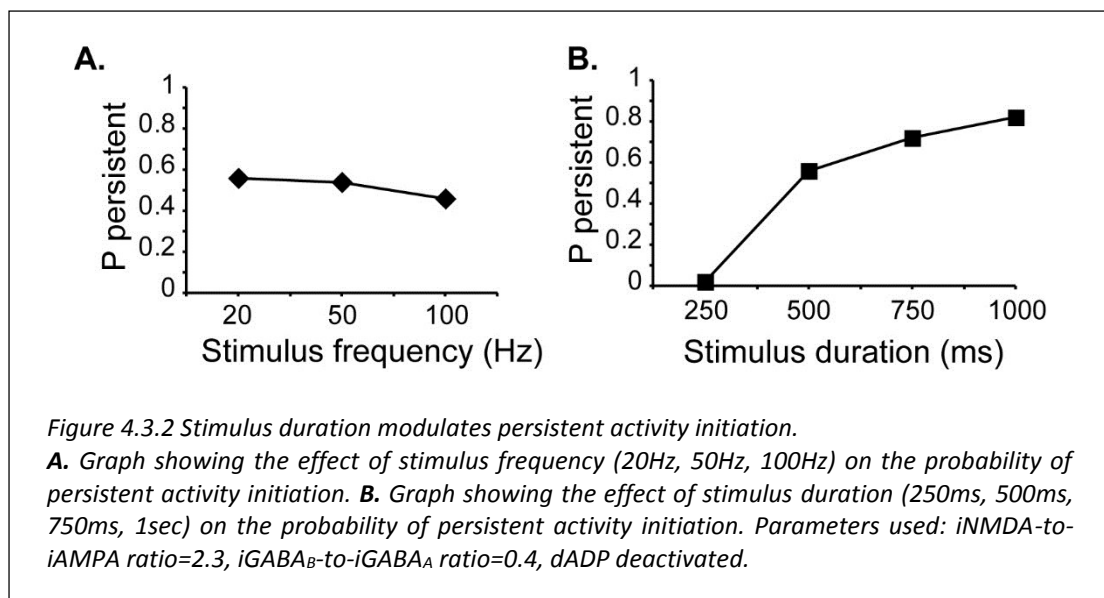


4.3.2 Stimulus effects on persistent activity

The firing frequency and stimulus-specificity of persistent activity during working memory tasks are modulated by various neurotransmitters, such as dopamine (Arnsten et al., 2012), although the exact mechanisms and effects of this

modulation remain unclear. In the following paragraphs, we investigated the stimulus-specific factors that can influence the firing characteristics of persistent activity.

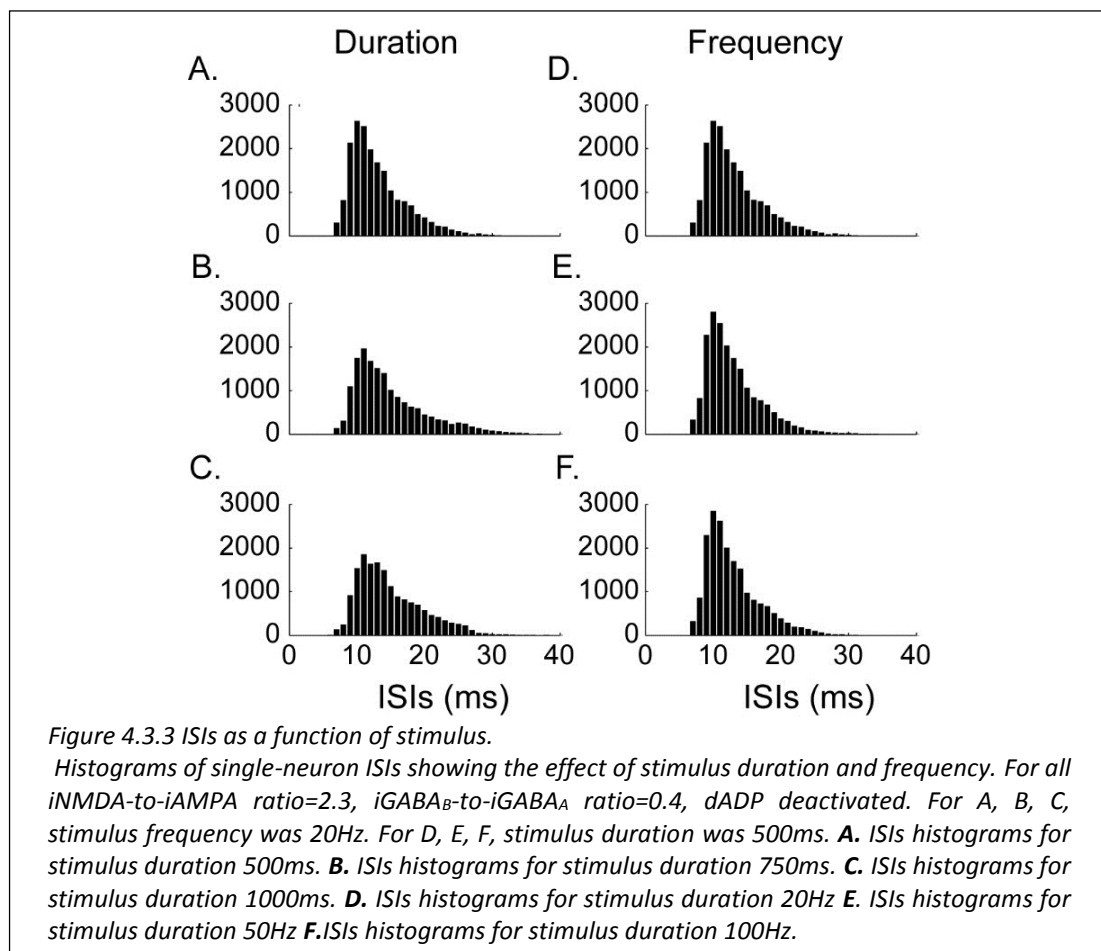
First, we asked whether the properties (firing frequency and duration) of the inducing stimulus alter the emergence and/or firing characteristics of persistent activity, using a range of input frequencies (20, 50 and 100 Hz, 10 synchronous events) and durations (0.25, 0.5, 0.75 and 1sec, input frequency 20Hz). We found that the input frequency had no significant effect on the probability of persistent activity initiation (Figure 4.3.2A), but the duration greatly altered the microcircuit's response to the stimulus: longer stimuli were more likely to induce persistent firing (Figure 4.3.2B).

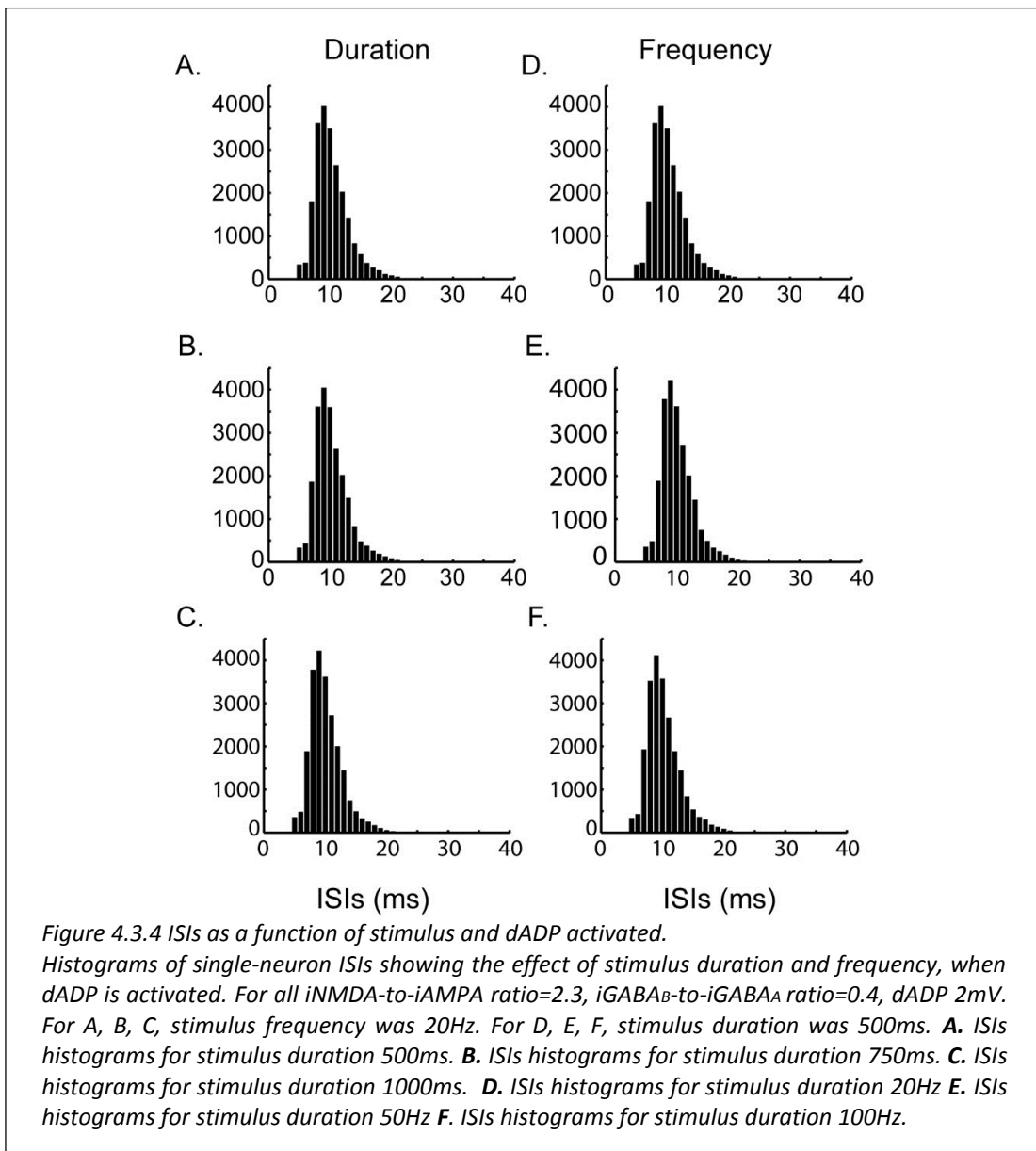


To investigate potential stimulus coding for different input frequencies and/or durations we compared the ISI distributions during persistent firing at a single pyramidal neuron and synchronization index in the microcircuit level. The single neuron ISI distributions were significantly different (Kruskal-Wallis test) between stimuli lasting 0.5, 0.75 and 1sec ($p < 0.001$), with median ISI values of 11.5, 12.9 and 13.2ms, respectively (Figure 4.3.3A, B, C). Although comparison of the synchronization index of the microcircuit was significantly different ($p < 0.001$), the pair-wise comparison (Mann-Whitney U-test) for stimuli lasting 0.75 and 1 sec were not statistically different. These results suggest that individual neurons in the microcircuit

may code for differences in the stimulus duration, but when looking at the population output of the microcircuit, this coding is weakened.

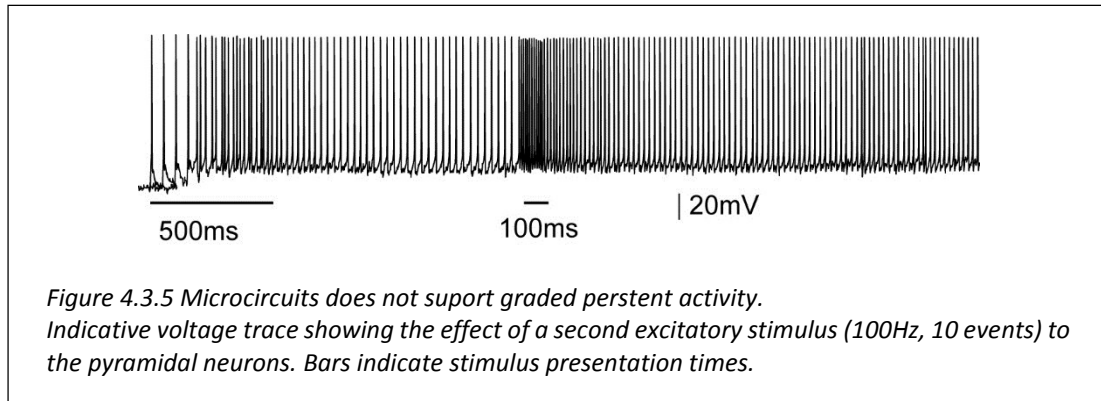
Similar results were obtained when altering the firing frequency of the input: the ISI distributions were significantly different for 20 *versus* 50 or 20 *versus* 100Hz inputs ($p < 0.001$ in both cases), but not for 50 *versus* 100Hz-inputs (Figure 4.3.3D, E, F). Median ISI values were 11.5ms for 20Hz, 11.4 for 50Hz and 11.3ms for 100Hz. No significant difference was found between the synchronization indexes of the microcircuit in any condition. The same analysis was performed with the dADP mechanism activated (at 2mV), as it was previously suggested to contribute to stimulus coding at the single neuron level (Egorov et al., 2002). The results were qualitatively the same (Figure 4.3.4). Overall, we do not find strong evidence for coding the firing characteristics of the input in our model microcircuit.





Stimulus coding may also be realized via the expression of graded persistent activity, whereby subsequent presentation of the same (or different) stimulus increases the firing frequency of persistent activity (Egorov et al., 2002). To test the microcircuit's ability to generate graded firing, we performed another set of experiments whereby a second excitatory stimulus of different frequency (90 synapses activated with 10 events at 50Hz or 100 Hz) was delivered 1sec after the initial stimulus to the proximal dendrites of all pyramidal neurons. Again, no differences were seen in the ISI distributions during persistent activity (Figure 4.3.5). Collectively, properties of spiking activity are independent of stimulus properties, and

fine-tuned stimulus coding may be realized in higher-level networks. We further investigated how persistent activity properties can be modulated by the synaptic and intrinsic properties.

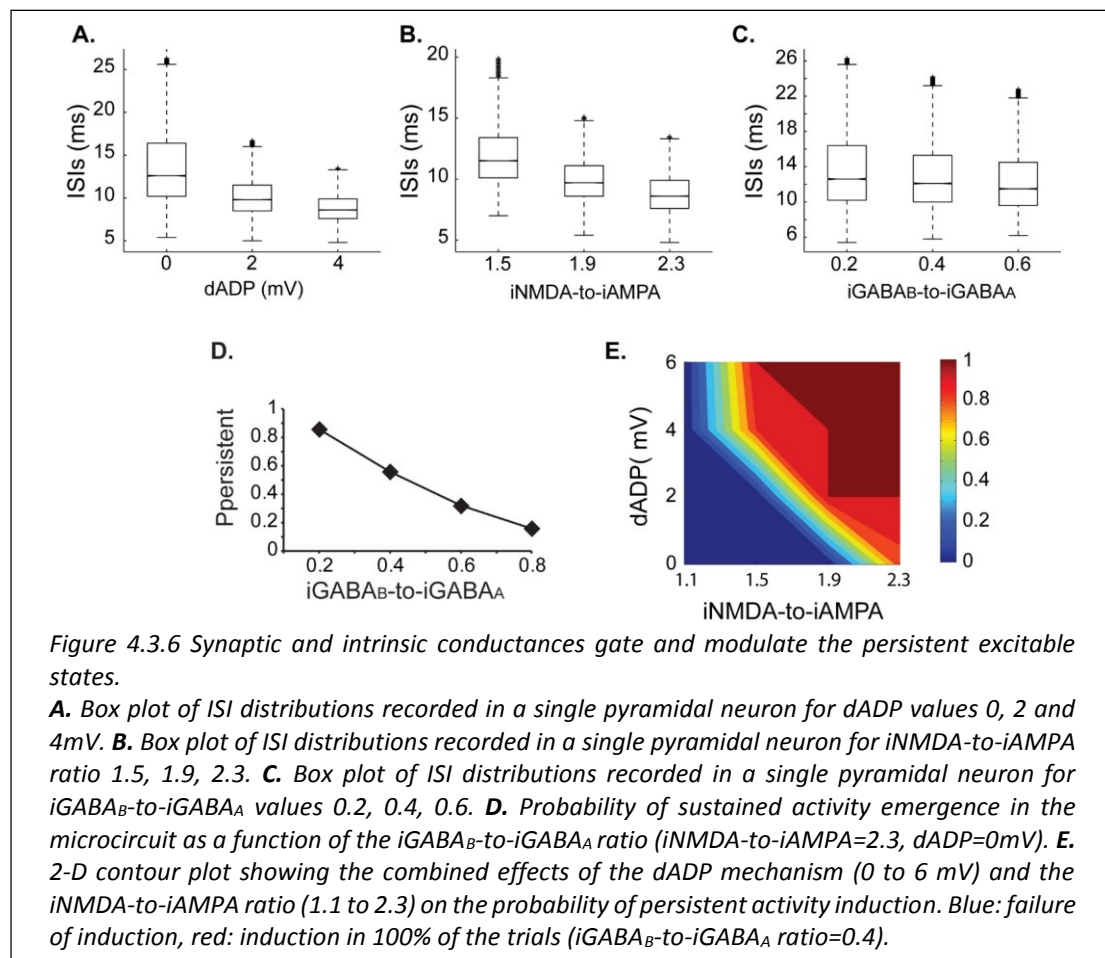


4.3.3 Excitation-inhibition balance and dADP effects on persistent activity induction

Working memory has been associated with the release of various neuromodulators that influence the balance of excitation-inhibition and the magnitude of the dADP in the PFC. Therefore, we asked whether changes in these mechanisms may influence persistent activity properties. We found that increasing the amplitude of the dADP (0mV, 2mV and 4 mV) (Figure 4.3.6A), the iNMDA-to-iAMPA ratio (1.5, 1.9, 2.3) (Figure 4.3.6B) or the iGABA_B-to-iGABA_A ratio (0.2, 0.4, 0.6) (Figure 4.3.6C) was associated with smaller average ISIs at the single neuron level (and thus larger average firing frequencies), although the effect in the median values for the different iGABA_B-to-iGABA_A ratios is small ($p < 0.001$ for all cases, Kruskal-Wallis test). These findings suggest that the release of a neuromodulator that influences any of the above mentioned mechanisms will significantly change both the average and the temporal firing characteristics of the microcircuit.

To further elucidate the effect of inhibition on persistent activity, we investigated whether slow inhibitory synaptic currents mediated by the GABA_B receptors can counteract the permissive effects of the NMDA current. We found that large iGABA_B-to-iGABA_A ratios (when iNMDA-to-iAMPA ratio=2.3) reduced, but did not eliminate the probability of persistent activity initiation (Figure 4.3.6D). Thus, activation of the GABA_B current modulated persistent activity initiation and adds a

novel parameter to the so far known biophysical mechanisms underlying persistent activity.



In addition to synaptic, intrinsic mechanisms and particularly the dADP have been linked to persistent firing at the single neuron level (Sidiropoulou and Poirazi, 2012; Sidiropoulou et al., 2009). As depicted in Figure 4.3.6E, incorporation of the dADP mechanism in a physiologically relevant range (2-6 mV) in the microcircuit model allows the emergence of persistent activity for smaller iNMDA-to-iAMPA ratios but not for a ratio of 1.1. These findings suggest that high NMDA current is a prerequisite for persistent activity initiation in the microcircuit when the dADP current is inactive, but this necessity weakens in the presence of dADP.

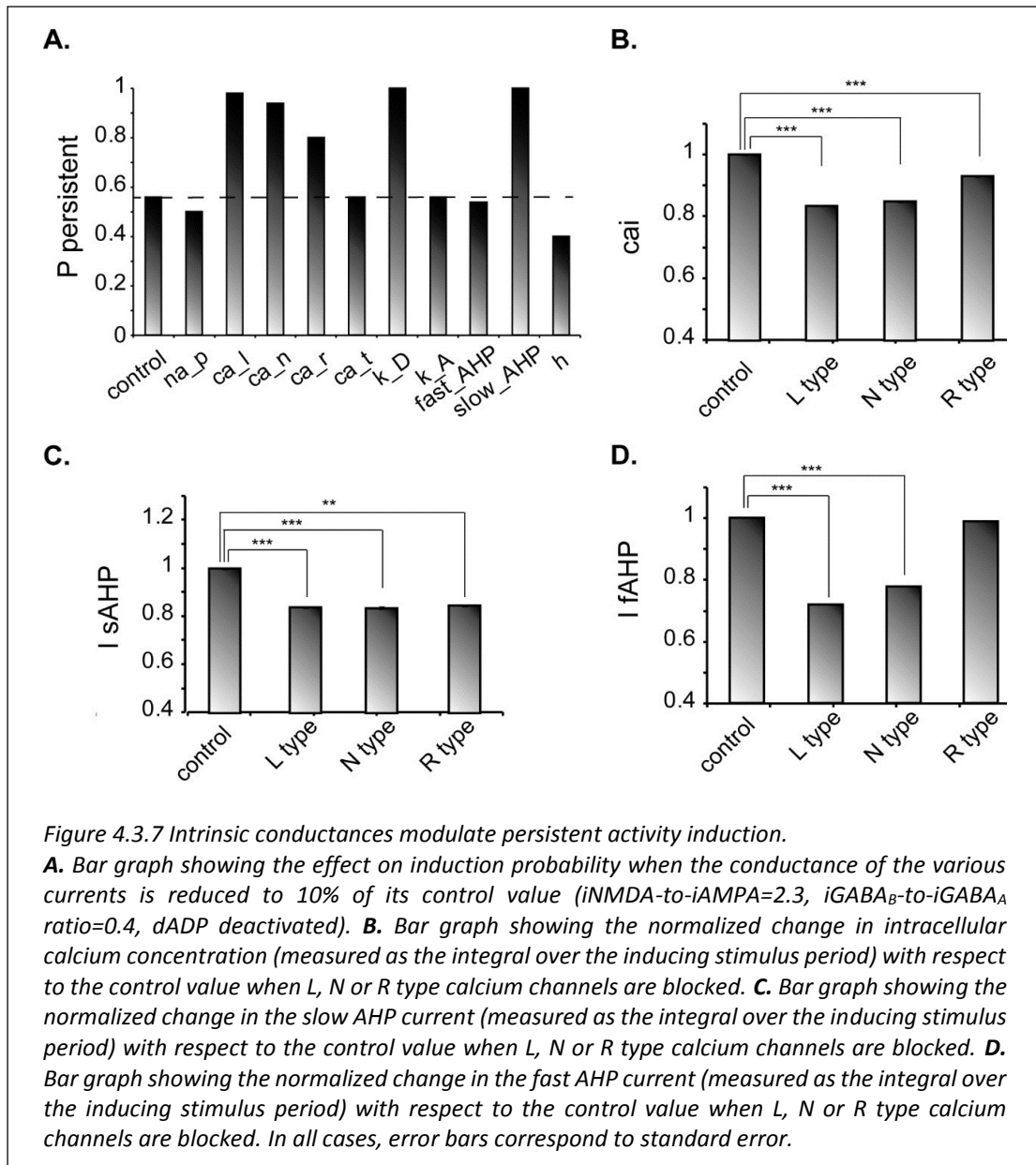
4.3.4 Intrinsic mechanisms involved in the initiation of persistent activity

We finally investigated how changes in the conductance values of membrane mechanisms, including ionic conductances, can interfere with the ability of the

microcircuit to express persistent activity. We examined the contribution of various intrinsic ionic mechanisms by independently reducing their conductance to 10% of their control value and assessing the effect on persistent activity emergence. The following mechanisms were investigated: the persistent Na⁺ current, the D-type K⁺ current, the A-type K⁺ current, the h-current, the L-, N-, T- and R-type Ca⁺⁺ currents and the currents underlying the fast and slow AHP mechanisms (I_{sAHP} , and I_{fAHP} , respectively). For these experiments iNMDA-to-iAMPA was 2.3, iGABA_B-to-iGABA_A was 0.4 and the dADP was deactivated, leading to an induction probability of 0.54. Figure 4.3.7A shows the effect of each mechanism blockade on the probability of persistent activity emergence relative to the control.

In general, independent blockade of the D-type K⁺ current, the h-current, the L-, N- and R-type calcium current and the I_{sAHP} led to more than 15% change in the induction probability: reducing the conductance of D -type K⁺ current, the L-, N- and R-type calcium current and the I_{sAHP} enhanced the probability of induction, whereas reducing the conductance of the h current reduced the probability of persistent activity emergence.

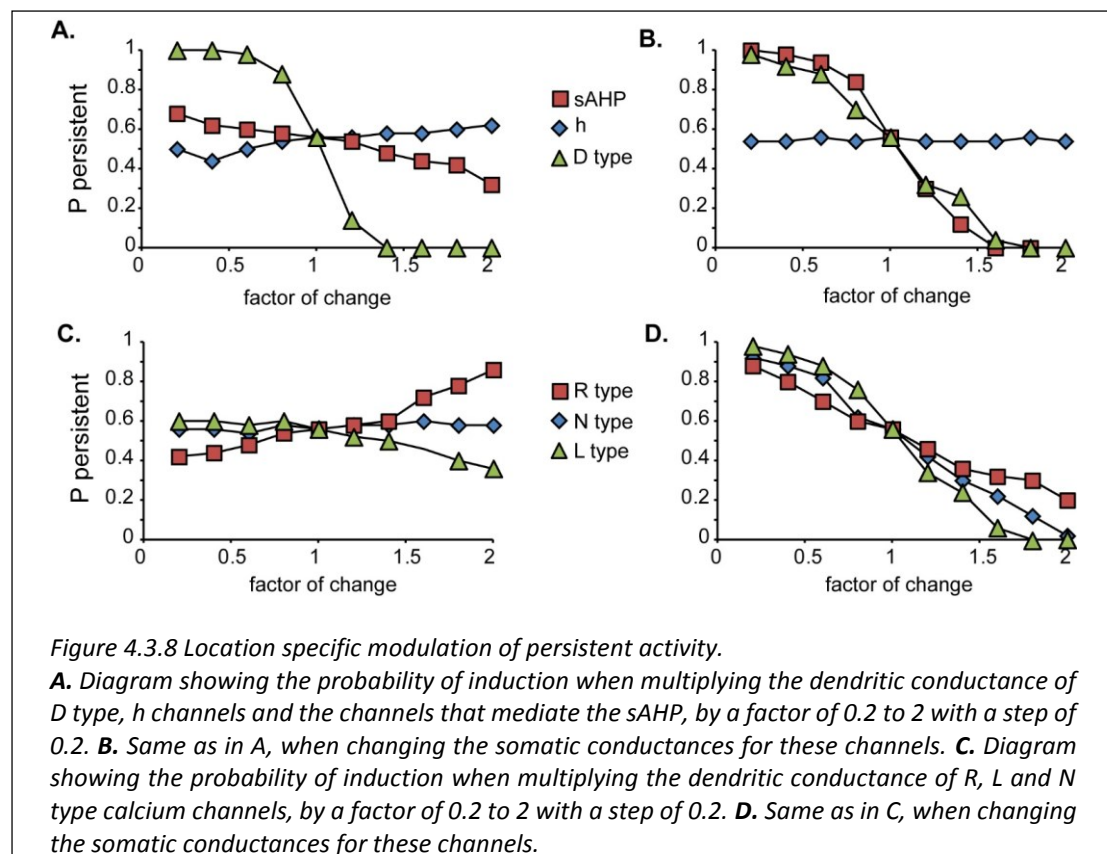
Counter intuitively, blockade of the L, N or R-type calcium currents increased the probability of persistent activity (Figure 4.3.7A). To further investigate this result, we compared the intracellular calcium accumulation (integral of the calcium concentration) and the cumulative (integral) I_{sAHP} , and I_{fAHP} currents during stimulus presentation under control and calcium channel blockade conditions (Figure 4.3.7B, C, D). As expected, the intracellular calcium accumulation and the cumulative I_{sAHP} current were both significantly lower ($[Ca^{++}]$: for L-type blockade $p < 0.001$, for N-type blockade $p < 0.001$ and for R-type blockade $p < 0.001$, I_{sAHP} : for L-type blockade $p < 0.0001$, for N-type blockade $p < 0.001$ and for R-type blockade $p = 0.001$) in all cases, while the cumulative I_{fAHP} was smaller when blocking the L, N but not the R type calcium channels (for L-type blockade $p < 0.001$, for N-type blockade $p < 0.001$ and for R-type blockade $p = 0.15$). Therefore blockade of calcium channels enhances persistent activity induction via the secondary reduction of the slow after hyperpolarization current.



For the mechanisms that affected persistent activity induction, we conducted a second set of experiments aiming to dissect the effects of dendritic versus somatic manipulations by altering their conductance values (multiplying with a factor of 0.2 to 2, with a step of 0.2) separately at the dendrites and the soma (Figure 4.3.8). We found that the h-current had a small effect on persistent activity only when conductance manipulations were done in the dendrites (Figure 4.3.8A diamonds), with the probability being proportional to the conductance. For IsAHP and the D-type K⁺ currents (ID) somatic conductances had a prominent, inversely proportional effect on the induction probability (Figure 4.3.8B squares and triangles). For IsAHP, this effect was scaled down when manipulations took place in the dendrites (Figure 4.3.8.A red

squares) while the opposite was true for ID (Figure 4.3.8A green triangles). Since both currents are potassium currents with slowly inactivating characteristics that contribute to prolonged membrane hyperpolarization, the different contributions seen for dendritic manipulations can be explained by the different distribution patterns of these channels: fewer sAHP channels are present in the dendrites whereas D-type channels increase in these regions, compared to their cell body values (Korngreen and Sakmann, 2000).

Similar to the I_{sAHP} , somatic VGCCs have a more prominent effect of the induction probability than the respective dendritic currents (Figure 4.3.8C, D). Again, induction probability is inversely proportional to the conductance values of these channels, presumably via the secondary activation of sAHP (Figure 4.3.7C). Changes in dendritic conductances of VGCC have more subtle effects. The N-type calcium current does not affect the induction probability, whereas the effect of L-type calcium current is greatly scaled down but with the same trend as the respective somatic conductance. The R-type calcium current however has opposite effects, depending on its somatic or dendritic localization: dendritic modifications are proportional while somatic modifications are inversely proportional to the induction probability. The possible



explanation for this observation is that R-type calcium channels contribute to bursting when located in the dendrites (Pissadaki et al., 2010; Takahashi and Magee, 2009) and to AHP when located at the soma. Thus, increasing R-type channel currents in the dendrites enhances local depolarization and perhaps contributes to dendritic spike generation, whereas increasing it in the soma does not contribute to dendritic events (Figure 4.3.8C, D).

Most importantly, our model predicts that location dependent manipulations of VGCCs and the sAHP conductances differentially influence signal integration and persistent firing.

4.4 Discussion

In this section we used the detailed in terms of biophysical mechanisms model of a layer 5 PFC microcircuit. The model was extensively constrained by experimental data (Angulo et al., 1999; Bacci et al., 2003; Buhl et al., 1997; Dombrowski et al., 2001; Durstewitz and Gabriel, 2007; Kawaguchi and Kubota, 1993; Van der Loos et al., 1972; Markram, 1997; Markram et al., 1997; Nasif et al., 2005; Sidiropoulou et al., 2009; Tamás et al., 1997a, 1997b; Thomson and Lamy, 2007; Wang et al., 2008; Woo et al., 2007) casting it as a faithful representation of a biologically realistic PFC microcircuit with morphologically simplified neurons. The model conclusively shows that the expression and modulation of persistent activity can be supported by small-sized clusters of cells (microcircuits), even though previous studies have suggested otherwise (Compte, 2006; Compte et al., 2000).

Indeed, computational studies investigating network properties have become more elaborate over the years, incorporating physiological intrinsic and synaptic currents in neurons as well as their connectivity properties in order to elucidate the functional advantages of cortical microcircuits (Haeusler and Maass, 2007; Litwin-Kumar and Doiron, 2012; Reimann et al., 2013; Sarid et al., 2007). This model network supports synaptically-induced persistent activity, which is tunable by changes in several intrinsic ionic conductances, namely the CAN current that underlies the dADP, the h-current, the I_{SAHP} and the R-type calcium current, uncovering a new role or providing further supporting evidence for these mechanisms that can be tested experimentally. Our work suggests that these microcircuits may serve as the anatomical substrate for the expression and tunable modulation of persistent activity, thus conferring a flexible short term memory system.

4.4.1 Minimal anatomical substrate of persistent activity

Most studies have suggested that intact large networks of neurons are necessary for induction and maintenance of persistent activity. This statement has been supported by the fact that persistent activity is primarily observed *in vivo*, while its generation in brain slices comes in the form of Up-and-Down states (McCormick, 2003). In single, isolated neurons persistent activity can only be induced in the presence of neuromodulators that activate the CAN current and generate dADP

(Egorov et al., 2002; Sidiropoulou and Poirazi, 2012; Sidiropoulou et al., 2009). Here, we constructed what recent experimental data claim to be the minimal functional neuronal network in the cortex and found that this network can support persistent activity in the absence of neuromodulators that activate the CAN current, but with enhanced NMDA conductance. In agreement with our predictions, small assemblies of neurons have also been reported to support persistent spiking activity in hippocampal cultures (Lau and Bi, 2005). Therefore, it is likely that the neuronal clusters shown to exist *in vivo* (Feldt et al., 2011; Ko et al., 2011; Seung, 2009; Yassin et al., 2010) represent the minimum anatomical substrate for the emergence of stimulus-induced persistent activity.

One prediction of our study is that stimulus-induced persistent activity can possibly be generated in brain slices, assuming that these network structures remain intact. Therefore, the absence of persistent activity firing in brain slices could reflect an anatomical compromise of these networks, such as cut dendrites due to the different planes that dendrites extend to in the prefrontal cortex (Day et al., 2005). The anatomical (Fiala et al., 2003) or synaptic (Gundersen et al., 1995; Kuenzi et al., 2000) changes that occur after slicing can potentially affect the normal physiological mechanisms needed for persistent activity to be generated, such as dendritic non-linear events. We propose that appropriate *in vitro* experiments in organotypic cultures of the prefrontal cortex alone, as has already been done with co-cultures of the prefrontal cortex, the ventral tegmental area (VTA), the hippocampus or the basal forebrain (Seamans, 2003), where a high degree of connectivity is reestablished, will elucidate the necessary neural substrate for persistent activity emergence in the PFC.

4.4.2 Pairing excitation to inhibition

Although many studies have proposed balanced excitation/inhibition to promote and stabilize persistent activity (Compte, 2006) and the NMDA current as the most widely accepted source of excitation, inhibitory effects remain under-characterized. In the entorhinal cortex, GABA_A currents are imperative for the stabilization of Up states, while GABA_B currents mediate the transition to the Down state (Mann et al., 2009). A recent simulation study has also shown that the NMDA/GABA_B currents are the perfect couple for the emergence of bistability: NMDA

promotes Up states, and the GABA_B current underlies the Down state (Sanders et al., 2013). Our work addresses for the first time the role of the GABA_B current in the generation of a strongly related phenomenon, namely persistent activity. Although this current has a slow time course, we show that it can gate the induction of persistent activity (without diminishing it in the range tested), a prediction that can be experimentally tested.

4.4.3 (No) Stimulus coding

We found little evidence for stimulus coding in the microcircuit model. We showed that prolonging the duration of the input enhances the probability of induction, a result that is in agreement with findings in the entorhinal cortex (Tahvildari et al., 2007). On the other hand, varying the firing frequency or the duration of the input does not consistently affect persistent firing properties. However, changes in the dADP, NMDA and GABA_B currents affect the temporal (ISI distribution) firing characteristics of persistent activity, suggesting that modulation of these mechanisms, e.g. by dopamine (Galloway et al., 2008; Seamans and Yang, 2004), may allow the selective tuning of different microcircuits, enabling the appearance of multiple, semi-independent processing modules, each with its own activity dynamics. Stimulus coding observed *in vivo* (Romo et al., 1999) could in turn result from the crosstalk of multiple microcircuits, and therefore, comprise a property of a larger neuronal network and not of a small cluster of neurons.

4.4.4 Role of Intrinsic Mechanisms

It is well known that the dADP contributes to persistent firing induction and maintenance, primarily at the single neuron level (Egorov et al., 2002; Sidiropoulou and Poirazi, 2012; Sidiropoulou et al., 2009). This long lasting depolarized state of neurons is evoked by stimulation of Gq-coupled receptors (mGluRs, muscarine Ach, 5-HT receptors) (Zhang et al., 2013) that results in the activation of the IP3 pathway and release of Ca⁺⁺ ions from the endoplasmic reticulum (Fowler et al., 2007). Elevation of the intracellular Ca⁺⁺ concentration activates the I_{CAN} (Haj-Dahmane and Andrade, 1998), mediated by the transient receptors potential channels (TRPCs) of both the prefrontal and entorhinal neurons (Fowler et al., 2007; Zhang et al., 2011). In the PFC

microcircuit model used here, persistent firing was induced in the absence of CAN current but required enhanced levels of NMDA receptor activation. Activating the CAN current allowed for persistent activity generation at lower, but not all NMDA-to-AMPA ratios, a similar finding observed in large-scale simplified networks (Tegnér et al., 2002). In addition, increasing the dADP values (within the normal physiological range) increased the firing frequency of persistent activity in agreement with earlier findings (Egorov et al., 2002). In sum, our results show that the dADP mechanism regulates the expression and properties of the persistent state in the microcircuit model.

The role of I_h in persistent activity in the microcircuit model is location-dependent: its reduction in the dendrites -but not the soma- lowers the induction probability. These findings are in agreement with some but not all experimental studies in the PFC, where the contribution of I_h to persistent firing remains unclear. In L5 PFC pyramidal neurons, the effect of the I_h is cell-type specific: CPn neurons (see 1.3 section) that are characterized of complex apical morphology, also display characteristic voltage sag and rebound depolarization in response to hyperpolarization (indicating high contribution of the I_h). These neurons express persistent activity in response to muscarinic-receptor activation with higher probability compared to COM neurons (that have lower levels of I_h) and support the generation of depolarizing plateau potential following activation of dopamine D2 receptors (Dembrow et al., 2010; Gee et al., 2012). Note that activation of noradrenergic, cholinergic and mGluR I receptors that induce dADP also reduce the I_h current (Dembrow et al., 2010; Kalmbach et al., 2013). In addition, data from the Arnsten laboratory have shown that an increase in dendritic I_h following $\alpha 2A$ activation, decreases the contribution of a specific synaptic input to persistent firing, thus eliminating noise or distractors, while inhibiting I_h promotes persistent firing (Wang et al., 2007).

On the other hand, I_h has been shown to directly participate in persistent firing induction in a subset of neurons sampled from both supragranular and infragranular layers by promoting graded firing (Winograd et al., 2008). In accordance, the most recent report of the role of the I_h in L5 PFC pyramidal neurons shows that deletion of the HCN1 channels reduces the probability of persistent activity induction and impairs performance in working memory related tasks. The proposed by the authors

underlying mechanism of this effect of the I_h current is the shifting the membrane potential to more depolarizing values and thus influences the ability of other conductances to promote persistent activity (Thuault et al., 2013). Our data are in-line with the latter studies since reduction of dendritic I_h lowers the induction probability. Further more elaborate experimental and/or computational studies will be required to resolve or clarify the role of I_h in persistent activity states.

D-type potassium channels also had a major effect on persistent activity: blockade of these channels either at the dendrites or the soma greatly enhanced the probability for persistent activity emergence. This result is primarily attributed to the long-lasting negative regulation of excitability exerted by I_D on pyramidal model neurons, which counteracts the currents that support persistent firing (Yang et al., 1996). Interestingly, this current is selectively suppressed under dopamine application in PFC slices, through activation of D1 receptors (Dong and White, 2003), supporting the predicted need for controlling its value in order to allow the emergence of persistent activity.

Reducing the I_{sAHP} enhances the induction probability, particularly when blocked at the soma, thus indicating that attenuation of synaptic transmission also has a gating effect on synaptic persistent activity initiation. This is in line with earlier work where dendritic SK channel activation decreases excitatory synaptic transmission (Faber, 2010), dopamine-mediated reduction of the sAHP increases synaptic gain *in vitro* (Thurley et al., 2008) and blockade of SK channels improves working memory *in vivo* (Brennan et al., 2008).

Blockade of voltage gated calcium channels in our model reduced both the fast and slow AHP, in agreement with experimental data (Faber, 2010; Hagenston et al., 2008; Sun et al., 2003). On the contrary, increasing calcium channel conductance at the soma, where the effect of I_{sAHP} is more prominent, increased the sAHP and decreased the induction probability. Dendritic modulation of VGCCs on the other hand had a more complex and type-specific effect. This may be attributed to the fact that dendritic intracellular calcium modulates both hyperpolarization and depolarization in these neurons: increase in dendritic, as opposed to somatic, calcium concentration is correlated with small amplitude of somatic hyperpolarization or even failure to activate SK channels (Hagenston et al., 2008). In addition, dendritic voltage and

calcium depolarizing plateaus at the basal dendrites of L5 prefrontal pyramidal neurons are due to the activation of NMDA receptors and in great part insensitive to blockade of voltage gated calcium channels (Milojkovic et al., 2007). In accordance, our results show that dendritic blockade of N calcium channels does not affect persistent activity initiation and of L type only slightly reduces excitability, similarly to the I_{SAHP} effect. Note that the dADP is inactivated in this part of the study. It is possible that in the presence of the dADP the effect of calcium currents may be different (Gee et al., 2012; Sidiropoulou et al., 2009).

On the other hand, enhancement of the dendritic conductance of R-type calcium channels facilitated persistent activity. R-type calcium channels are known to promote bursting in hippocampal neurons (Metz et al., 2005) and possibly PFC pyramidal neurons (Sidiropoulou and Poirazi, 2012). Due to the absence of a specific blocker of these channels, their study is greatly hampered. In our study, we have uncovered a novel role of R-type calcium channels, and particularly dendritic R-type channels, that of facilitating persistent activity, that can possibly be examined experimentally.

Overall, we predict an important role for several diverse intrinsic mechanisms in both gating and modulating the probability of persistent activity emergence, which in most cases is at least indirectly supported by experimental findings. Specifically, our study reinforces the significant role of I_h in persistent firing, which should be examined further experimentally, while for the first time the D-type K current, the I_{SAHP} and the R-type calcium current are linked at the cellular level with modulating persistent activity emergence.

5 Dendritic nonlinearities reduce size requirements and mediate ON and OFF states of persistent activity in a PFC microcircuit model

5.1 Preamble

Having established that L5 PFC microcircuit models can serve as tunable modules of persistent activity shaped by the intrinsic make-up of active ion channels along the somato-dendritic compartments, several extensions to the basic idea deserved further consideration. One such idea is to thoroughly investigate the effect of network size effect on persistent activity emergence. As mentioned, in earlier studies the structure and size of the network studied varied greatly, from a couple of cells with unrealistic connectivity properties (e.g. long conduction delays) (Gutkin et al., 2001) to networks of hundreds to thousands of neurons (*in silico*) (Compte, 2006; Compte et al., 2000). As a result, the minimum size of a network capable of expressing persistent activity under physiological conditions remains debatable, yet critical for understanding the mechanisms underlying its induction (Lau and Bi, 2005). We showed in the previous section (Section 4.3.1) that when a basic microcircuit

consisting of 7 pyramidal neurons and 2 inhibitory interneurons is stimulated and the ratio of iNMDA/iAMPA is 2.3, then persistent activity is induced with a probability of 86%. What will happen if the number of pyramidal neurons in the network is reduced or increased? Will the probability of induction increase or decrease?

Like network size, the role of dendritic nonlinearities in persistent activity emergence is also ambiguous. We showed that the NMDA current, that provides slow excitation, is imperative for the initiation of persistent activity, in accordance with the *in vivo* data (Wang et al., 2013). Also we showed that increased CAN current supports persistent activity induction, but for iNMDA-to-iAMPA ratio 1.1 (Section 4.3.3). How does the activation of the NMDA receptors contribute to persistent firing? Is this due to slow excitation that temporally binds together synaptic events, or more specialized mechanisms are needed, such as dendritic regenerative events?

Finally, little is known about how key characteristic features of PFC persistent activity like resistance to distracters and termination induced by behavioral actions (Miller, 2000) can be implemented by neuronal tissue. The only candidate mechanism for termination is inhibitory input which was shown to cease Up states in the entorhinal cortex (Mann et al., 2009). Regarding stimulus-specificity, Sidiropoulou and Poirazi, 2012 used a computational model of a single L5 PFC pyramidal neuron to show that location of activated synapses along the basal dendrites and action potential timing could serve as encoding and decoding mechanisms, respectively, of stimulus-selective induction (Sidiropoulou and Poirazi, 2012). Identifying such information in the response pattern of these neurons is particularly important as it may signal the upcoming state transitions to downstream neurons, setting the ground for the subsequent behaviour actions. However, whether such mechanisms are also relevant at the network level or whether other mechanisms are implicated is not known.

In this section, we use the same microcircuit model to investigate the mechanisms that underlie persistent activity emergence (ON) and termination (OFF) at the dendritic, neuronal and network levels and search for the minimum network size required for expressing these states within physiological regimes. Moreover, we search for mechanisms that may underlie persistent activity maintenance upon presentation of distracting stimuli and identify network characteristics that code for the upcoming state transitions.

5.2 Materials and Methods

Model microcircuit was as before. In addition, a linear Support Vector Machine (SVM) classifier was used to examine whether certain features of the microcircuit responses (network activity features, single cell response properties and synaptic currents) could predict state transitions.

Features: The input features used to train and test the linear SVM classifier were: (a) single neuron inter-spike intervals (ISIs) and number of spikes during stimulus presentation, (b) the number of spikes from all the pyramidal neurons during stimulus presentation, (c) synaptic currents (i_{AMPA} , i_{NMDA} , i_{GABA_A} , i_{GABA_B}) measured at a single neuron by summing its synaptic current traces and (d) ratio of excitatory ($i_{\text{AMPA}} + i_{\text{NMDA}}$) transmission to inhibitory transmission ($i_{\text{GABA}_A} + i_{\text{GABA}_B}$). Since traces were acquired with a sampling frequency of 10kHz (simulation time step 0.1ms), synaptic currents were processed using the Chebyshev Type I low pass filters in Matlab resulting in a sampling frequency of 100Hz ($dt = 10\text{ms}$). The i_{NMDA} and i_{GABA_B} traces were also processed with a low-pass Butterworth filter to eliminate fast fluctuations in order to unravel the potential impact of the slow kinetics of these currents. Both filtered and unfiltered versions of NMDA and GABA_B currents were used as discriminator parameters.

Classification: To classify each feature matrix, a random training and test set were initially selected. The training set consisted of 100 (50 'persistent' and 50 'no persistent') trials. The linear SVM was then used to predict the classification of the blind test set of 30 (15 'persistent' and 15 'no persistent') trials. This procedure was repeated 20 times by picking randomly different training and test sets. We calculated the average prediction accuracy (number of correctly predicted trials over the 20 repetitions), the sensitivity (number of correctly predicted 'persistent' trials over the total number of 'persistent' trials) and the specificity (number of correctly predicted 'no persistent' trials over the total number of 'no persistent' trials) and the standard error for each prediction. The performance threshold was set to 70% (for both sensitivity and specificity) on the test set.

5.3 Results

5.3.1 Network size vs. network connectivity

To investigate the effect of network size on persistent activity emergence, we varied the number of pyramidal neurons in the microcircuit and recorded the result of this manipulation on the probability of induction. We found that reducing the number of pyramidal neurons from 7 to 5 completely abolished persistent activity, whereas adding more neurons increased the probability of induction to 100% (Figure 5.3.1A, diamonds). The latter could be due to stronger synaptic drive within the network (a connectivity effect) or due to having more neurons that propagate signals (a size effect). To discriminate between these two possibilities, we varied the network size while keeping the number of recurrent connections per neuron fixed to that of a size 7 network (31 synapses per neuron: 6 x 5 pyramidal-to-pyramidal inputs plus 1 autapse). Persistent activity emerged in all cases tested (Figure 5.3.1A, squares), even in a microcircuit of size 2. On the contrary, changing the synaptic drive of each neuron (in a network of size 7) had a strong effect: reducing the pyramidal-to-pyramidal synaptic contacts by 20%, from 5 to 4 (total inputs per neuron: from 31 to 25) abolished persistent activity, whereas the respective increase in connections from 5 to 6 (total inputs per neuron: from 31 to 37) led to 100% probability of induction (Figure 5.3.1B, diamonds). Varying the connectivity strength between pyramidal and

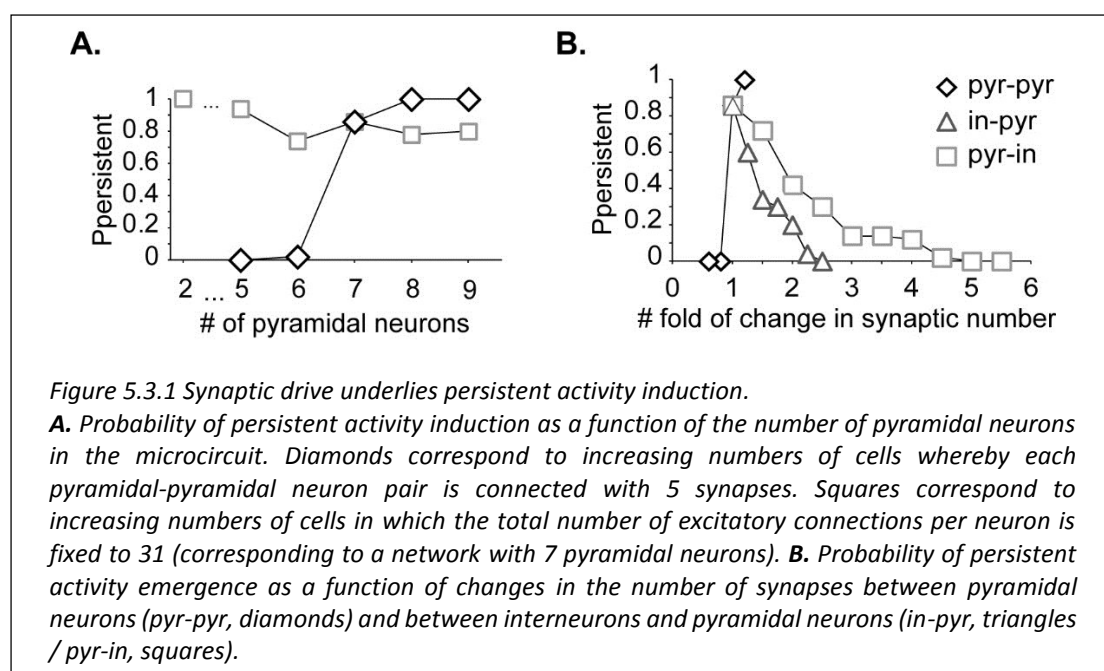


Figure 5.3.1 Synaptic drive underlies persistent activity induction.

A. Probability of persistent activity induction as a function of the number of pyramidal neurons in the microcircuit. Diamonds correspond to increasing numbers of cells whereby each pyramidal-pyramidal neuron pair is connected with 5 synapses. Squares correspond to increasing numbers of cells in which the total number of excitatory connections per neuron is fixed to 31 (corresponding to a network with 7 pyramidal neurons). **B.** Probability of persistent activity emergence as a function of changes in the number of synapses between pyramidal neurons (pyr-pyr, diamonds) and between interneurons and pyramidal neurons (in-pyr, triangles / pyr-in, squares).

interneurons had less pronounced effects: persistent activity could emerge even when the pyramidal-to-interneuron connections tripled (Figure 5.3.1B, squares) or the interneuron-to-pyramidal connections doubled (Figure 5.3.1B, triangles). These results suggest that the strength of excitatory-to-excitatory transmission, as opposed to the network size, is the crucial factor for persistent activity induction in the microcircuit.

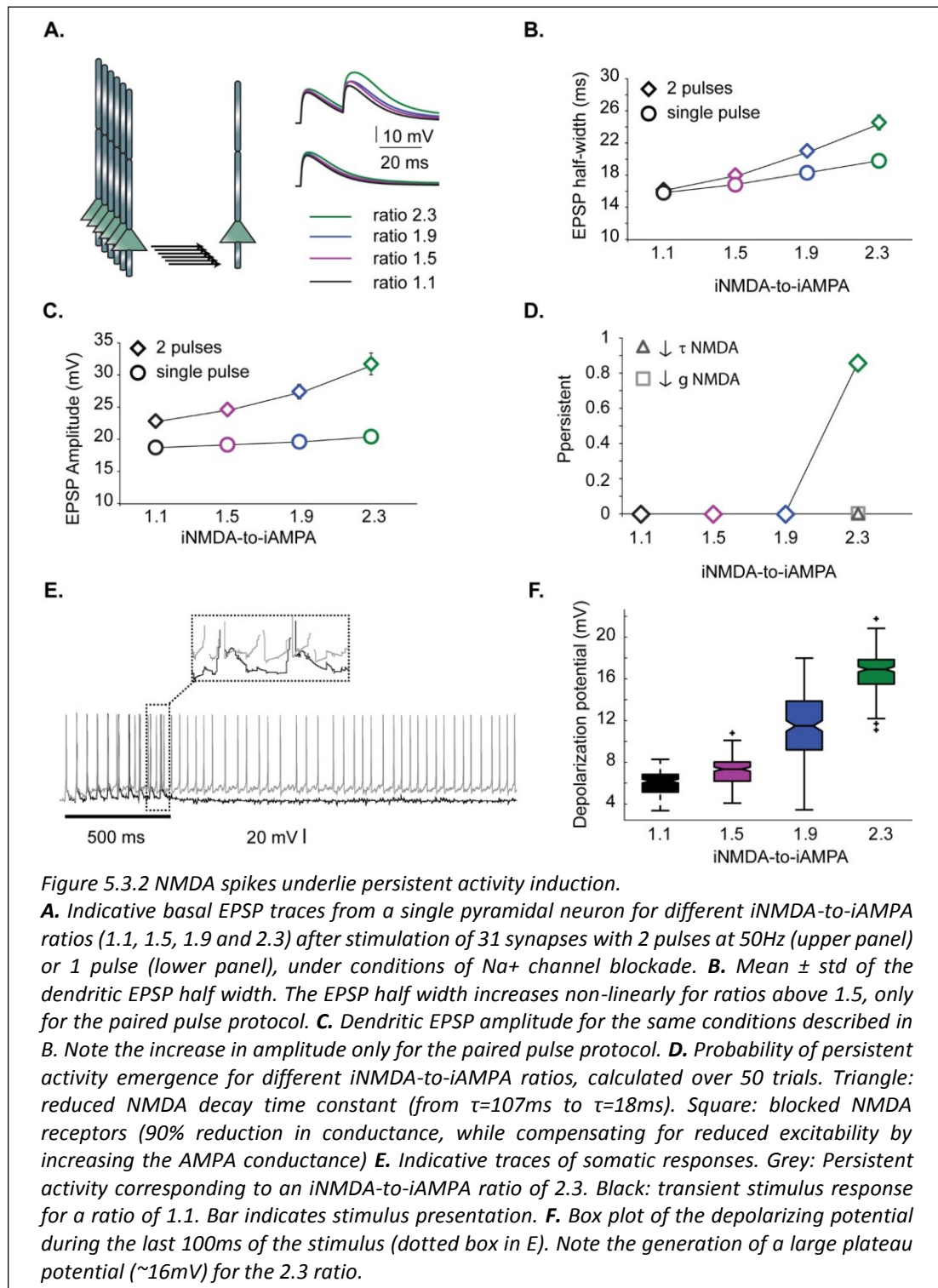
5.3.2 Network size vs. NMDA spikes

Given that excitatory-to-excitatory transmission is crucial for induction and NMDA receptors play a key role in shaping excitatory synaptic transmission in L5 PFC pyramidal neurons (Chalifoux and Carter, 2011; Wang et al., 2008), we next examine their contribution to the size *versus* synaptic drive argument. Activation of NMDA receptors was recently found to be imperative for persistent activity emergence *in vivo* (Wang et al., 2013) and the generation of Up-states in acute slices (Oikonomou et al., 2012; Shu et al., 2003; Tseng and O'Donnell, 2005). Since both of these phenomena are characterized by long-lasting depolarizations, it can be assumed that the role of NMDA currents is to provide or sustain these depolarizations through regenerative dendritic events such as NMDA spikes (Chalifoux and Carter, 2011). We thus investigate whether and how the generation of NMDA spikes may influence persistent activity induction in the microcircuit model.

We first assessed whether NMDA spikes are inducible in our pyramidal neuron models using the four different iNMDA-to-iAMPA ratios: 1.1, 1.5, 1.9, and 2.3. In all cases, only the NMDA current increased and the ratios were calculated under voltage clamp conditions (Figure 3.3.1A). Representative traces resulting from the activation of 31 synapses (2 pulses at 50 Hz: diamonds or 1 pulse: squares) in the basal dendrite of a pyramidal neuron model, under blockade of Na⁺ channels are shown in Figure 5.3.2A. The dendritic EPSP half width and amplitude are shown in Figure 5.3.2B and Figure 5.3.2C, respectively. An enhancement of EPSP amplitude, reminiscent of NMDA spike generation (Chalifoux and Carter, 2011), was seen only for a ratio of 2.3 and a

double –but not single- pulse stimulation, suggesting that ratios 1.1-1.9 do not support NMDA spikes after stimulation with 2 pulses at 50 Hz.

Emergence of persistent activity was strongly correlated with the generation of NMDA spikes. As shown in Figure 5.3.2D, lack of NMDA spikes (ratio 1.1-1.9) was associated with zero probability of persistent activity whereas generation of large NMDA spikes (2.3 ratio) was associated with an induction probability of 86%.



Importantly, reducing the NMDA decay time constant (from $\tau=107\text{ms}$ to $\tau=18\text{ms}$, Figure 5.3.2D, triangle) or blocking the NMDA receptors (90% reduction in conductance, while compensating for reduced excitability by increasing the AMPA conductance) under conditions that normally supported persistent activity (Figure 5.3.2D, square) also abolished the persistent state.

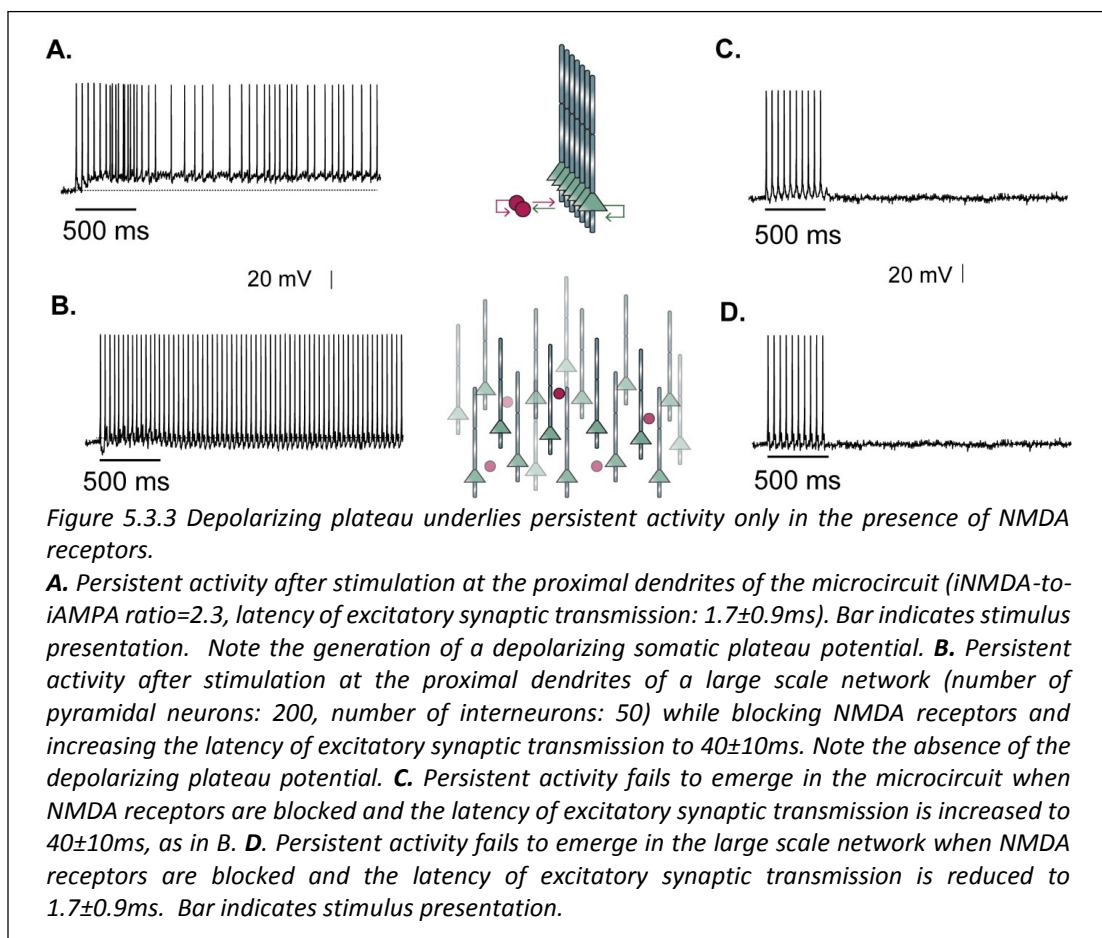
To test whether NMDA spikes provide long-lasting somatic depolarizations on top of which persistent activity can ride, we measured the somatic depolarization of a pyramidal neuron model during the last 100ms of stimulus presentation (Figure 5.3.2E, dotted box) for the four different ratios. Generation of NMDA spikes for a ratio of 2.3 induced, on average (calculated over 50 trials), a large plateau potential ($\sim 16\text{mV}$) at the soma; smaller plateaus were seen for ratios of 1.1-1.9 (Figure 5.3.2F). This depolarized state, which is not seen for small ratios, is proposed to underlie the persistent spiking activity. Representative traces for the two cases are shown in Figure 5.3.2E (black trace: ratio 1.1, grey trace: ratio 2.3). To further investigate this hypothesis we asked whether the 100ms depolarizing potential is also different between trials that led to persistent firing *versus* trials that didn't, this time for a fixed NMDA-to-AMPA ratio. Indeed, for a ratio of 2.3, this plateau potential was significantly larger in the persistent compared to the transient response trials (p value <0.001) (Figure 5.3.6A). In sum, our simulations predict that dendritic nonlinearities alone, through the generation of NMDA spikes and a subsequent built up of somatic depolarization, act as a switch for entering a sustained firing state in PFC microcircuits.

5.3.3 NMDA is critical for small but not large scale networks

The predicted dependence on NMDA dendritic spikes may seem contradictory to previous work, whereby both large- (Compte et al., 2000) and small- scale neuronal network models (Gutkin et al., 2001) without NMDA receptors supported persistent activity. However, those models were not biophysically constrained in several aspects, including their connectivity properties. Moreover, blockade of NMDA receptors in the PFC was shown to abolish prolonged spiking activity (McCormick, 2003; Wang et al., 2013), suggesting that this dependence may be a region-specific effect. To further investigate this issue, we simulated a large scale network of fully connected 250 neurons (200 pyramidal and 50 interneurons) whereby NMDA and GABA_B receptors

were completely blocked (as in earlier reports) and constrains regarding synaptic delays between pyramidal neurons were relaxed (delays for excitatory-to-excitatory connections were drawn from a Gaussian distribution with $\mu = 40\text{ms}$ and $\sigma = 10\text{ms}$). We found that the resulting asynchronicity in conjunction with the much larger size of the network were sufficient for persistent activity to emerge (Figure 5.3.3B) with high probability (90%), in agreement with earlier work (Gutkin et al., 2001).

Note the elimination of the somatic plateau potential during persistent firing generated in our large-scale networks (Figure 5.3.3B) compared to the microcircuit (Figure 5.3.3A). To test whether asynchronicity produced by long conduction delays was sufficient to replace NMDA-induced depolarizations, we blocked NMDA receptors in the microcircuit model and allowed for conduction delays similar to the ones used in Figure 5.3.3B. In this case, no persistent activity could be induced in any of the trials tested (Figure 5.3.3C). Similarly, we asked if reverberating activity in a large scale network with short conduction delays (similar to the ones used in the microcircuit) could support persistent firing under NMDA blockade (Figure 5.3.3D) and again failed to see sustained responses. Taken together, these findings suggest that in small



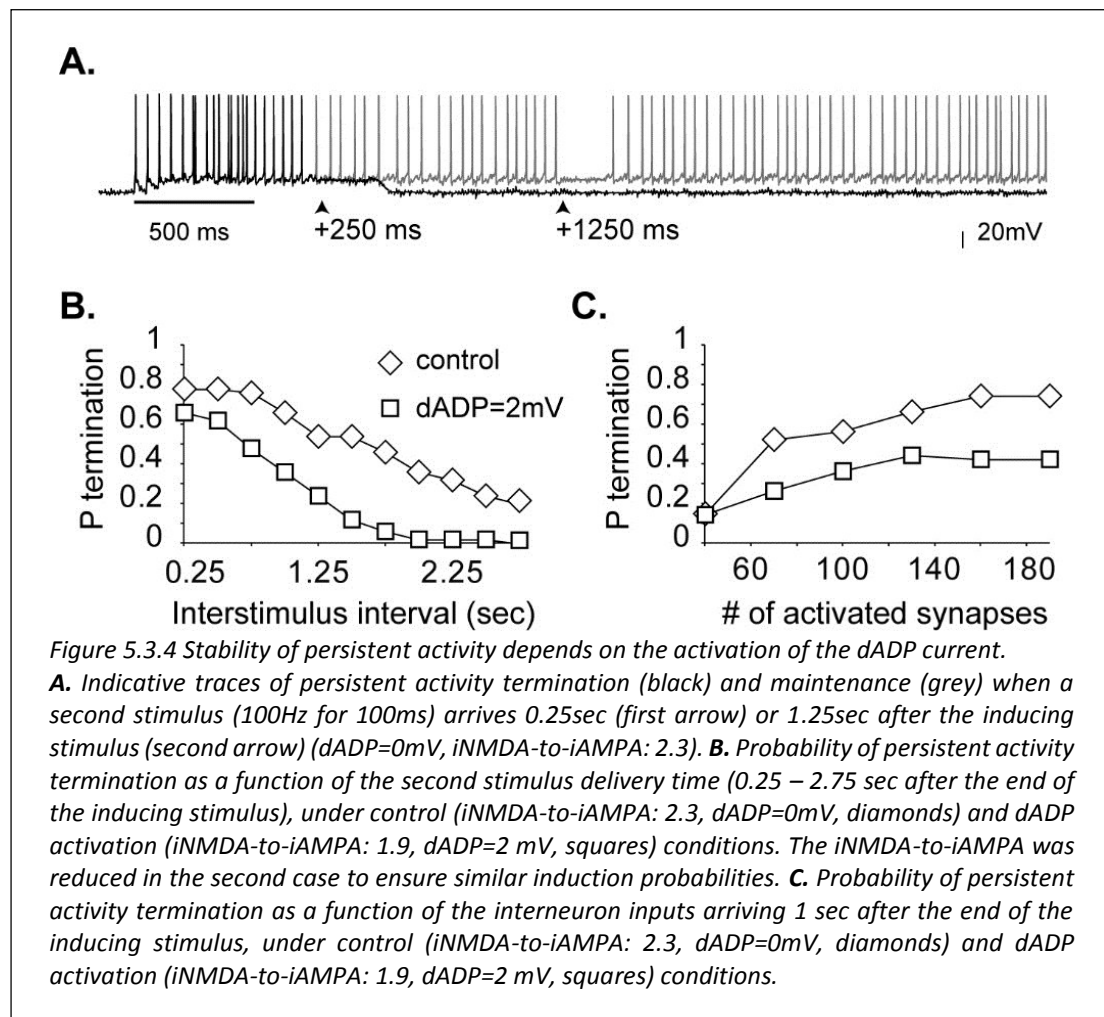
biophysically constrained PFC microcircuits, where conduction delays are short, NMDA receptors are necessary for persistent activity induction. This necessity disappears in large scale networks whereby long conduction delays in conjunction with multiple reverberating connections are sufficient to bridge depolarisations over time, thus prolonging spiking.

5.3.4 Persistent activity termination is strength, time and dADP dependent

Persistent activity recorded during working memory terminates normally upon the execution of motor actions (Funahashi et al., 1989) or prematurely as a result of distracting stimuli, in which case performance drops significantly (Miller et al., 1996). However, the mechanisms underlying persistent activity termination remain unclear. Inhibition is currently the primary candidate as it has been found that Up states, a condition similar to persistent firing, are terminated by activation of interneurons (Mann et al., 2009). Since PFC interneurons receive feed forward excitation during working memory tasks (Diester and Nieder, 2008; Kuroda et al., 1998), we investigated their role in persistent activity termination. Delivery of a second excitatory stimulus (100 synapses activated with 10 events at 100 Hz) to the interneuron models at variable time points showed that termination is most probable if the second stimulus arrives at least 250ms after persistent activity emergence. Representative traces for delivery times of 250ms and 1250ms are shown in Figure 5.3.4A. Increasing the delivery time from 0.25 to 2.75 seconds (while maintaining the same stimulus strength), resulted in a gradual decrease in the probability of persistent activity termination (Figure 5.3.4B, diamonds). These findings suggest that inhibition is more effective in terminating the persistent state if it is activated soon after induction.

Interestingly, cessation was strongly modulated by the dADP mechanism, which has thus far been implicated with the emergence of persistent firing (Sidiropoulou and Poirazi, 2012; Sidiropoulou et al., 2009). Specifically, we showed that dADP activation (2mV) led to a significant decrease (~26%) in the termination probability for all delivery times (Figure 5.3.4B, squares). Since the dADP primarily emerges following acetylcholine or glutamate action and is modulated by dopamine (Sidiropoulou et al., 2009), our data suggest that neuromodulatory effects are likely to have a key role in the maintenance of persistent firing.

In a second set of experiments we kept the inter-stimulus interval fixed at 1 second and varied the number of activated synapses (Figure 5.3.4C). As expected, stronger inhibitory stimuli facilitated termination (Figure 5.3.4C, diamonds), before reaching ceiling and this facilitation was reduced in the presence of dADP (Figure 5.3.4C, squares). These results show that termination of persistent activity by a second stimulus delivered to the inhibitory neurons depends on the strength and timing of the input and is negatively modulated by dADP activation.



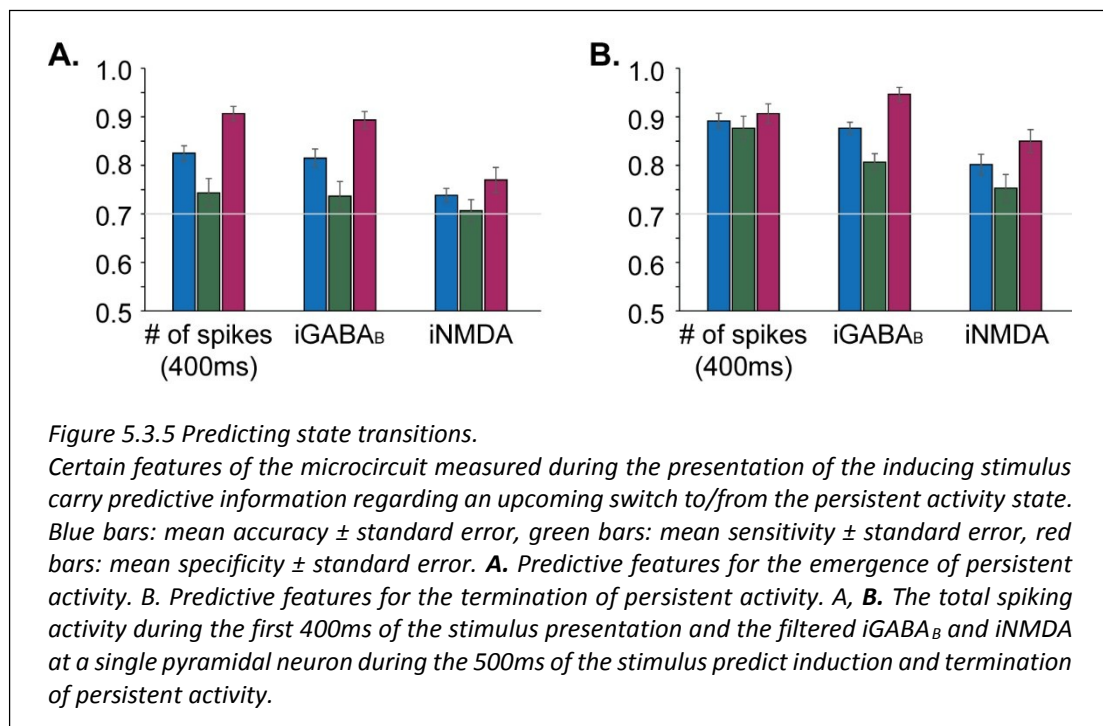
5.3.5 Predicting state transitions

Previous work from Poirazi's lab showed that the stimulus-induced response of a single L5 PFC pyramidal neuron model codes for an upcoming transition to a persistent state (Sidiropoulou and Poirazi, 2012). We thus tested whether this type of coding is preserved at the microcircuit level. Specifically, we asked whether the response of the microcircuit during stimulus presentation contained predictive

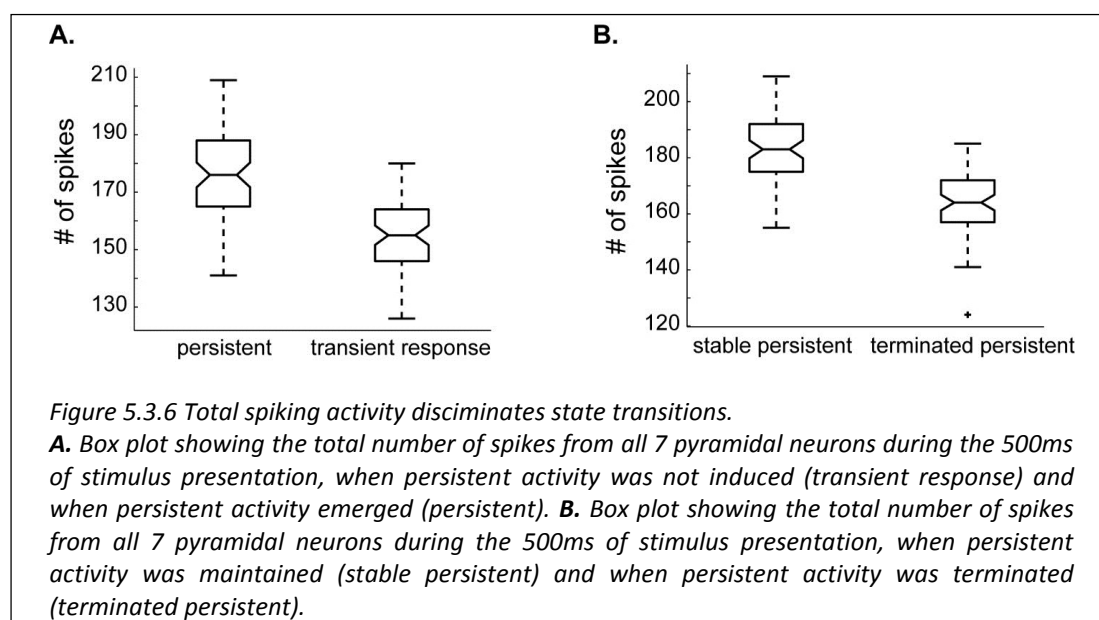
information regarding both the induction and the termination of the persistent state. Termination was caused by a second stimulus delivered to the interneurons 1 sec after the inducing stimulus (100 synapses activated with 10 events at 100Hz). Induction and termination were evaluated under control conditions over 500 and 423 trials, respectively.

We used a linear SVM classifier (see Methods for details) to identify features of the stimulus-induced response that can serve as predictive markers for the microcircuit output. The examined features included measures of a) network spiking activity, b) single-cell spiking activity and c) single-cell synaptic currents. For each feature tested, the SVM was trained with 100 trials (training set) exhibiting the desired phenotypes (i.e. persistent activity *versus* transient response or terminated *versus* stable persistent activity) and prediction accuracy, sensitivity and specificity were estimated on a set of 30 previously unseen trials (test set). In all cases, a strict threshold of 70% sensitivity and specificity was used for the identification of informative features.

We started by testing whether the first few ISIs of the pyramidal neuron responses could predict state transitions, as dictated by previous work in a single PFC model cell (Sidiropoulou and Poirazi, 2012). This was not the case for the microcircuit model. A possible explanation is the lack of a detailed dendritic morphology for



pyramidal neurons, which could account for different responses generated by location specific inputs, as previously argued (Sidiropoulou and Poirazi, 2012). However, we found that both the induction and the termination of persistent activity could be accurately predicted by the total number of spikes from all pyramidal neurons measured over the first 400ms of the stimulus presentation. This feature predicted persistent activity emergence with an accuracy of $83\pm 7\%$ (Figure 5.3.5A) and termination with an accuracy of $89\pm 6\%$ (Figure 5.3.5B), respectively. In both cases, the total number of pyramidal neuron spikes during stimulus presentation was higher for the persistent *versus* transient (p value <0.001 , Figure 5.3.6A) and stable *versus* terminated states (Figure 5.3.6B), respectively.



We also examined the predictive power of synaptic currents measured at a single pyramidal neuron. We found that both NMDA-mediated slow excitation and GABA_B-mediated slow inhibition coded for upcoming state transitions. Specifically, the iGABA_B during stimulus presentation predicted induction and termination with an accuracy of $82\pm 8\%$ (Figure 5.3.5A) and $88\pm 5\%$ (Figure 5.3.5B), respectively. Although counterintuitive, the total GABA_B current was significantly larger in persistent than transient response trials (p value <0.001 , non-parametric parametric U test, Figure 5.3.7C). The same was true for stable compared to terminated trials (p value <0.001 , non-parametric parametric U test, Figure 5.3.7D). A similar trend was seen for the NMDA current, which predicted induction and termination with accuracies of $74\pm 6\%$ (Figure 5.3.5A) and $80\pm 9\%$ (Figure 5.3.5B), respectively. In

this case, the total NMDA current during stimulus presentation was significantly larger in persistent than transient response trials (p value <0.05 , non-parametric parametric U test, Figure 5.3.7E) but not in stable *versus* terminated trials (p value >0.05 , non-

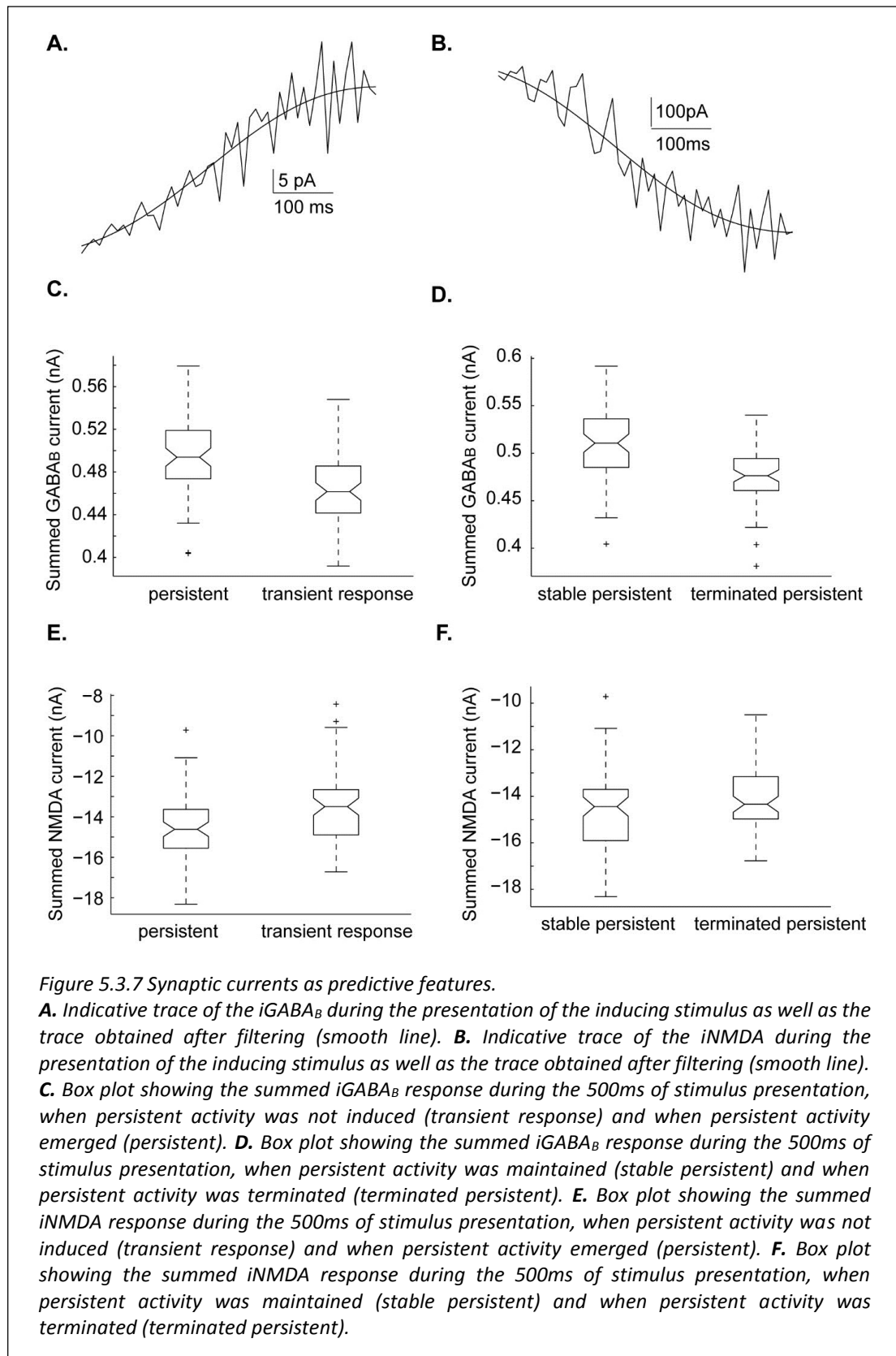
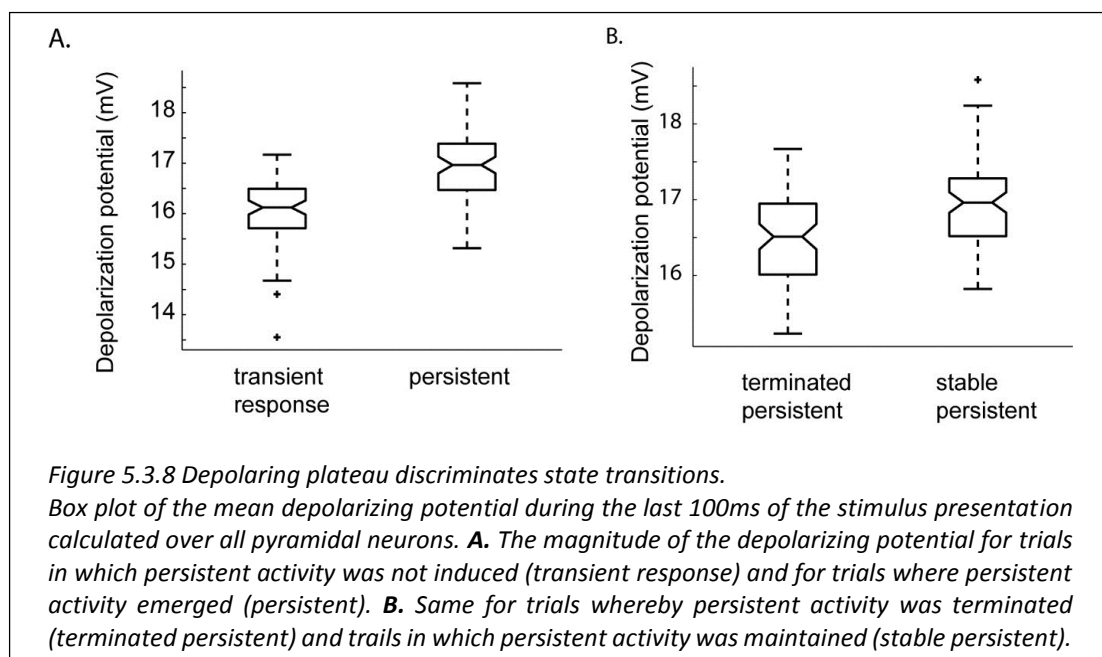


Figure 5.3.7 Synaptic currents as predictive features.

A. Indicative trace of the $iGABA_B$ during the presentation of the inducing stimulus as well as the trace obtained after filtering (smooth line). **B.** Indicative trace of the $iNMDA$ during the presentation of the inducing stimulus as well as the trace obtained after filtering (smooth line). **C.** Box plot showing the summed $iGABA_B$ response during the 500ms of stimulus presentation, when persistent activity was not induced (transient response) and when persistent activity emerged (persistent). **D.** Box plot showing the summed $iGABA_B$ response during the 500ms of stimulus presentation, when persistent activity was maintained (stable persistent) and when persistent activity was terminated (terminated persistent). **E.** Box plot showing the summed $iNMDA$ response during the 500ms of stimulus presentation, when persistent activity was not induced (transient response) and when persistent activity emerged (persistent). **F.** Box plot showing the summed $iNMDA$ response during the 500ms of stimulus presentation, when persistent activity was maintained (stable persistent) and when persistent activity was terminated (terminated persistent).

parametric U test, Figure 5.3.7F). Note that, in order to study the impact of their slow kinetics, the NMDA and GABA_B currents were filtered using a Butterworth low pass filter. Indicative traces before and after the filtering of the NMDA and GABA_B currents are shown in Figure 5.3.7A, B.

The predictive power of NMDA and GABA_B currents during stimulus presentation does not explain *how* these mechanisms determine the induction and termination of persistent activity. We hypothesize that their interactions shape the somatic plateau potential towards the end of the stimulus as described in Figure 5.3.2F. We thus tested whether this plateau potential is significantly different not only between persistent and transient response trials as shown in Figure 5.3.8A, but also between stable and terminated trials. Indeed, the somatic depolarization (measured in the last 100ms of the stimulus presentation) in stable trials was significantly larger than in terminated ones (p value <0.001) (Figure 5.3.8B), suggesting that the magnitude of the somatic membrane depolarization is a determining factor for both the emergence and termination of persistent firing in the PFC microcircuit.



Overall, our findings show that both spiking characteristic of the network activity and slow synaptic currents, presumably through their effect on somatic membrane depolarization, mediate induction as well as termination of persistent activity in the microcircuit model.

5.4 Discussion

In this section we used the biophysical model of a L5 PFC microcircuit to investigate the contributions of dendritic, somatic and network events to persistent activity emergence (ON) and termination (OFF).

5.4.1 NMDA spikes *versus* network properties

Our study predicts that regenerative events occurring in the basal dendrites of PFC pyramidal neurons, in particular NMDA spikes, gate the induction of persistent firing in a biophysically validated PFC microcircuit, but not in large scale neuronal networks with relaxation of biophysical constraints. A number of studies have suggested that NMDA receptors are critical for persistent firing (Lim and Goldman, 2013; Wang, 1999; Wang et al., 2013), however, this study is the first one to provide a direct link between NMDA spike generation in dendrites and the probability of persistent activity induction. These findings concur with a reported association between NMDA spikes and stimulus-specificity at the single neuron level (Sidiropoulou and Poirazi, 2012) and with reports that dendritic NMDA spikes are crucial for the generation of Up-states in L5 PFC pyramidal neurons *in vitro* (Oikonomou et al., 2012).

Furthermore, we find that the minimum network size required for persistent activity induction is inversely proportional to the synaptic drive of each excitatory neuron: if synaptic input is sufficient to induce NMDA spikes, the network can be reduced down to 2 cells. A number of modeling and experimental studies have focused on the effect of network size/synaptic strength/neuronal clustering in the emergence of various physiological phenotypes (Börgers et al., 2012; Lau and Bi, 2005; Litwin-Kumar and Doiron, 2012; Oswald et al., 2009). In fact, persistent activity was generated in very small networks but only under conditions that are far from the physiological ones (Gutkin et al., 2001). This is the first study where a heavily constrained microcircuit model is used to infer a link between network size and dendritic nonlinearities with respect to persistent firing.

Finally, we find that relaxation of connectivity and synaptic delay constrains eliminates the gating effect of NMDA spikes, albeit at a cost of much larger networks. Large scale networks were classically assumed necessary for persistent activity

induction (Compte et al., 2000). Our study suggests that different mechanisms underlie persistent firing in small *versus* large scale networks, at least in the PFC: NMDA-dependent dendritic spikes underlie persistent firing in small, biophysically constrained, microcircuits via the generation of long lasting somatic depolarizations; in large scale networks, these plateau potentials are replaced by massive, asynchronous inputs that are sufficient to maintain activity. Our predictions concur with *in vitro* studies in the visual cortex where NMDA blockade does not eliminate Up and Down states (Sanchez-Vives and McCormick, 2000) and *in silico* studies in large-scale networks (Compte et al., 2000) which support persistent firing without NMDA receptors, under the assumption of asynchronous spiking activity.

5.4.2 Mechanisms underlying persistent activity termination: new roles for old players

We find that persistent activity can be terminated by increasing feed-forward inhibition, but only if the inhibitory signal is appropriately timed. Inhibition was previously suggested to terminate persistent firing, mainly during UP states (Mann et al., 2009), but a timing effect has never been reported. Our results predict that interfering signals are more effective if presented earlier than later during the delay period of a working memory task. We also find that termination can be prevented by the activation of the afterdepolarization mechanism (dADP) mediated by the CAN current. This finding points to a new functional role for the dADP, which has thus far been suggested to underlie the emergence of persistent activity (Sidiropoulou and Poirazi, 2012; Sidiropoulou et al., 2009) rather than its maintenance. We claim that the dADP, regulated by neuromodulators, may play a key role in preventing interfering signals from distracting the animals and thus improving working memory performance. An experimentally testable prediction made by our model based on these findings is that termination would be more easily achieved in the absence of dADP and when interneurons are strongly stimulated within 750 ms from the onset of persistent activity.

5.4.3 Predictive features of upcoming state transitions

Finally, we show that network activity (number of spikes) and slow synaptic mechanisms (NMDA and GABA_B currents), contain predictive information regarding the ability of a given stimulus to turn ON or OFF persistent firing in the microcircuit model. Interestingly, an upcoming ON state can be predicted by the microcircuit spiking activity, several milliseconds before the transition occurs. More importantly, a switch from the ON to the OFF state caused by a second inhibitory input can be predicted by the microcircuit response properties (total number of spikes) during the inducing stimulus, which is presented seconds before the termination takes place. This ability to predict ON and OFF states is in agreement with previous modeling (albeit with a different feature) work (Sidiropoulou and Poirazi, 2012) and conforms with experimental work showing that single neurons can categorize signals *in vivo* at the onset of stimulus presentation (Yamada et al., 2010). This information is readily available to downstream regions (Balleine et al., 2011; Tziritidis et al., 2009), presumably contributing to the preparation of a specific movement.

The predictive roles of GABA_B and NMDA are in accordance with our previous finding (Section 4.3.3) that slow excitation and inhibition gate persistent activity induction and further provides a mechanisms for this gating effect: the built-up of somatic depolarizations. In support, recent findings that slow synaptic currents mediate persistent activity (Sanders et al., 2013) and stimulus-outcome discrimination (van Wingerden et al., 2012), respectively. The finding that both iNMDA and iGABA_B code for state transitions, by shaping the somatic plateau potential, indicates that the balance of slow excitation/inhibition is crucial for the stability of the persistent state, as proposed by (Sanders et al., 2013). This is consistent with *in vivo* experiments in the PFC where Up states are generated through a temporal enhancement of fast excitation, whereas balanced synaptic events promote their stability (Haider et al., 2006).

6 Role of dendritic morphology in neuronal function

6.1 Preamble

So far, pyramidal models used were chosen to be morphologically simplified, in order to dissect the role of intrinsic and synaptic currents from the contribution of detailed dendritic morphology at the microcircuit level. Yet, having established that dendritic regenerative events support persistent activity, and given the complexity of dendritic integration, the next natural question that emerged is the relevance of our results in pyramidal neurons with detailed morphology. Even further, and motivated by recent findings suggesting that morphological features strongly influence the excitability of PFC compared to V1 neurons (Amatrudo et al., 2012), we searched for a systematic link between dendritic morphology, dendritic integration mode and persistent activity induction in L5 PFC neurons. Since basal dendrites of L5 PFC pyramidal neurons decrease in total basal dendritic length, branching frequency, and terminal dendritic length with age (de Brabander et al., 1998; Dickstein et al., 2007; Petanjek et al., 2007) and in schizophrenia (Black et al., 2004; Broadbelt et al., 2002), linking morphology of basal dendrites with neuronal function can contribute to better understanding of related diseases. Thus, at the final part of this study, we extended our model to include detailed dendritic morphology and showed how dendritic

integration at different branches contributes to the output of L5 PFC pyramidal neurons. Towards this goal, we first investigated how morphology shapes dendritic integration and second how morphology shapes functional output of the neurons.

6.2 Materials and Methods

6.2.1 Pyramidal Neuron Models

6.2.1.1 Morphologies

We used 56 reconstructed morphologies of pyramidal L5 PFC neurons derived from adult male Long-Evans rats at 64–78 days of age (Bergstrom et al., 2008), available from the Neuromorpho database, Smith laboratory (<http://neuromorpho.org/neuroMorpho/bylab.jsp#top>).

In order to focus on the effect of the basal dendritic tree morphology, we replaced the somatic and apical dendritic trees morphologies of all neuron models with identical copies of generic versions described below, while maintaining their original basal trees. The generic soma was the one with the median volume among the 56 cells ($V = 819.23 \mu\text{m}^3$ of the 35-2 pyramidal neuron). We selected the generic apical tree from neuron h-2b (shown in Figure 6.2.1A) because of its low complexity (9 dendrites, total dendritic length: $810.1 \mu\text{m}$, number of branch points: 5). The simple dendritic morphology was selected because complex apical trees have been associated with bursting phenotypes (van Elburg and van Ooyen, 2010) and this could bias our results. Neurons with the generic compartments were used throughout the experiments, except for the experiments involving the unaltered, original morphologies.

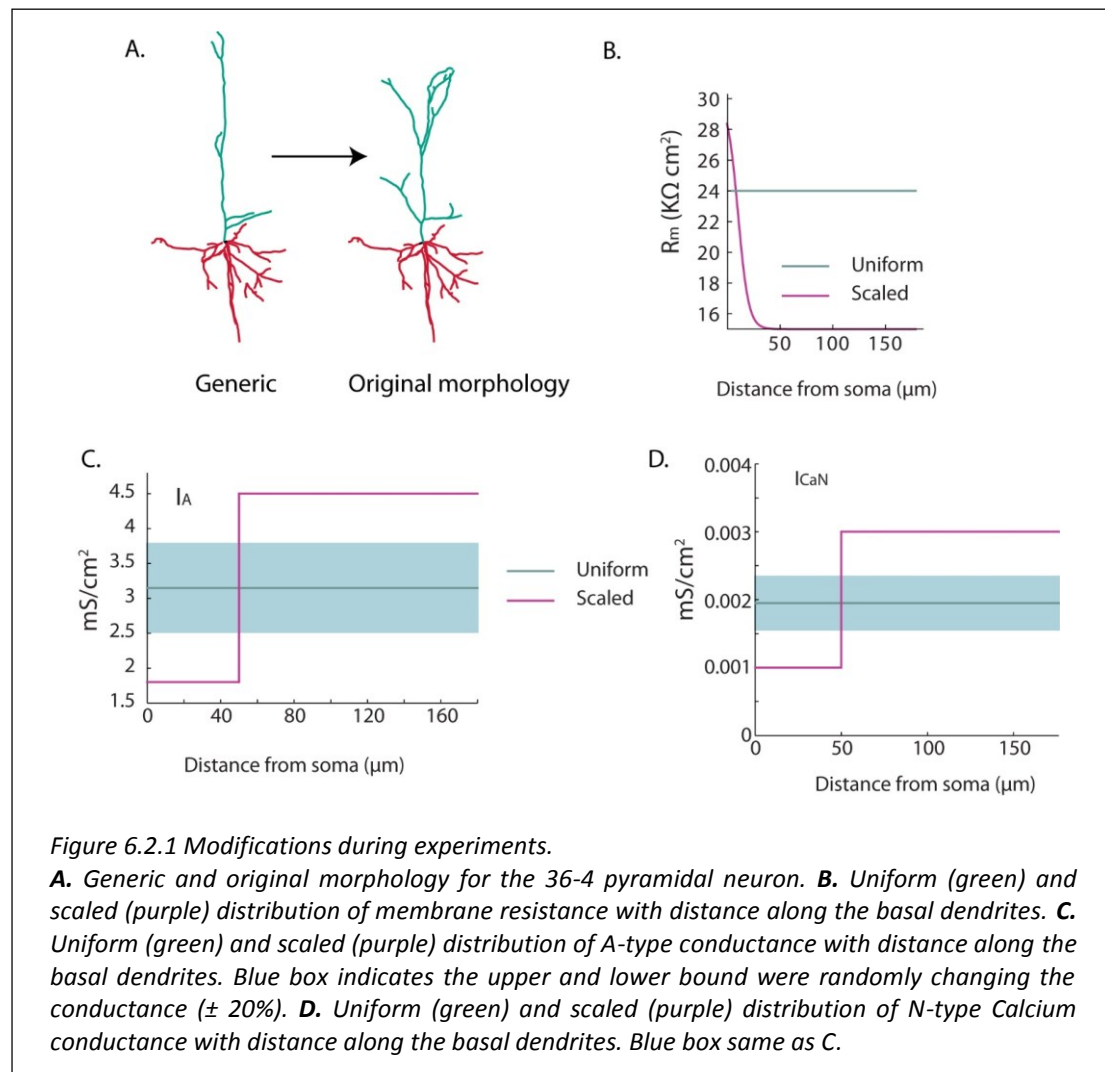
6.2.1.2 Biophysical properties

Biophysical properties of the model were adapted from (Sidiropoulou and Poirazi, 2012). In order to isolate the effect of the gradients of biophysical properties with distance from the effect of the morphology of the basal dendritic (Krichmar et al., 2002) we implemented the following modifications:

1. For the basic set of experiments, the membrane resistance R_m and the conductances of the basal L-type Ca^{++} current and A-type K^+ current were uniform throughout the neurons (Table 10.1.4, Figure 6.2.1B-D).

2. For the experiments investigating intrinsic properties, the active and passive conductances were scaled throughout the length of dendritic trees (Table 10.1.4, Figure 6.2.1B-D).

3. Finally in another set experiment, all active ionic conductances in the basal tree were randomly varied uniformly by $\pm 10\%$ and $\pm 20\%$ from their original values, in order to assess the effect of ionic mechanisms on dendritic integration (Figure 6.2.1A-D).



6.2.1.3 Synaptic mechanisms

The AMPA and NMDA currents were modeled and validated as per (Sidiropoulou and Poirazi, 2012). In all experiments, the iNMDA-to-iAMPA ratio at the basal dendrites was set to 1.5 (Wang et al., 2008) in order to mimic the $\sim 40\%$ increase in the NMDA current observed during working memory tasks that results after application of dopamine (Wang and O'Donnell, 2001), the recruitment of

extrasynaptic receptors (Chalifoux and Carter, 2011) or due to glia related processes (Oikonomou et al., 2012). The conductance of the GABA_A current was set so that the amplitude of the mIPSC was 10pA at a holding potential of -65 mV, as per (Woo et al., 2007) and the GABA_B conductance was set to the 0.3 of the GABA_A conductance.

6.2.2 Characterization of dendritic integration mode

For each basal dendrite of the 56 neurons, dendritic and somatic depolarization was measured in response to increasing strength of excitatory synaptic stimulation. Specifically, a number of 5, 10, 15....100 synapses (AMPA/NMDA) were evenly distributed along a given dendritic branch and stimulated with 2 pulses at 50Hz. This stimulation protocol was selected because of its ability to reliably induce NMDA spikes in basal dendrites of L5 pyramidal neurons (Chalifoux and Carter, 2011; Nevian et al., 2007), thus maximizing nonlinear dendritic responses. Somatic sodium channels were blocked to prevent firing of action potentials.

Integration mode was defined as sublinear or sigmoid depending on how the somatic response (peak EPSP) to multiple synapses (e.g. 100 synapses) compares to the arithmetic sum of equal number of responses to 5 synapses (e.g. sum of 20 unitary responses). The following approach was used: given a basal dendrite, we subtracted the actual peak EPSP minus the expected arithmetic-sum peak EPSP for each synaptic input level. If the maximum difference was equal or below 0.2mV, we characterized the integration mode of the dendrite as sublinear (SUB), whereas if it was above 0.2mV we characterized the dendrite as sigmoidal (SIG). In cases where expected EPSP was approximately the same as the actual EPSP, dendrites were categorized as linear.

6.2.3 Classification of dendrites using their morphological/passive features

In order to test whether the morphology of basal dendrites determines their integration mode, we extracted a number of morphological features and used them as input to a statistical classifier. Features with high classification power can be used to predict the dendritic integration mode of a branch without explicitly measuring it.

6.2.3.1 Characteristic features of basal dendrites

The following morphological features of all basal dendritic branches were extracted:

1) branch length, 2) branch diameter, 3) path length - i.e. the total length of all branches forming the dendritic path from the soma to a given dendrite, 4) path diameter -i.e. the average diameter of all branches in a dendritic path, 5) branch order 6) branch Electrotonic Length (EL) –i.e. the natural length (L_i) of a branch i , normalized to its electrotonic length constant λ_i (lambda),

$$\lambda_i = \sqrt{\frac{d_i R_m}{4R_a}}$$

where d_i is the diameter of branch i

$$EL_i = \frac{\lambda_i}{L_i}$$

and 7) path Electrotonic Length or Mean Electrotonic Pathway (MEP) -i.e. the sum of the ELs of all branches forming the path from the soma to the tip of the studied branch,

$$MEP = \frac{1}{n} \sum_{i=1}^n EL_i$$

where n is the number of branches in the path (van Elburg and van Ooyen, 2010).

Features 1-5 are purely anatomical while features 6-7 depend on the passive properties of neurons. Statistical comparisons were performed using non-parametric tests in Matlab (The MathWorks Inc.). The Mann–Whitney–Wilcoxon test and the Kruskal–Wallis one-way analysis of variance were performed for two-group and three-group comparisons, respectively.

6.2.3.2 Assessing the predictive power of characteristic features

After characterizing the integration mode of all basal dendrites and extracting their characteristic features, we used a Bayesian classifier to search for a link between morphology and dendritic integration. Out of the dataset of 1393 dendrites, 200 randomly selected dendrites (100 sigmoidal and 100 sublinear dendrites) were retained for testing our method (test set). Each characteristic feature set for the remaining 1193 dendrites was used as input to a simple probabilistic Bayesian classifier, assuming a Gaussian distribution of examples. A Bayesian classifier uses the

input examples to extract a simple probabilistic relationship that assigns a class label (e.g. sigmoidal-SIG or sublinear-SUB integration) to a new example, based on the value of its characteristic feature (e.g. its diameter). Using this classifier, we categorized the 200 previously unseen dendrites (test set) into one of the two classes (SIG or SUB) and calculated the accuracy, sensitivity and specificity for the predicted classification. This procedure was repeated ten times, where a new training and testing data set were randomly selected. The mean and the standard deviation of the accuracy, sensitivity and specificity over the ten repetitions was calculated for each characteristic feature.

In order to calculate the threshold that best separates the two classes, we analytically solved the Bayes probability equation, under the assumption of Gaussian distributions for all features in both classes.

6.2.4 Neuronal input-output gain function

In order to evaluate the input-output function of neurons, we characterized their gain function by fitting a Hill function of coefficient 2 to the somatic EPSP amplitude response curves (Murphy and Miller, 2003):

$$\Delta V = R_{max} \frac{I^2}{I^2 + I_{50}^2}$$

The parameter I_{50} is the synapses that corresponds to the half of the maximum depolarization amplitude ΔV_{max} of the dendrite and characterizes the additive gain of the neuron (Silver, 2010). The maximum depolarization amplitude ΔV_{max} is the somatic response for 100 synaptic inputs. In order to evaluate the effect of the different experimental conditions, we used the generic neuronal models as controls, and plotted the changes of the parameters I_{50} and ΔV_{max} in the following conditions: original morphologies, scaled membrane resistance, 10% perturbation in ionic conductances and 20% perturbation.

6.2.5 The PFC microcircuit model

We constructed a small microcircuit as described in Section 3: Model development that comprised of 9 pyramidal neurons and 2 interneurons and studied its ability to generate persistent activity. The 9 pyramidal neurons were selected from the 56 reconstructed neurons based on their percentage of SIG and SUB dendrites: 3

with the highest percentage of SIG dendrites, 3 with 50% of SIG and SUB dendrites and 3 with the highest percentage of SUB dendrites were selected. The generic neuron models were used (that is uniform distribution of passive and active mechanisms along the basal dendrites, the simple apical dendrite and the median soma).

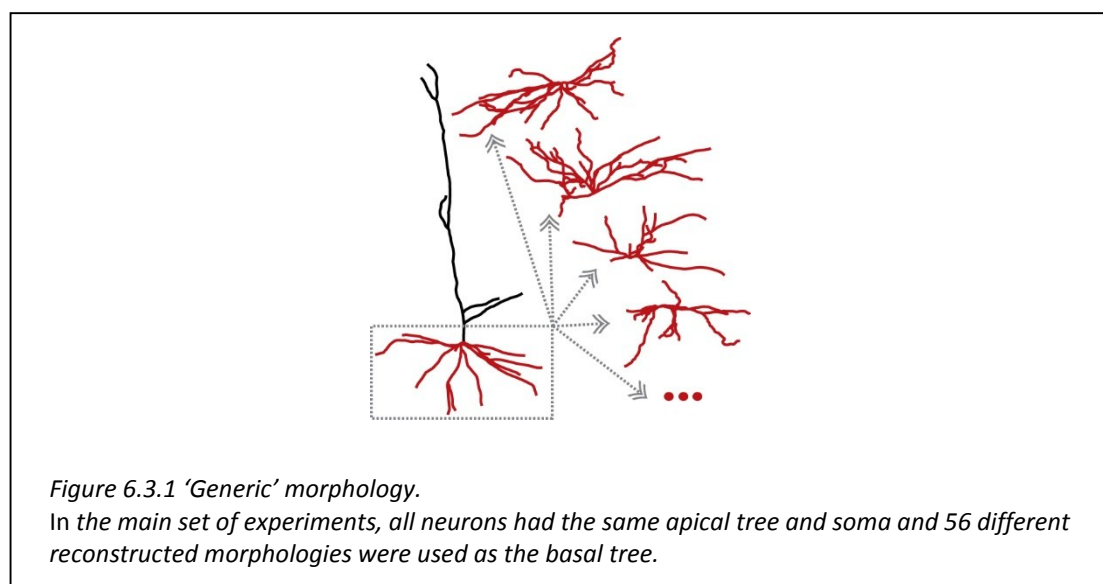
As before, the microcircuit model was assessed for its ability to support persistent activity induction. During the stimulation period, 100 synapses were randomly distributed along the apical dendritic trees of pyramidal neurons (Petreanu et al., 2009) and were activated with 10 pulses at 20 Hz. The probability of persistent activity induction was calculated over 50 consecutive repetitions during which both the synapses of the stimulus and the connecting synapses between neurons were randomly distributed along the apical and basal tree respectively. Positioning of synapses along a single dendrite and selection of dendrites were done using a uniform distribution (i.e. equal probability of selection). In these experiments, instead of enhancing the iNMDA-to-iAMPA ratio, we increased the number of reciprocal synapses to study initiation persistent activity.

6.3 Results

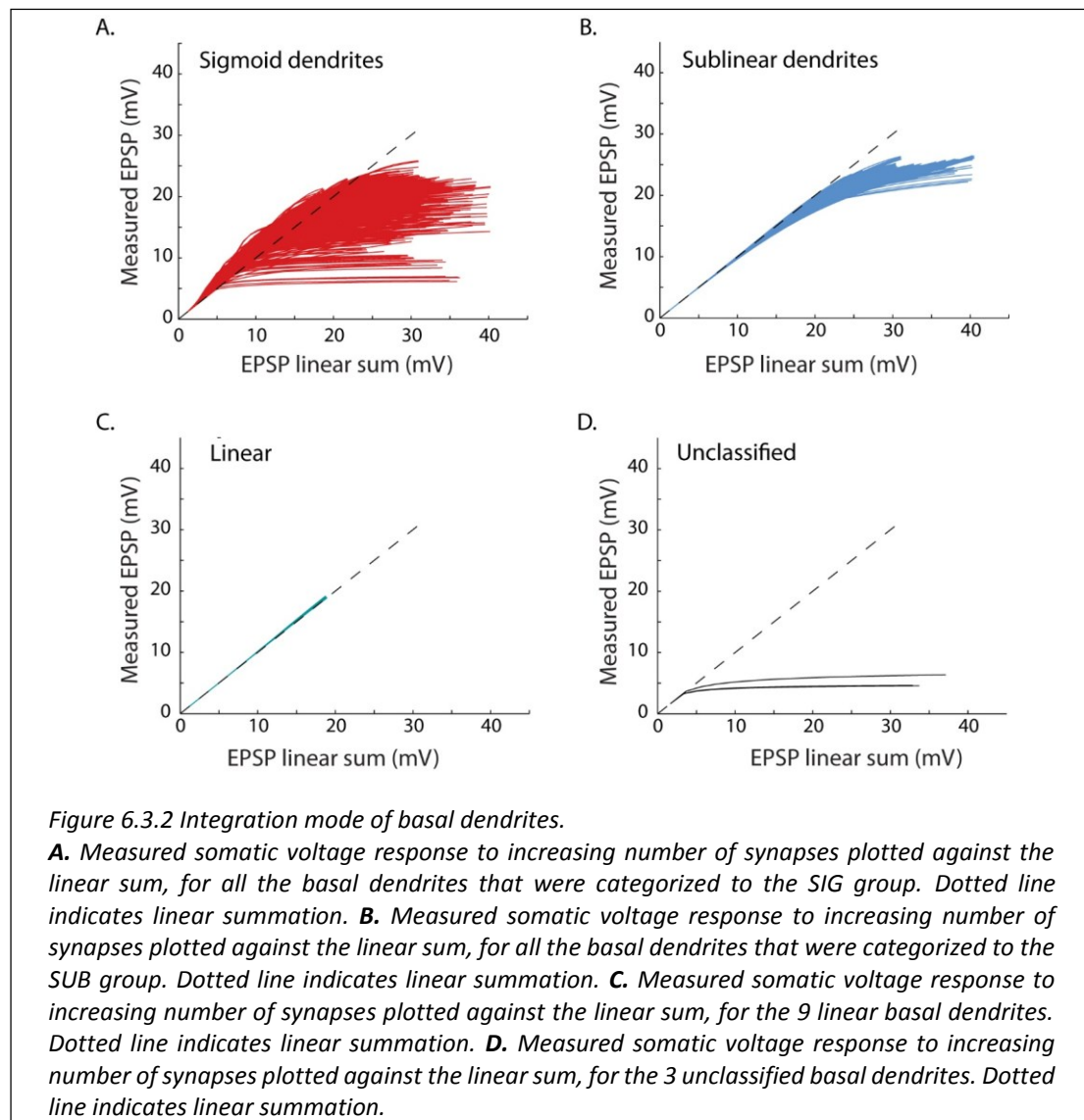
6.3.1 Morphology of the basal dendrites shapes dendritic integration

6.3.1.1 Basal dendrites integrate inputs sublinear or sigmoidal

As mentioned in previous sections, connections between pyramidal neurons are primarily realized at the basal dendrites (Markram, 1997; Markram et al., 1997). Thus we studied the effect of basal dendritic morphology in synaptic integration, in isolation from the morphology of the soma or the apical dendrite. Therefore, the "generic" pyramidal soma and apical tree model were constructed (see Materials and Methods). Also, active channels and passive properties were distributed evenly across the basal dendrites of cells so that the differences observed in the neurons would only be due to morphological differences of the basal dendrites. The 56 reconstructed basal dendritic trees were inserted in the "generic" pyramidal soma and apical tree model (Figure 6.3.1). The EPSPs responses of all 1401 dendrites in a 2 spikes at 50Hz were measured both locally at the dendrite and at the cell body while increasing the number of exciting synapses from 5 to 100, with step 5. Note that in this range of synapses both subthreshold and suprathreshold responses were investigated (although under sodium channel blockade at the soma to avoid action potential generation). Based on the somatic peak EPSP values, basal dendrites were categorized in one of three synaptic integration modes: sublinear (SUB), sigmoidal (SIG) or linear.



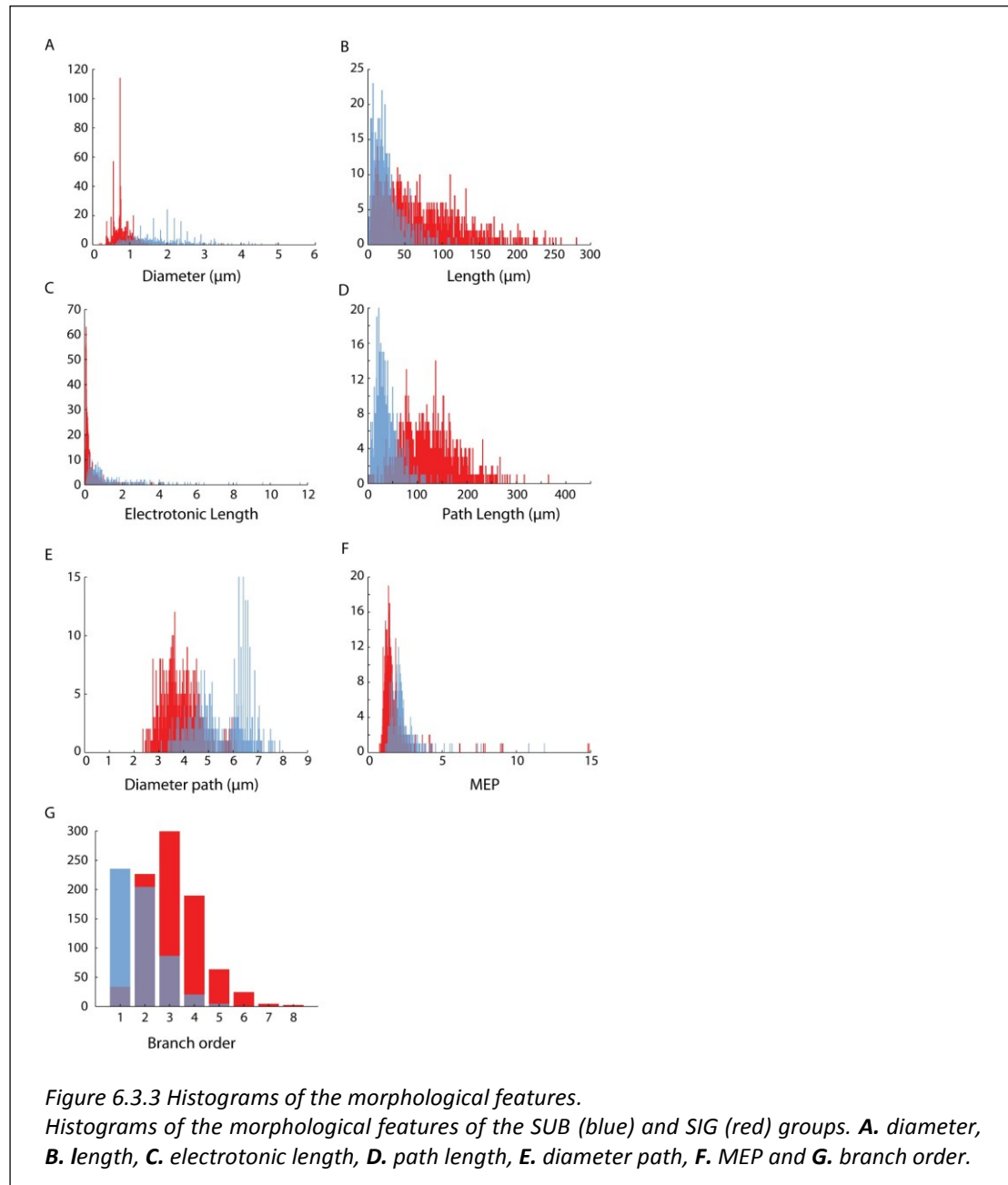
Out of the 1401 dendrites of the 56 neurons, 840 belonged to the SIG group (60%), 549 to the SUB group (39.2%), 9 to the linear group (0.6%) and 3 remained unclassified (0.2%). Actual-versus-expected somatic EPSP values of dendrites are shown in Figure 6.3.2. Note that in the case of SUB dendrites, integration was linear and shifted to sublinear in higher voltages (presumably supra-threshold). Due to the low number of linear dendrites, they were not analyzed in this study.



6.3.1.2 Morphology shapes dendritic integration in basal dendrites

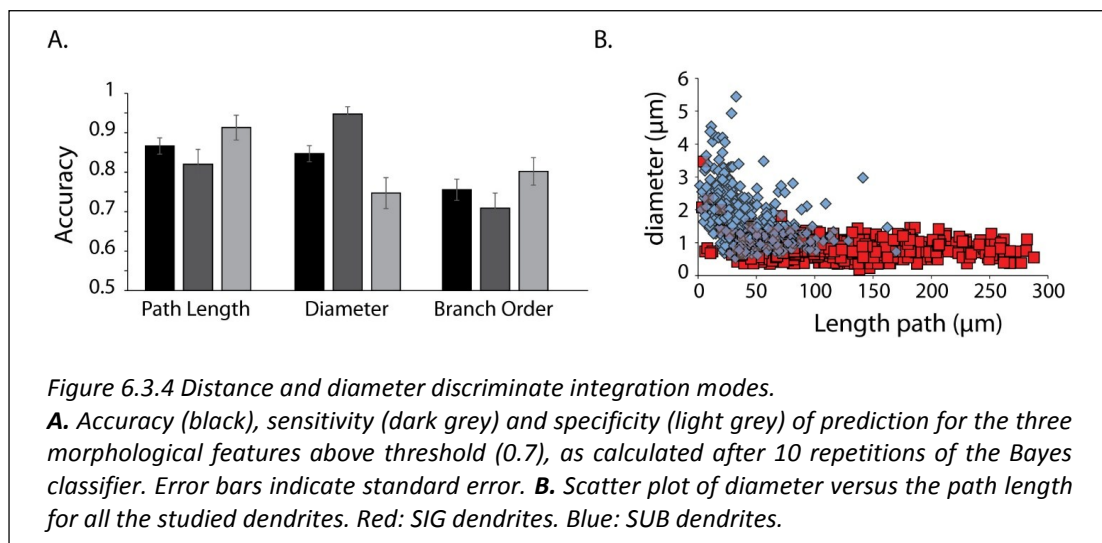
Having categorized the synaptic integration mode of the basal dendrites, we investigated which morphological characteristics between the SUB and SIG classes were substantially different. Seven morphological features, described in Materials and Methods, were studied. We found statistically significant differences (p value <0.001 ,

Mann-Whitney U test) for all seven morphological features. Class-specific distributions are shown in Figure 6.3.3 and their means \pm standard deviation values for each feature are shown in Table 10.1.8.



These results suggest that morphological features alone may be sufficient for determining the integration mode of any basal dendrite in L5 PFC pyramidal neurons. To test this hypothesis we used a Naïve Bayes Classifier to extract the probabilities that a dendritic branch is classified as sublinear or sigmoidal based on each one of its morphological features. The branch was assigned to the class (SUB or SIG) for which it

was predicted to belong with the maximum probability. Prediction accuracy was estimated for a total of 200 branches (test set) that were not used to train the classifier. Training and testing was performed 10 times and results were averaged. All scores all are listed in Table 10.1.9. The threshold for accuracy, sensitivity and specificity was 0.7. Figure 6.3.4A shows the mean accuracy, sensitivity and specificity achieved on this classification task for the three morphological features that were above threshold.



Path length, namely the path distance from the soma to the tip of a given branch, was the most informative feature as it achieved a mean prediction accuracy of 0.87 ± 0.02 . This suggests that the path distance of a given basal dendrite from the cell body is the most reliable predictor of its integration mode. Dendrites with path length $\geq 76.45 \mu\text{m}$ (classifier threshold) were assigned to the SIG class and the rest were assigned to the SUB class. Branch diameter is the second best predictive feature, achieving a mean accuracy of 0.85 ± 0.02 . Dendrites with diameter $\leq 1.19 \mu\text{m}$ were assigned to the SIG and the rest to the SUB class. Finally, branch-order could classify SIG and SUB dendrites with accuracy 0.76 ± 0.03 . Dendrites with branch order ≥ 3 were classified to the SIG group.

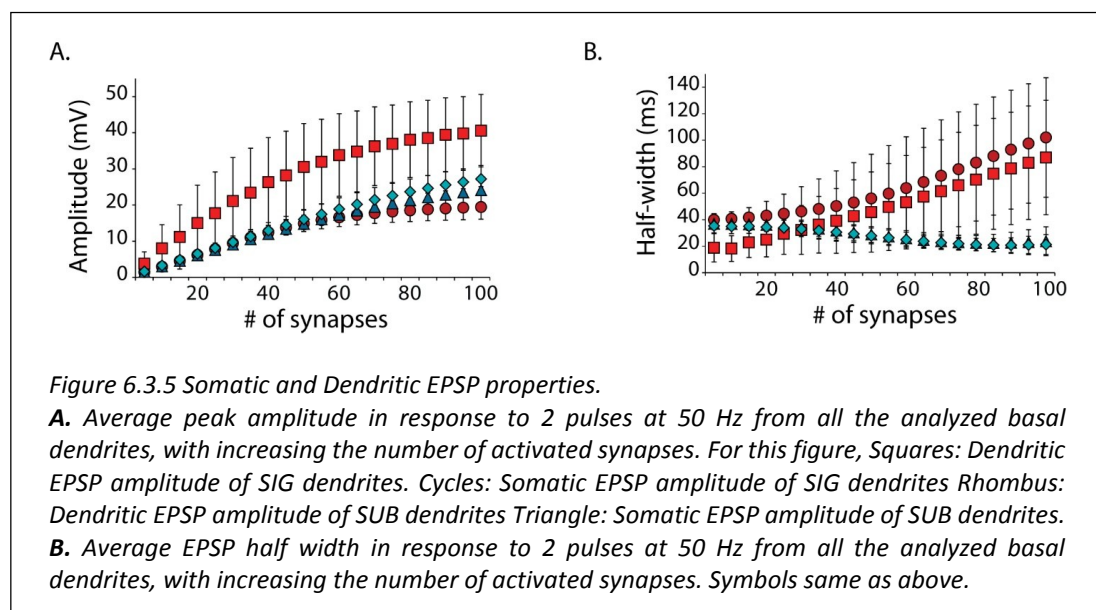
As seen in Figure 6.3.4B, distant dendrites are more likely to be thin and belong to the SIG group; however this is not true for proximal dendrites: the diameter of proximal dendrites (0-100μm) has a wide range. When a proximal dendrite has large diameter it is assigned to the SUB group but when a proximal dendrite has small

diameter ($< 1.2 \mu\text{m}$) it can either be assigned to the SUB or the SIG class (Figure 6.3.4B). A reason for the sublinear integration of the thin proximal dendrites may be the dominance of K^+ conductances of the soma. Thus, the path length, which incorporates both features (distance from the soma and indirectly diameter) is the more significant predicting feature for the integration mode of the dendrite.

Taken together, these results suggest that that sigmoidal integration is primarily realized by dendrites that are thin and located far away from the soma while sublinear integration is seen in more proximal, thicker branches. Importantly, the integration mode of a completely new branch can be predicted with $\sim 90\%$ accuracy when knowing just one morphological parameter: its path distance from the soma. It should be noted that such anatomical characteristics are very easy to compute given an image of the cell or even part of it and such images are now readily available both *in vivo* and *in vitro*.

6.3.1.3 Integration mode depends on dendritic spikes

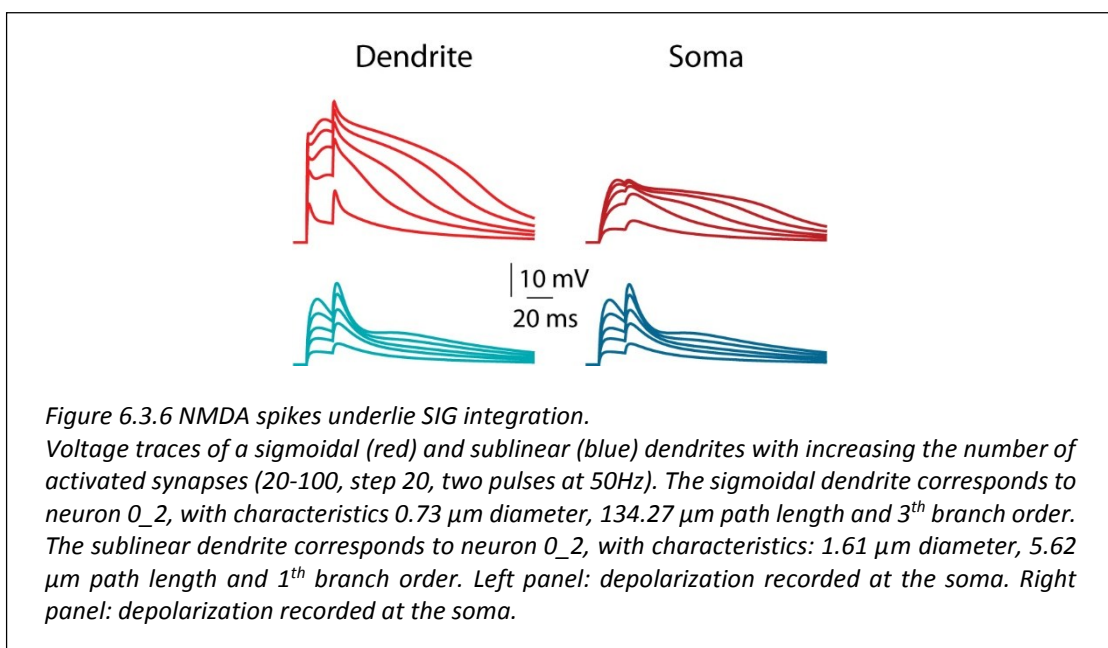
Dendritic spikes, and particularly NMDA spikes, have been associated with supralinear integration in multiple neuron types (Gómez González et al., 2011; Losonczy and Magee, 2006; Poirazi et al., 2003a; Polsky et al., 2004). However, location-specific summation of inputs can lead to different integration modes thus altering the local computations the dendrites perform (Branco and Häusser, 2011;



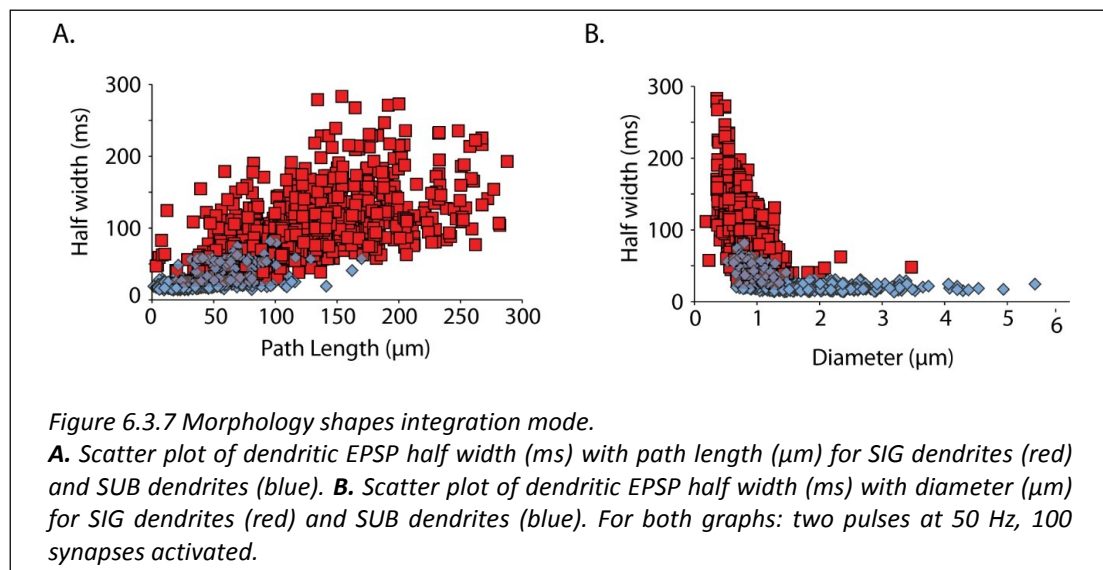
Major et al., 2008). We thus studied the properties of dendritic EPSPs resulting from synaptic stimulation in both SIG and SUB branches.

Dendritic EPSPs of SIG group had both larger amplitude and half width (Figure 6.3.5 C, D, squares; half width is henceforth defined as the time duration for which the EPSP is above its half-amplitude), compared to dendritic EPSPs of the SUB group (Figure 6.3.5 C, D, diamonds). Differences in half width were preserved in the somatic traces and increased with synaptic intensity (Figure 6.3.5D, cycles vs. triangles) but differences in amplitude (Figure 6.3.5 C, cycles vs. triangles) disappeared completely (0-60 synapses) or emerged attenuated for more strong stimuli (> 60 synapses). This is due to signal attenuation that is much larger for sigmoidal than sublinear branches, since they are located more distally. Note also the increased variance of both the amplitude and half-width EPSPs of SIG dendrites.

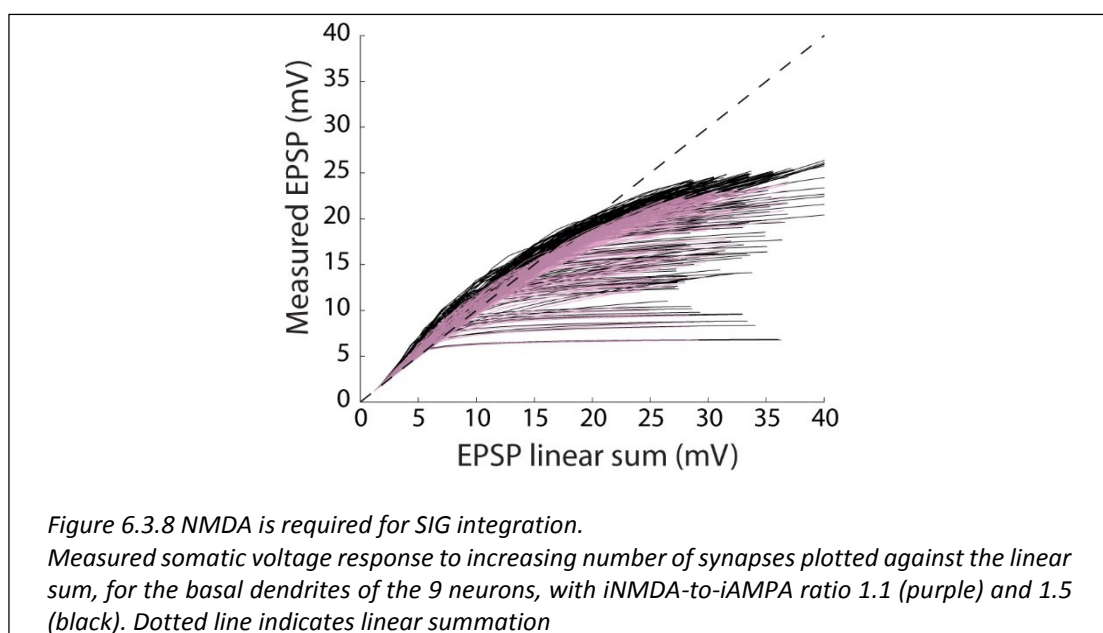
Larger and longer EPSPs in SIG dendrites resulted from the generation of NMDA spikes (Figure 6.3.6, red) which are characterized by a sharp increase in the peak amplitude of the EPSP upon induction and a progressive increase in the duration of the EPSP “plateau”. EPSPs in SUB dendrites on the other hand exhibited a gradual increase in amplitude and almost no change in half width (Figure 6.3.6, blue). Since the biophysical properties of both types of dendrites are identical, the reasons underlying the lack of NMDA spikes in SUB dendrites lie exclusively in their morphological features. Somatic EPSP half-width is increased with stimulating more



distant dendrites and with smaller diameter, the two morphological features that determined the sigmoidal and sublinear integration mode (Figure 6.3.7).



In another set of experiments, we reduced the iNMDA-to-iAMPA ratio to 1.1 (Wang et al., 2008), and again investigated the integration mode of the basal dendrites. For this and the following studies 9 neurons were used: 3 with the highest percentage of SIG dendrites, 3 with 50% percentage of SIG and SUB and 50% with high percentage of SUB dendrites. In total the 9 neurons had 188 dendrites, of which the 111 were SIG and 77 were SUB. Reducing the NMDA conductance altered the integration mode in 23.4 % (44 out of 188 tested) of dendrites, while the rest 76.6 %

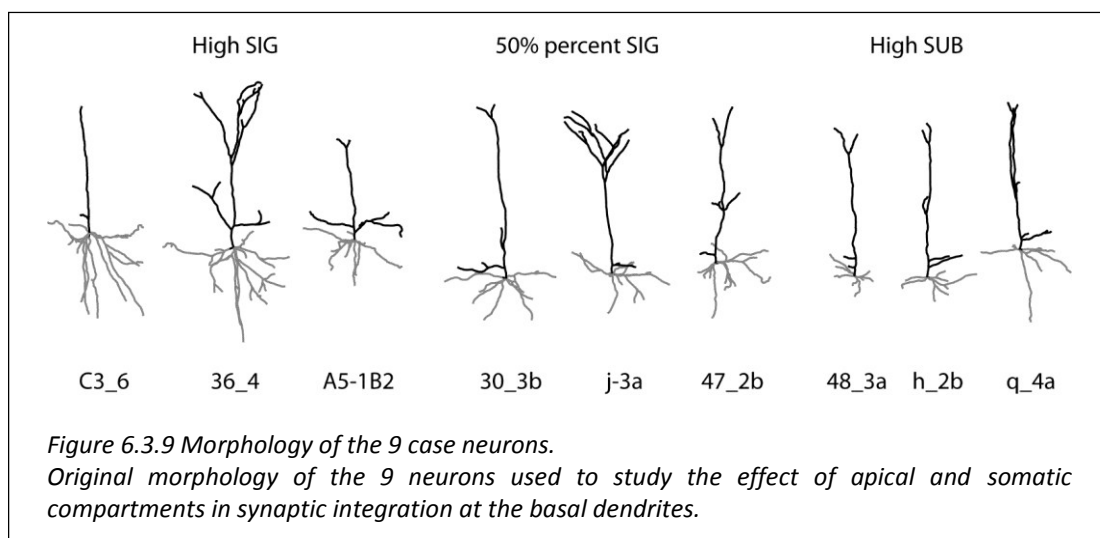


remained unaltered. As expected, all dendrites that changed were of the SIG class, and changed to the SUB class (44 of the 111 SIG dendrites in total, 40%). Integration mode of the 188 dendrites for the ratio 1.1 and for the ratio 1.5 are shown in Figure 6.3.8.

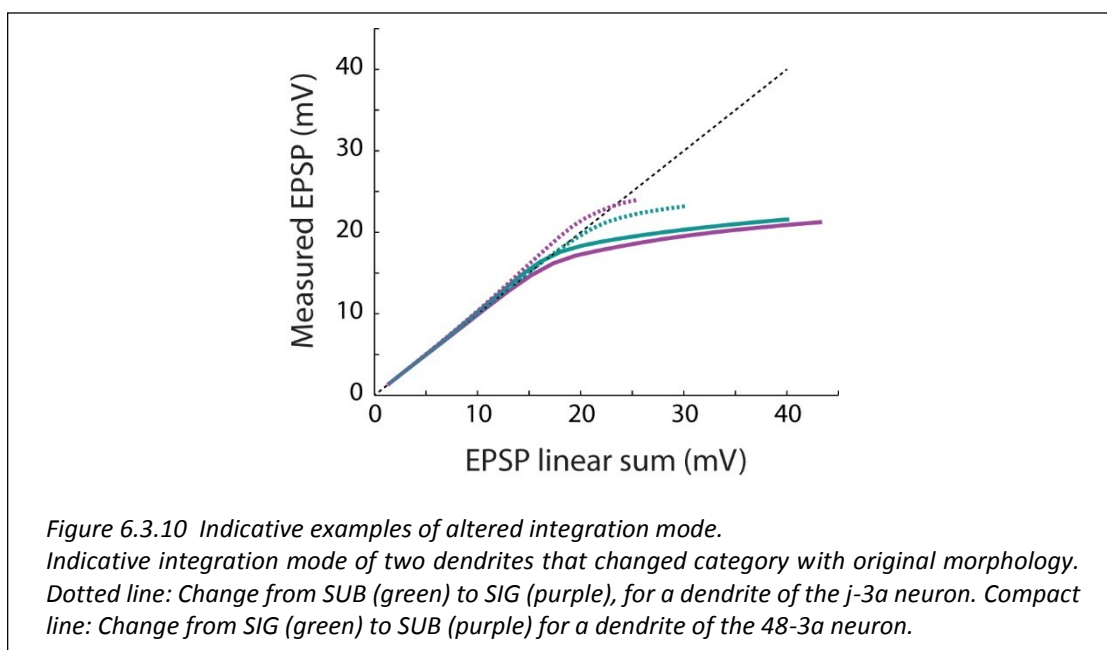
We further tested the NMDA dependence of sigmoidal integration by reducing the NMDA time constant τ_{NMDA} from 102 ms to 4.4 ms, in which case all dendrites were categorized to the SUB class, indicating that the observed enhanced EPSP half width in SIG dendrites is dependent on the generation of NMDA spikes.

6.3.1.4 Basal integration mode does not depend on apical tree and somatic morphologies

As previously mentioned, all experiments were performed using the ‘generic’ neuron with fixed morphology for the apical tree and the somatic compartment. Thus, we reassessed dendritic integration at the basal dendrites using the original reconstructed morphologies of both the apical and somatic compartments. The nine pyramidal cells were studied as in the previous section: three with the highest percentage of sigmoid dendrites, three with 50% sigmoid-sublinear dendrites and three with highest percentage of sublinear dendrites. Original morphology of the 9 neurons is shown in Figure 6.3.9.



Unexpectedly, changing the apical and somatic compartments did not alter the integration mode in most of the dendrites (176 from 188 tested, 93.62%). In the cases that categorization was altered, this could go to either direction (SIG to SUB or SUB to SIG), depending on the original morphology (indicative examples are shown in Figure 6.3.10). Thus, integration mode of the basal dendrites is dictated by their morphological properties alone.



6.3.1.5 Basal integration mode does not depend on ionic mechanism distribution or conductance fluctuations.

In the previous experiments, passive and active ionic conductances were uniform along the basal dendrites, in order to isolate the effect of morphology. We next investigate whether a) a realistic, non-uniform distribution of ionic mechanisms and b) random fluctuations in their conductances influence the integration mode of basal dendrites. These experiments were performed using the “generic” type (same apical and somatic compartments) of the nine representative pyramidal neuron models (as in the previous sections).

Pyramidal neuron models were first modified to account for distance-dependent scaling of passive and active conductances within basal dendrites (see Material and Methods) and integration curves were re-assessed. Scaling the passive and active properties along the basal dendrites did not change the integration mode

of 184 dendrites out of 188 tested (97.87%). In all four dendrites for which categorization was altered, they changed from SUB to the SIG group, although the integration curve was close to threshold of categorization (max difference of measured EPSP from expected EPSP equal to 0.2 mV).

In a second set of experiments, the conductances of all the ionic mechanisms in the basal dendrites were randomly altered by 10% or 20% of their value for a set of 5 trials (given the uniform distribution, indicative manipulation is shown in Figure 6.2.1). Interestingly, the classification did not change in either the 10% or the 20% manipulations.

Overall, the integration mode (SUB or SIG) remained the same, irrespectively of the morphology of the apical and somatic compartments (generic or original), the distribution of ionic and passive mechanisms in the basal tree (uniform or non-uniform) or the variability in the conductance values of ionic mechanisms ($\pm 10\%$ or $\pm 20\%$).

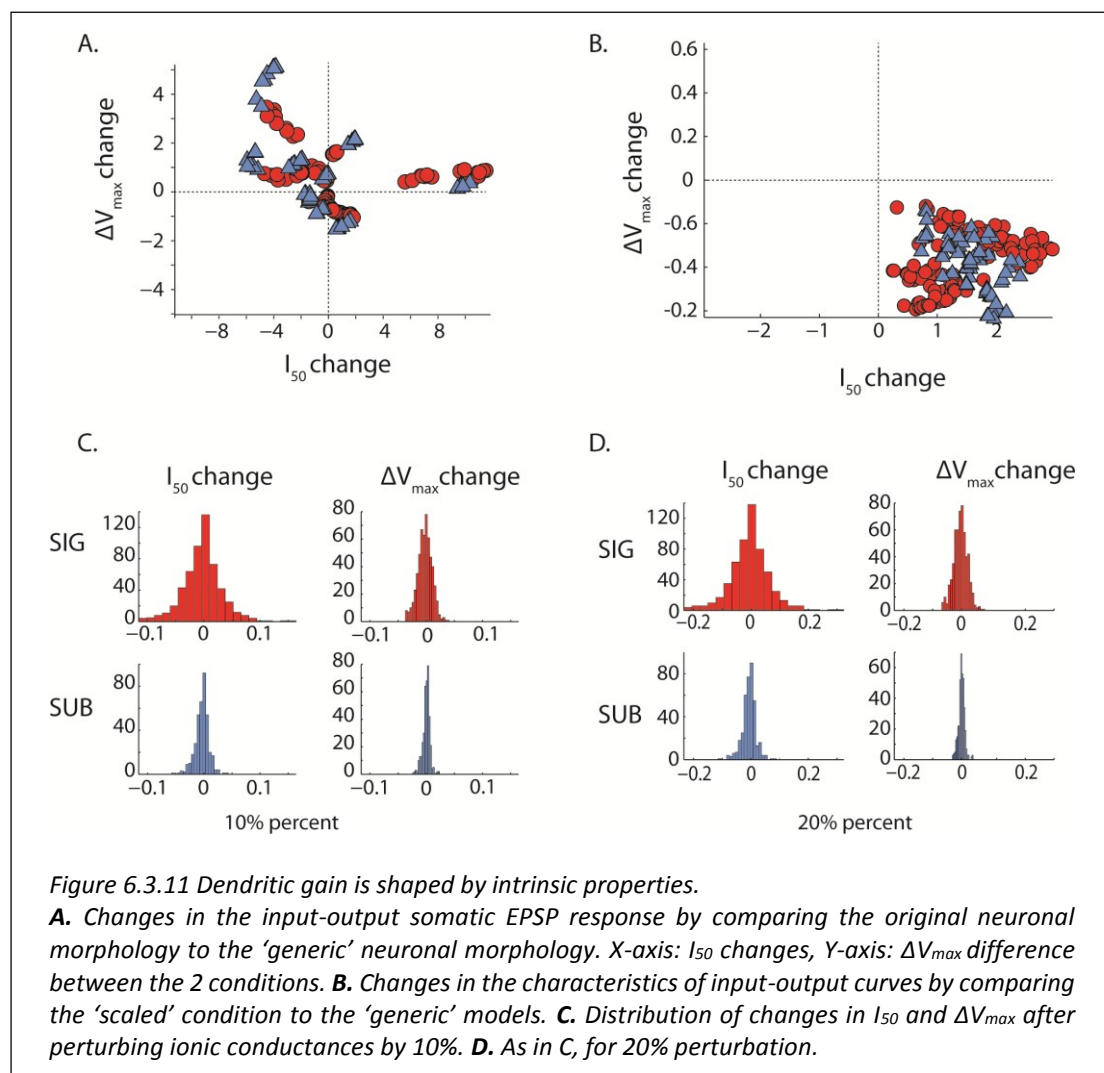
6.3.1.6 Gain depends on the morphological and ionic properties.

The finding that neither the morphology of the soma and the apical dendrites or the passive and active biophysical properties did not alter the integration mode raised the question about the effect of the above properties in the input-output function of neurons. Thus, we investigated the change in the gain (both in the amplitude and the additive gain, see Materials and Methods) compared to control in the above conditions. When changing to the original morphology of neurons, significant changes were observed in the input-output gain characteristics of most dendrites compared to the generic versions (average I_{50} difference: 0.004 ± 3.708 , V_{max} difference: 0.588 ± 1.477) (Figure 6.3.11A). Note that a decrease in the I_{50} (x-axis) and increase in the V_{max} (y-axis) correspond to increase of excitability. The change in the excitability could follow either direction.

When investigating the gain modulation in the case of passive and active properties scaling, it was changed and in general a decrease in excitability was observed: V_{max} was decreased on average 0.371 ± 0.128 and I_{50} was increased by 1.496 ± 0.611 (Figure 6.3.11B). This is primarily an effect of the reduced membrane resistance (R_m) along the basal dendrites: reduced R_m results in reduced voltage

depolarization. Finally, when randomly changing the active ionic conductances along the basal dendrites either $\pm 10\%$ or $\pm 20\%$ gain modulation was changed, however, with SIG dendrites displaying in general higher variability with respect to perturbations, as shown in Figure 6.3.11C, D.

Taken together, these results suggest that while ionic and passive mechanisms play an important role in shaping the input-output function of basal dendrites as expected, it is their morphology that determines whether regenerative NMDA spikes can emerge and turn a branch from purely sublinear to sigmoidal.

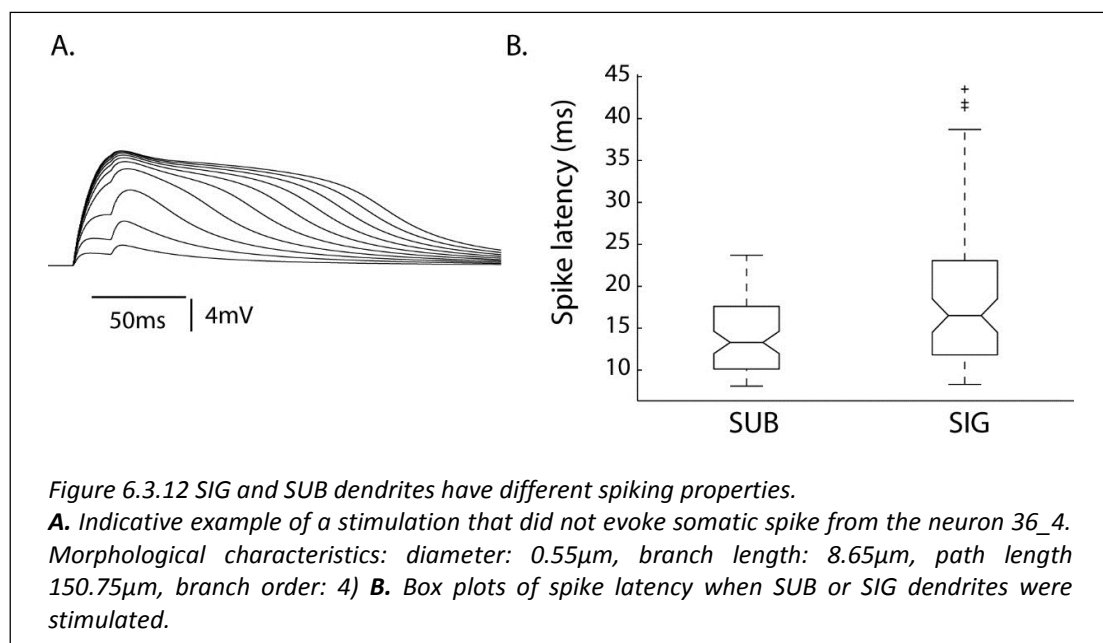


6.3.2 Morphology of the basal dendrites shapes neuronal function

The above experiments using the heavily validated models of L5 PFC pyramidal neurons showed that the basal dendrites integrate inputs in either a sublinear or a sigmoidal manner, depending on their morphological properties. The natural question

to ask next is what are the implications in the function of L5 PFC microcircuits. We first evaluated the spiking properties of the two groups of dendrites for the 9 neurons used in the previous studies, and then we constructed a PFC microcircuit model as before and used it to study the contribution of SUB and SIG dendrites in the expression of persistent activity.

For evaluating the spiking properties we repeated the synaptic stimulation of the basal dendrites with step 10 synapses, without simulating the ttx condition. We investigated differences in (a) threshold for spiking activity (number of synapses required for spike generation) (b) spike latency and (c) number of spikes when 100 synapses were activated, between the SIG and SUB dendrites. Counterintuitively, stimulation in 22 out of the 111 SIG dendrites (19.82%) did not result in spiking activity at the soma (maximum number of synapses tested: 100). This was never the case when the SUB dendrites were stimulated. The morphological characteristics of the 22 SIG dendrites that did not evoke an action potential at the soma were: diameter: $0.51 \pm 0.08 \mu\text{m}$, branch length: $65.1 \pm 71.06 \mu\text{m}$, path length $180.38 \pm 45.62 \mu\text{m}$, branch order: 3.31 ± 0.99 . Stimulation of these dendrites builds a long-lasting depolarizing plateau at the soma without spiking activity (Figure 6.3.12A).



We then investigated differences between SIG and SUB dendrites, in the cases that a somatic action potential was generated at the soma. No statistical significant

difference (p value >0.05) was found between the two groups (mean synapses 65.18 ± 11.71 for the SIG and 65.32 ± 5.75 for the SUB). Yet the maximum synapses to evoke an action potential never surpassed the 70 for the SUB group, but reach 100 in 3 SIG dendrites. Spike latency of the SUB group was statistically significant lower in the SUB group than spike latency of the SIG group (Figure 6.3.12B) (p value < 0.001). In conjunction with the previous results, signal transmission is systematically more reliable in the SUB dendrites. On the other hand, the number of spikes evoked by stimulation of dendrites with 100 synapses was higher (p value <0.001) for the SIG (1.46 ± 0.5 spikes) compared to the SUB (1.06 ± 0.25 spikes).

Overall, SIG dendrites displayed lower probability of evoking a somatic spike, and had higher spike latency, both of which can be explained in terms of their longer path distance (Table 10.1.10). On the other hand, generation of NMDA spikes in the case of SIG dendrites enhanced the probability of bursty activity. Thus we finally asked whether reliable spiking transmission (mediated by the SUB dendrites) or depolarizing plateau potentials (as predicted from our previous results) contribute to persistent activity.

The microcircuit (Figure 6.3.13) was developed and validated as in previous sections, but with detailed morphologies for the L5 PFC pyramidal neurons. It comprised of the 9 'generic' pyramidal neurons, also used in the above sections. Passive and active properties were uniformly distributed along the basal dendrites. This allowed the investigation of the effect of morphology of basal dendrites alone in shaping persistent activity. Three sets of experiments were conducted: in the first all

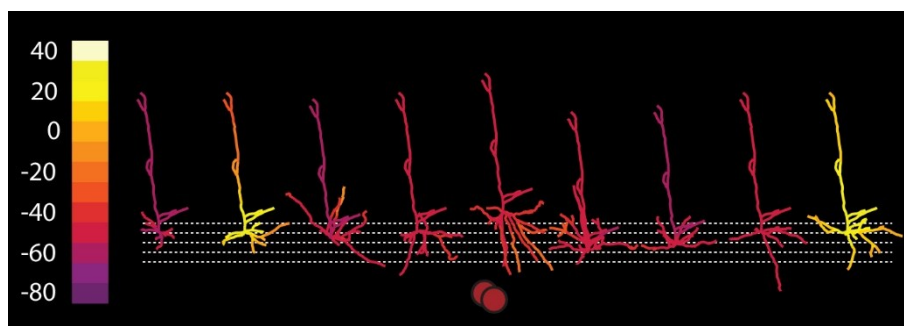
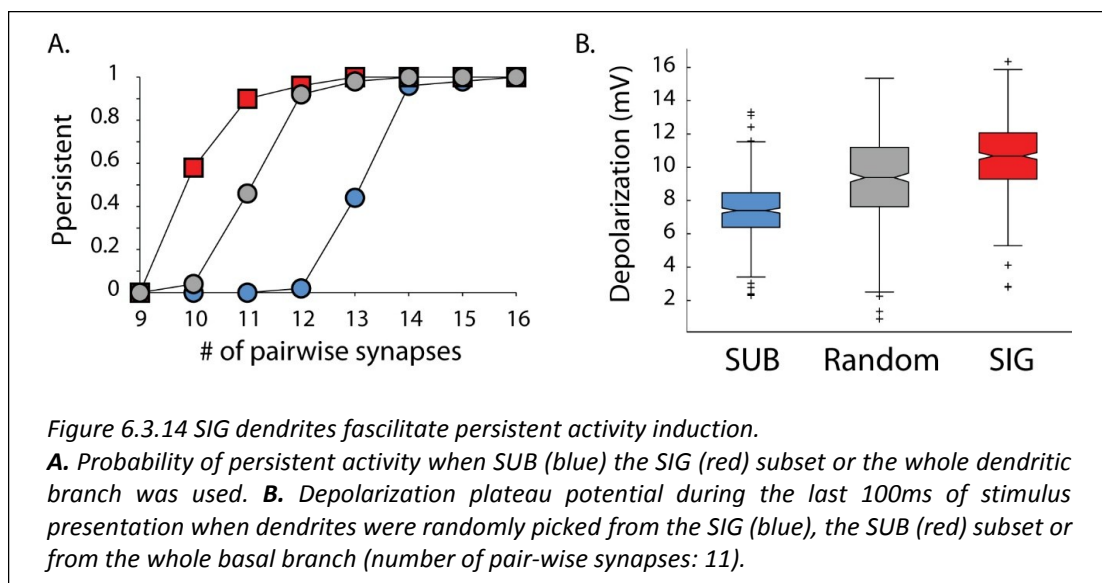


*Figure 6.3.13 Detailed microcircuit.
Indicative instance of the 9 neuron microcircuit. Color bar in pyramidal neurons shows voltage potential.*

pairwise synapses between pyramidal neurons were randomly positioned exclusively along basal dendrites of the SIG group (SIG experiment), in the second excitatory synapses between pyramidal neurons were randomly positioned exclusively along basal dendrites of the SUB group (SUB experiment) and in the third experiment excitatory synapses between pyramidal neurons were randomly positioned without biases along basal dendrites (Random experiment). In order to account for different clustering of synapses between neurons with more/less basal dendrites, two dendrites from the SIG or SUB group or the whole dendritic tree from each neuron were randomly picked in each simulation.

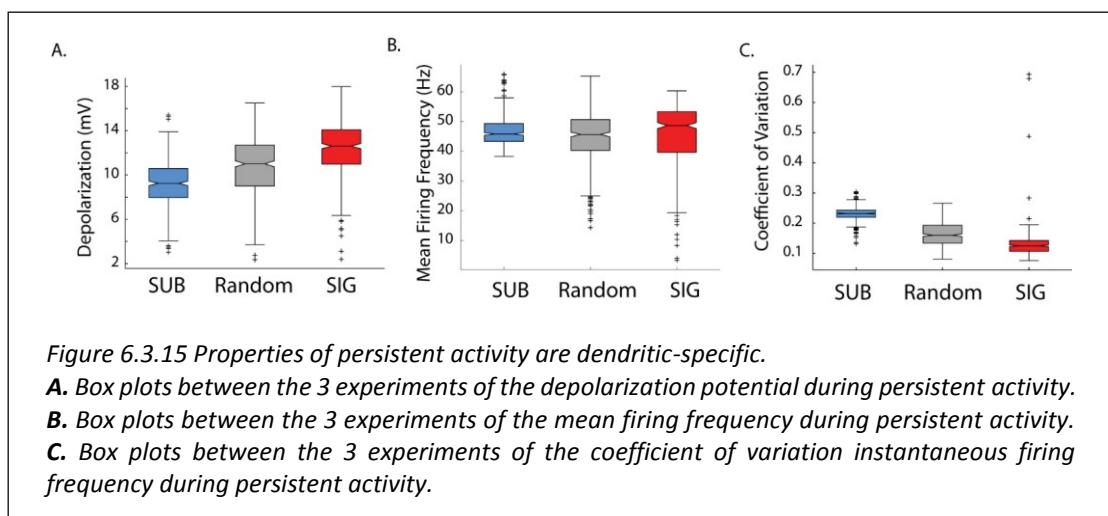
In accordance with the simplified microcircuit, persistent activity was induced by stimulating a total of 100 synapses (10 synchronous events at 20 Hz) randomly positioned along the apical dendrites. Probability of induction was estimated over 50 trials during which only the synaptic location was changed. Induction probability was assessed for increasing numbers of pyramidal-to-pyramidal connections within each microcircuit (ranging from 9 to 16).

Positioning pairwise synapses exclusively to the SIG basal dendrites of the 9 neurons, resulted significant lower threshold of probability for persistent activity induction (Figure 6.3.14A). SIG dendrites of the 9 neurons were more distally from the soma, had smaller diameter and higher branch order compared to the SUB group (Table 10.1.10). On the other hand, positioning pairwise synapses more closely to the soma, to the SUB subset, considerable reduced the probability of persistent activity

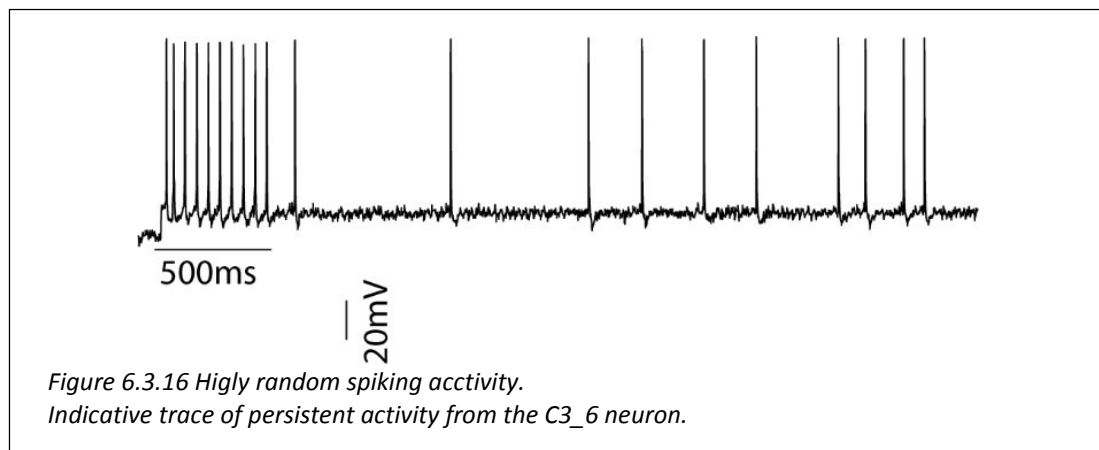


induction. Random position of synapses along the basal tree resulted in an intermediate probability (Figure 6.3.14A). Not that in the Random experiment SIG dendrites are overrepresented (111 out of 188) compared to the SUB dendrites (77 out of 188). Therefore, positioning synapses to the tips of the basal tree facilitates the induction of persistent spiking activity. In order to further investigate how SIG dendrites promote prolonged spiking activity, we calculated the depolarization potential during the last 100ms of stimulus presentation in the three sets of experiments, as in Section 5.3, when 11 synapses were used in the pairwise connections. Under this condition persistent activity is not induced when the SUB group of dendrites is used (Figure 6.3.14A). Depolarization was statistically significant higher ($p < 0.001$) when synapses were located at the SIG dendrites, indicating that NMDA spike generation facilitates persistent activity induction through the built up of plateau potential at the soma, as also predicted in the previous sections (Figure 6.3.14B).

We further investigated how dendritic integration shapes firing properties during persistent activity. Persistent activity properties were studied when pyramidal neurons were connected by 16 synapses (100% probability of induction in both SIG, Random and SUB experiments). Interestingly, all features examine were statistically significant different between the three sets of experiments. In The SIG experiments, during persistent activity depolarizing plateau potential was higher (12.34 ± 2.48) compared to the Random (10.84 ± 2.68) or SUB (9.2 ± 2.1) experiment (p value < 0.001) (Figure 6.3.15A).



When investigating the spiking properties, the mean firing frequency during persistent activity (number of spikes/persistent activity time) had similar median value in the three experiments (SUB experiment: 45.83, Random experiment: 45.67, SIG: 48.67 Hz), yet their variation was higher for the SIG experiment to the Random, to the SUB (p value <0.05) (Figure 6.3.15B). This is because when stimulating at the SIG dendrites, the mean firing frequency between neurons is shows high heterogeneity. An indicative example is shown in Figure 6.3.16 where the stimulated SIG dendrites in the neuron were far from the soma and thus providing enough depolarization for the generation of plateau potential at the soma, but not for high frequency spiking activity. On the other hand, the coefficient of variation of the instantaneous firing frequency, is larger for the SUB (0.23 ± 0.02) compared to the Random (0.16 ± 0.04) and the SIG (0.13 ± 0.05) experiments (p value <0.001). Again the outliers in the case of the SIG experiments are due to cases as in Figure 6.3.16.



These result suggest that generation of NMDA spikes at the distal basal dendrites of L5 prefrontal neurons supports the generation of depolarizing plateau potential at the soma able to induce persistent activity. The firing properties of persistent activity exhibit higher variation when the SIG dendrites are stimulated. These results suggest that different combinations of SUB and SIG dendrites can be utilized by the brain to exert a fine modulation on expression of persistent activity, thus providing a robust and flexible system that can be used for the expression of working memory.

6.4 Discussion

Investigations of how structure relates to function have argued that heterogeneity of pyramidal cells provides the anatomical substrate of different functions performed in different regions (Elston, 2003). Here we argue that inter-neuronal morphological differences also support different functions. In this study, we linked the morphological characteristics of basal dendrites to the mode of synaptic integration and to selectivity of persistent activity initiation and persistent activity properties.

In particular, we developed a simple tool, based on a Bayes classifier which allows the evaluation and prediction of the effect of each dendritic morphological feature in synaptic integration. We found that the length of the dendritic path from the soma, as well as the diameter and the branch order, are predictors of whether a dendrite will summate inputs sublinearly or sigmoidally. The predictability of the dendritic path length criterion is consistent with the fact that the thinner distal dendrites generate larger local EPSPs due to their higher resistance. Larger EPSPs, in turn, facilitate the generation of dendritic spikes, which equips these dendrites with sigmoidal integration capabilities (Branco and Häusser, 2011; Major et al., 2008). An unexpected finding is that the path length is a better predictor of sublinear *versus* supralinear integration than the diameter of the dendrite. Distant dendrites are more likely to be thin; however this is not true for proximal dendrites. It may thus be the case that the dominance of K^+ conductances of the soma may be responsible for the observed sublinear integration, even when the diameter of the dendrite is small, thus rendering diameter a less significant predicting feature compared to the distance from the soma. It should be noted that such anatomical characteristics are very easy to compute given an image of the cell or even part of it and such images are now readily available both *in vivo* and *in vitro*. Recent data from L5 PFC neurons confirm that the distance from the soma of contact sites between neighbouring neurons are in the majority above our calculated threshold ($\geq 76.45 \mu\text{m}$) (Morishima et al., 2011).

Another important finding is the robustness of the categorization of dendritic branches as SIG or SUB to changes of ionic mechanism concentrations. Our experiments show that, while the input-output function is affected by the passive

properties, the distribution of ionic conductances and the morphological characteristics of the apical tree and of the soma, the mode of integration remains unaltered regardless of all the aforementioned manipulations. This propounds the view that morphology is the main determinant of the mode of integration in cortical pyramidal dendritic trees and is in agreement with robustness of synaptic transmission due to morphological diversity (Ramaswamy et al., 2012). Since the morphological branching patterns of dendrites are stable over long periods of time (Trachtenberg et al., 2002), while their intrinsic properties can be changed by experience (Zhang and Linden, 2003) our results suggest that learning and experience do not alter the mode of integration of dendrites but can alter their input-output gain.

Synaptic transmission was more reliable in evoking timely action potentials when SUB dendrites were stimulated. On the other hand, stimulation of SIG dendrites evoked depolarizing plateaus and higher number of action potentials. We thus investigated their contribution to persistent activity. The different integration modes of basal dendrites had clear functional implications for the emergence of persistent activity in the microcircuit. We found that, when the basal dendrites chosen were exclusively from the SIG subset, the threshold for persistent induction was decreased and the probability of induction was systematically higher. This finding is in agreement with our previous results (Section 5) that showed that persistent activity depends on the built-up of depolarizing plateau, shaped by NMDA spikes. Additionally, persistent activity initiated by SIG dendrites was qualitatively different from the activity initiated by SUB dendrites, the former having a higher baseline plateau potential and higher variation of spiking frequency. This suggests that neurons may exploit the selective allocation of synapses at the basal dendritic tree during the formation of a memory circuits: important inputs may be biased to distal regions within the dendritic tree, which will promote persistent activity induction. Selective stimulation of the SUB dendrites may occur in other functions of the prefrontal cortex, when reliable synaptic transmission is important, such as monitoring of sensory information processed in other brain areas (Champod and Petrides, 2007), or other task-related responses (apart from delay-period activity) such as cue-, response- or reward period activity (Funahashi and Inoue, 2000). We propose that the hyper-reciprocally microcircuits of

L5 PFC (Wang et al., 2006) may selectively participate in persistent activity induction through the generation of NMDA spikes at their basal dendrites.

Overall, although when it comes to electrophysiological profiles and synaptic responses, various combinations in the parameter space of ionic conductances replicate the physiological observed phenotypes in neurons with different morphologies (Achard and De Schutter, 2006; Hay et al., 2013; Weaver and Wearne, 2008), contributing to functional homeostasis between neurons with different morphologies, here we argue that this is not the case when the integration mode of dendrites is examined. We propose that morphological differences enhanced the computational capabilities of neurons by enhancing the repertoire of computations they can perform beyond summation properties, such as the construction of functional selective microcircuits. This study corroborates with recent findings from *in vivo* experiments, showing that dendritic spikes mediate sensory-motor integration and angular tuning in the barrel cortex (Lavzin et al., 2012; Xu et al., 2012) and direction selectivity in retinal ganglion neurons (Sivyer and Williams, 2013). Note that although sublinear integration is in principle essential for selectivity to emerge, it contributes to other functions of these neurons. For example, in the visual cortex, sublinear integration is involved in binocular processing (Longordo et al., 2013), whereas NMDA spikes in angular tuning (Smith et al., 2013).

7 Conclusions

Computational studies investigating neuronal circuit dynamics have become more elaborate over the years (Haeusler et al., 2009; Sarid et al., 2007). The incorporation of anatomical, biophysical and connectivity constrains in these models facilitates the search for the functional relevance of cortical microcircuits with respect to cognition. In agreement, complex cognitive processes such as those involving working memory, depend upon functional properties of the circuit of the prefrontal cortex and thus knowledge of the realist architecture of connectivity is crucial to understanding the neural mechanisms that sub-serve persistent activity.

This study zooms out from dendrites to cell assemblies and suggests a tight interaction between dendritic non-linearities and assembly properties (size/connectivity) that support the short-term memory function of the PFC. It produces a number of experimentally tested predictions, such as that (a) stimulus-induced persistent activity can be generated in brain slices, assuming that these network structures remain intact, (b) slow inhibition (GABA_B current) gates the induction of persistent activity, (c) intrinsic currents, such as the h, the D-type, the sAHP and the R-type calcium currents modulate persistent activity emergence, (d) regenerative events, in particular NMDA spikes, gate the induction of persistent firing, (e) persistent activity has a time-dependent profile and (f) learning and experience do not alter the

mode of integration of dendrites but can alter their input-output gain. In summary, our results show that:

1) Small-sized PFC microcircuits serve as the anatomical substrate for the expression of persistent activity (Section 4.3.1). In the PFC, L5 neurons form discrete functional clusters of neurons, among which pyramidal neurons with complex (more branching) basal dendrites are hyper-reciprocally connected (Morishima et al., 2011; Wang et al., 2006), with the same afferent and efferent projections (Morishima and Kawaguchi, 2006; Otsuka and Kawaguchi, 2008). At the functional level, activation of PFC assemblies mediates rule learning on a trial-to-trial basis (Durstewitz et al., 2010) and also encodes for the rule-learning related memory (Ferrari et al., 2013; Peyrache et al., 2009). Sequential recruitment of these assemblies in the PFC *in vivo* is correlated with the animal's choice during a working memory task (Fujisawa et al., 2008). Here, we establish for the first time that these independent modules can support persistent activity, and this can be experimentally tested *in vitro* given an appropriate experimental set-up that will leave the micro-architecture intact.

2) In these microcircuits, persistent activity has a thresholding nature that depends on the generation of a plateau potential at the soma of pyramidal neurons (Section 3.3.5). Generation of the somatic plateau potential is primarily underlined by NMDA spike generation at the basal dendrites (Sections 5.3.2 and 6.3.2), shaped by the NMDA/GABA_B balance (Section 5.3.5) and can be facilitated by slow depolarizing currents, such as the dADP (Section 4.3.3). A recent biophysically constrained modelling study put forward the idea that short-term function depends critically upon the presence of thresholding mechanisms that could be either synaptic, or result from the circuit's recurrent connectivity (e.g. feedback inhibition) (Fisher et al., 2013). In support, in a very interesting experiment Durstewitz et al. investigated neuronal activity in PFC during the transition between two rules. When analyzed in steady-state (no rule changing), the two rules were represented by discrete patterns of network activity. During the learning of a new rule, they reported abrupt transitions of the excitability of PFC microcircuits, rather than gradual changes that were also correlated with abrupt transition in the behavioral performance. These data cast doubt to the

role of slow and gradual changes of synaptic connections in rule learning and also reinforce the notion of thresholding. Our results are in agreement with this notion and indicate that generation of a somatic plateau potential acts as a threshold for persistent activity induction. We propose that, driven by neuromodulators such as dopamine, enhancement of the NMDA conductance at the basal dendrites in specific microcircuits can mediate this abrupt transition via the generation of all-or-none NMDA spikes that result in long-lasting somatic plateau potentials.

3) Driven by the vast amount of data indicating compartmentalization of neuronal integration, we attempted to decipher the role of dendritic morphology as determinant factor of neuronal function. We identified a crucial role for morphological features, mainly the distance from the soma, in shaping the integration mode of basal dendrites (to sigmoidal or sublinear) (Section 6.3.1). We established simple criteria for inferring the integration mode of dendritic branches based on their anatomical characteristics, which can greatly simplify the study of dendritic function. The different integration modes also displayed different spiking properties at the supra-threshold regime: Sublinear basal dendrites mediated timely and reliable spiking activity, whereas sigmoidal dendrites contributed to the built-up of somatic depolarizing plateau (Section 6.3.2). Moreover, we found that persistent activity emergence depended on the synaptic location in the microcircuit that allowed for the generation of the somatic plateau potential. Therefore, there seems to be a functional role of the documented increased (compared to sensory areas) complexity of PFC dendritic trees. We propose that proximal inputs carry different information than distal ones: when reliable synaptic transmission is needed proximal dendrites are recruited, whereas biasing the connections towards the tips of dendrites mediates the persistent activity emergence. Note that in this scenario, parallel functional pathways may exist, depending on the branches activated.

4) The above thresholding depolarizing plateau is no longer needed when persistent activity is induced within large-scale networks (Section 5.3.3), indicating that different mechanisms contribute to prolonged firing in small *versus* large networks. Our findings are particularly important from an optimization/energy conservation point of view as

they suggest that active dendrites enable small microcircuits to express memory related processes such as persistent activity without requiring the recruitment of large neuronal networks and the associated energy costs. Since persistent activity has been documented in various brain regions and given different local connectivity properties between different regions, it is possible that both strategies can be implemented by neuronal tissue in different areas.

5) Properties of persistent firing in the microcircuit are not stimulus-specific, but depend on intrinsic features of individual neurons and the microcircuit connectivity. In particular, firing frequency during persistent activity depends on the amplitude of NMDA, GABA_B and dADP mechanisms (Section 4.3.3) as well as the location of recurrent synapses along the basal dendrites (Section 6.3.2). This indicates that PFC microcircuits can be tuned by the variety of neuromodulators that alter excitation/inhibition balance and dADP amplitude (Arnsten et al., 2012; Sidiropoulou et al., 2009). In addition, functional studies of circuits have shown that the cell-type identity (e.g. interneuron class but also projection sites for pyramidal neurons) have different their connectivity properties (Brown and Hestrin, 2009; Morishima and Kawaguchi, 2006). These independent processing assemblies with different functional outputs can interact to mediate higher order computations, such as coding of stimulus properties.

6) Stability of persistent activity critically depended on the balance of NMDA/GABA_B currents (Section 5.3.5) (the 'perfect couple' for bistability, (Sanders et al., 2013)) and this dependence could be modulated by the dADP current (Section 5.3.4). dADP has thus far been implicated in initiation of persistent activity (Sidiropoulou and Poirazi, 2012; Sidiropoulou et al., 2009), and this the first study that points to a role of dADP in the stability of persistent activity. We propose that the functional role of the dADP and NMDA currents in persistent activity may be segregated: NMDA spikes have a pivotal role in the *initiation* of persistent spiking activity, whereas dADP is crucial *during* the persistent state, as it provides robustness against noise and distractors.

7) Information about up-coming state transitions (both initiation of persistent activity and termination) was encoded in network spiking activity during the stimulus presentation, corroborating the reported categorization of signals *in vivo* at the onset of stimulus presentation *in vivo* (Yamada et al., 2010). This information is readily available to downstream regions (Balleine et al., 2011; Tziridis et al., 2009), presumably contributing to the preparation of a specific movement.

8) Intrinsic active mechanisms altered the gain but not the integration mode of basal dendrites. To our knowledge this is the first study that segregates the role of morphology and intrinsic ionic currents in neuronal output: integration that depends on NMDA spikes is shaped solely by the morphological properties of dendrites, whereas dendritic gain is modulated by intrinsic currents (Section 6.3.1). Enhancement or decrease of the gain due to ionic manipulations was also correlated with different probabilities for persistent activity induction (Section 4.3.4). In this work we revealed the role of the H-current, the D-type K current, the I_{sAHP} and the R-type calcium current, in persistent activity generation. Two results were the most important: enhancement of somatic voltage-gated calcium channels dampened neuronal excitability through a secondary recruitment of sAHP currents and the R-type calcium current, that has been under-investigated, seems to selectively (among the other VGCCs) enhance dendritic excitability and promote persistent activity. Future experimental and/or computational studies will be required to resolve or clarify the role of I_h in persistent activity states, given the high degree of discrepancy in the literature.

Overall, our work can be viewed in the broader framework of working memory (or stimulus) representation. The classical approach that relies on Hebbian plasticity refers to the storage of external information in networks through adapting connections. This learning procedure results in the formation of stable states, the attractors, and such networks are considered classical tools when investigating PFC function (Brody et al., 2003). On the other hand the formation of independent cell assemblies, whose bistability can be dynamically regulated by neuromodulators, indicates that the interplay of intrinsic circuit dynamics and single neuron properties

is a fundamental aspect in dynamic and adaptive view of memory (or stimulus) representation. In this framework, it is possible that each microcircuit (and each neuron) can participate in more than one representations, forming parallel functional pathways, through location-specific activation of synapses (Harris, 2005).

What may be the computational advantages of this modular micro-architecture remains in great part an open question. Sequential activation of microcircuits during Up and Down states in L5 somatosensory neurons has been proposed to allow for serial execution of multiple steps in an information processing task (Luczak et al., 2007) and dynamic activation of these assemblies in the PFC has been found to underlie successful decision making (Lapish et al., 2008). We propose that modulation of these reciprocal microcircuits during learning may serve as a mechanism for generating different subpopulations in the PFC that integrate inputs semi-independently, by using different persistent activity induction thresholds and generating firing patterns with different temporal dynamics.

8 Future Directions

It was beyond the purpose of this work to explore how the various subtypes of interneurons contribute to persistent firing. Rather we choose to simplify our approach by incorporating a fast spiking interneuron providing somatic inhibition. In light of recent findings regarding the role of inhibition in controlling dendritic regenerative events (Gidon and Segev, 2012; Jadi et al., 2012) and display behavioral correlates (Kvitsiani et al., 2013), extension of the detailed microcircuit with different interneuron subtypes will also provide new insights to the function of microcircuits. Moreover, we assume that implementation of physiological procedures that result in synaptic modifications, such as short-term depression and facilitation and presynaptic GABA_B receptors, may unravel other aspects of persistent activity features, such as its temporal irregularity.

Most importantly, advances in parallel computing have allowed simulations of larger scale networks of biophysically and morphologically detailed neurons. Implementation of such networks that will allow to simultaneously simulate multiple L5 PFC assemblies, as well as neurons not participating in these clusters, will provide fundamental insights as to how these clusters can co-operate to produce a function (e.g. stimulus coding). In principle this approach can investigate how highly specific reciprocal sub-networks operate in synergy in a pool of sparse connections with moderate synaptic strengths (Song et al., 2005). Note that in this framework a neuron

may exhibit persistent activity without belonging to a reciprocally connected cell assembly: convergent input to a single neuron from spatially dispersed neurons of a cell assembly/assemblies may drive neurons to persistent firing. Future investigations could also address the role of plasticity (synaptic or intrinsic) in the formation and function of these clusters in a circuit of pyramidal and inhibitory cells with detailed dendritic morphologies.

9 References

- Achard, P., and De Schutter, E. (2006). Complex parameter landscape for a complex neuron model. *PLoS Comput. Biol.* 2, e94.
- Van Aerde, K.I., and Feldmeyer, D. (2013). Morphological and Physiological Characterization of Pyramidal Neuron Subtypes in Rat Medial Prefrontal Cortex. *Cereb. Cortex*.
- Van Aerde, K.I., Mann, E.O., Canto, C.B., Heistek, T.S., Linkenkaer-Hansen, K., Mulder, A.B., van der Roest, M., Paulsen, O., Brussaard, A.B., and Mansvelder, H.D. (2009). Flexible spike timing of layer 5 neurons during dynamic beta oscillation shifts in rat prefrontal cortex. *J. Physiol.* 587, 5177–5196.
- Agmon-Snir, H., and Segev, I. (1993). Signal delay and input synchronization in passive dendritic structures. *J. Neurophysiol.* 70, 2066–2085.
- Amatrudo, J.M., Weaver, C.M., Crimins, J.L., Hof, P.R., Rosene, D.L., and Luebke, J.I. (2012). Influence of highly distinctive structural properties on the excitability of pyramidal neurons in monkey visual and prefrontal cortices. *J. Neurosci.* 32, 13644–13660.
- Angulo, M.C., Rossier, J., and Audinat, E. (1999). Postsynaptic glutamate receptors and integrative properties of fast-spiking interneurons in the rat neocortex. *J. Neurophysiol.* 82, 1295–1302.
- Antic, S.D., Zhou, W.-L.W.-L., Moore, A.R., Short, S.M., and Ikonomu, K.D. (2010). The decade of the dendritic NMDA spike. *J. Neurosci. Res.* 88, 2991–3001.
- Ariav, G., Polsky, A., and Schiller, J. (2003). Submillisecond precision of the input-output transformation function mediated by fast sodium dendritic spikes in basal dendrites of CA1 pyramidal neurons. *J. Neurosci.* 23, 7750–7758.
- Arnsten, A.F.T. (2009). Stress signalling pathways that impair prefrontal cortex structure and function. *Nat. Rev. Neurosci.* 10, 410–422.
- Arnsten, A.F.T. (2013). The Neurobiology of Thought: The Groundbreaking Discoveries of Patricia Goldman-Rakic 1937-2003. *Cereb. Cortex*.
- Arnsten, A.F.T., Wang, M.J., and Paspalas, C.D. (2012). Neuromodulation of thought: flexibilities and vulnerabilities in prefrontal cortical network synapses. *Neuron* 76, 223–239.
- Aron, A.R., Robbins, T.W., and Poldrack, R. a (2004). Inhibition and the right inferior frontal cortex. *Trends Cogn. Sci.* 8, 170–177.
- Asaad, W.F., Rainer, G., and Miller, E.K. (2000). Task-specific neural activity in the primate prefrontal cortex. *J. Neurophysiol.* 84, 451–459.
- Bacci, A., and Huguenard, J.R. (2006). Enhancement of spike-timing precision by autaptic transmission in neocortical inhibitory interneurons. *Neuron* 49, 119–130.
- Bacci, A., Huguenard, J.R., and Prince, D. a (2003). Functional autaptic neurotransmission in fast-spiking interneurons: a novel form of feedback inhibition in the neocortex. *J. Neurosci.* 23, 859–866.
- Balleine, B.W., Leung, B.K., and Ostlund, S.B. (2011). The orbitofrontal cortex, predicted value, and choice. *Ann. N. Y. Acad. Sci.* 1239, 43–50.

- Barbas, H. (2000). Connections underlying the synthesis of cognition, memory, and emotion in primate prefrontal cortices. *Brain Res. Bull.* *52*, 319–330.
- Barbas, H., and Zikopoulos, B. (2007). The prefrontal cortex and flexible behavior. *Neuroscientist* *13*, 532–545.
- Beltramo, R., D’Urso, G., Dal Maschio, M., Farisello, P., Bovetti, S., Clovis, Y., Lassi, G., Tucci, V., De Pietri Tonelli, D., and Fellin, T. (2013). Layer-specific excitatory circuits differentially control recurrent network dynamics in the neocortex. *Nat. Neurosci.* *16*, 227–234.
- Bergstrom, H.C., McDonald, C.G., French, H.T., and Smith, R.F. (2008). Continuous nicotine administration produces selective, age-dependent structural alteration of pyramidal neurons from prelimbic cortex. *Synapse* *62*, 31–39.
- Black, J.E., Kodish, I.M., Grossman, A.W., Klintsova, A.Y., Orlovskaya, D., Vostrikov, V., Uranova, N., and Greenough, W.T. (2004). Pathology of layer V pyramidal neurons in the prefrontal cortex of patients with schizophrenia. *Am. J. Psychiatry* *161*, 742–744.
- Börgers, C., Talei Franzesi, G., Lebeau, F.E.N., Boyden, E.S., and Kopell, N.J. (2012). Minimal size of cell assemblies coordinated by gamma oscillations. *PLoS Comput. Biol.* *8*, e1002362.
- De Brabander, J.M., Kramers, R.J., and Uylings, H.B.M. (1998). Layer-specific dendritic regression of pyramidal cells with ageing in the human prefrontal cortex. *Eur. J. Neurosci.* *10*, 1261–1269.
- Branco, T., and Häusser, M. (2011). Synaptic integration gradients in single cortical pyramidal cell dendrites. *Neuron* *69*, 885–892.
- Brennan, A.R., Dolinsky, B., Vu, M.-A.T., Stanley, M., Yeckel, M.F., and Arnsten, A.F.T. (2008). Blockade of IP3-mediated SK channel signaling in the rat medial prefrontal cortex improves spatial working memory. *Learn. Mem.* *15*, 93–96.
- Broadbelt, K., Byne, W., and Jones, L.B. (2002). Evidence for a decrease in basilar dendrites of pyramidal cells in schizophrenic medial prefrontal cortex. *Schizophr. Res.* *58*, 75–81.
- Brody, C.D., Romo, R., and Kepecs, A. (2003). Basic mechanisms for graded persistent activity: discrete attractors, continuous attractors, and dynamic representations. *Curr. Opin. Neurobiol.* *13*, 204–211.
- Brown, S.P., and Hestrin, S. (2009). Cell-type identity: a key to unlocking the function of neocortical circuits. *Curr. Opin. Neurobiol.* *19*, 415–421.
- Buhl, E.H., Tamás, G., Szilágyi, T., Stricker, C., Paulsen, O., and Somogyi, P. (1997). Effect, number and location of synapses made by single pyramidal cells onto aspiny interneurons of cat visual cortex. *J. Physiol.* *500 (Pt 3)*, 689–713.
- Cash, S., and Yuste, R. (1999). Linear summation of excitatory inputs by CA1 pyramidal neurons. *Neuron* *22*, 383–394.
- Cauli, B., Audinat, E., Lambolez, B., Angulo, M.C., Ropert, N., Tsuzuki, K., Hestrin, S., and Rossier, J. (1997). Molecular and physiological diversity of cortical nonpyramidal cells. *J. Neurosci.* *17*, 3894–3906.
- Cazé, R.D., Humphries, M., and Gutkin, B. (2013). Passive dendrites enable single neurons to compute linearly non-separable functions. *PLoS Comput. Biol.* *9*, e1002867.

- Chalifoux, J.R., and Carter, A.G. (2011). Glutamate spillover promotes the generation of NMDA spikes. *J. Neurosci.* *31*, 16435–16446.
- Chen, G., Greengard, P., and Yan, Z. (2004). Potentiation of NMDA receptor currents by dopamine D1 receptors in prefrontal cortex. *Proc. Natl. Acad. Sci. U. S. A.* *101*, 2596–2600.
- Compte, A. (2006). Computational and in vitro studies of persistent activity: edging towards cellular and synaptic mechanisms of working memory. *Neuroscience* *139*, 135–151.
- Compte, A., Brunel, N., Goldman-Rakic, P.S., and Wang, X.-J. (2000). Synaptic mechanisms and network dynamics underlying spatial working memory in a cortical network model. *Cereb. Cortex* *10*, 910–923.
- Constantinidis, C., and Steinmetz, M. a (1996). Neuronal activity in posterior parietal area 7a during the delay periods of a spatial memory task. *J. Neurophysiol.* *76*, 1352–1355.
- Constantinidis, C., and Wang, X.-J. (2004). A neural circuit basis for spatial working memory. *Neurosci.* *10*, 553–565.
- Constantinidis, C., Forest, W., Carolina, N., Inseem, U., Fédératif, I., and Procyk, E. (2004). The primate working memory networks. *Cogn. Affect. Behav. Neurosci.* *4*, 444–465.
- Cossart, R., Aronov, D., and Yuste, R. (2003). Attractor dynamics of network UP states in the neocortex. *Nature* *423*, 283–288.
- Curtis, C.E., and Lee, D. (2010). Beyond working memory: the role of persistent activity in decision making. *Trends Cogn. Sci.* *14*, 216–222.
- Day, M., Carr, D.B., Ulrich, S., Ilijic, E., Tkatch, T., and Surmeier, D.J. (2005). Dendritic excitability of mouse frontal cortex pyramidal neurons is shaped by the interaction among HCN, Kir2, and K_{leak} channels. *J. Neurosci.* *25*, 8776–8787.
- Dembrow, N.C., Chitwood, R.A., and Johnston, D. (2010). Projection-specific neuromodulation of medial prefrontal cortex neurons. *J. Neurosci.* *30*, 16922–16937.
- Dickstein, D.L., Kabaso, D., Rocher, A.B., Luebke, J.I., Wearne, S.L., and Hof, P.R. (2007). Changes in the structural complexity of the aged brain. *Aging Cell* *6*, 275–284.
- Diester, I., and Nieder, A. (2008). Complementary contributions of prefrontal neuron classes in abstract numerical categorization. *J. Neurosci.* *28*, 7737–7747.
- Dodt, H.U., Frick, A., Kampe, K., and Zieglgänsberger, W. (1998). NMDA and AMPA receptors on neocortical neurons are differentially distributed. *Eur. J. Neurosci.* *10*, 3351–3357.
- Dombeck, D. a, Graziano, M.S., and Tank, D.W. (2009). Functional clustering of neurons in motor cortex determined by cellular resolution imaging in awake behaving mice. *J. Neurosci.* *29*, 13751–13760.
- Dombrowski, S.M., Hilgetag, C.C., and Barbas, H. (2001). Quantitative architecture distinguishes prefrontal cortical systems in the rhesus monkey. *Cereb. Cortex* *11*, 975–988.
- Dong, Y., and White, F.J. (2003). Dopamine D1-class receptors selectively modulate a slowly inactivating potassium current in rat medial prefrontal cortex pyramidal neurons. *J. Neurosci.* *23*, 2686–2695.

Van Drongelen, W., Koch, H., Elsen, F.P., Lee, H.C., Mrejeru, A., Doren, E., Marcuccilli, C.J., Hereld, M., Stevens, R.L., and Ramirez, J.-M. (2006). Role of persistent sodium current in bursting activity of mouse neocortical networks in vitro. *J. Neurophysiol.* *96*, 2564–2577.

Durstewitz, D., and Gabriel, T. (2007). Dynamical basis of irregular spiking in NMDA-driven prefrontal cortex neurons. *Cereb. Cortex* *17*, 894–908.

Durstewitz, D., and Seamans, J.K. (2002). The computational role of dopamine D1 receptors in working memory. *Neural Netw.* *15*, 561–572.

Durstewitz, D., Seamans, J.K., and Sejnowski, T.J. (2000). Dopamine-mediated stabilization of delay-period activity in a network model of prefrontal cortex. *J. Neurophysiol.* *83*, 1733–1750.

Durstewitz, D., Vittoz, N.M., Floresco, S.B., and Seamans, J.K. (2010). Abrupt transitions between prefrontal neural ensemble states accompany behavioral transitions during rule learning. *Neuron* *66*, 438–448.

Eder, M., Rammes, G., Zieglgänsberger, W., and Dodt, H.U.U. (2001). GABAA and GABAB receptors on neocortical neurons are differentially distributed. *Eur. J. Neurosci.* *13*, 1065–1069.

Egorov, A. V., Hamam, B.N., Fransén, E., Hasselmo, M.E., and Alonso, A.A. (2002). Graded persistent activity in entorhinal cortex neurons. *Nature* *420*, 173–178.

Van Elburg, R. a J., and van Ooyen, A. (2010). Impact of dendritic size and dendritic topology on burst firing in pyramidal cells. *PLoS Comput. Biol.* *6*, e1000781.

Elston, G.N. (2003). *Cortex, Cognition and the Cell: New Insights into the Pyramidal Neuron and Prefrontal Function.* *Cereb. Cortex* *13*, 1124–1138.

Elston, G.N., Benavides-Piccione, R., Elston, A., Manger, P.R., and Defelipe, J. (2011). Pyramidal cells in prefrontal cortex of primates: marked differences in neuronal structure among species. *Front. Neuroanat.* *5*, 2.

Faber, E.S.L.S.L. (2010). Functional interplay between NMDA receptors, SK channels and voltage-gated calcium channels regulates synaptic excitability in the medial prefrontal cortex. *J. Physiol.* *588*, 1281–1292.

Feldmeyer, D., and Sakmann, B. (2000). Synaptic efficacy and reliability of excitatory connections between the principal neurones of the input (layer 4) and output layer (layer 5) of the neocortex. *J. Physiol.* *525 Pt 1*, 31–39.

Feldt, S., Bonifazi, P., and Cossart, R. (2011). Dissecting functional connectivity of neuronal microcircuits: experimental and theoretical insights. *Trends Neurosci.* *34*, 225–236.

Fellous, J.-M., and Sejnowski, T.J. (2003). Regulation of persistent activity by background inhibition in an in vitro model of a cortical microcircuit. *Cereb. Cortex* *13*, 1232–1241.

Ferrante, M., Migliore, M., and Ascoli, G.A. (2013). Functional impact of dendritic branch-point morphology. *J. Neurosci.* *33*, 2156–2165.

Ferrari, U., Tavoni, G., Battaglia, F.P., Cocco, S., and Monasson, R. (2013). Inferred Ising model unveils potentiation of pairwise neural interactions and replay of rule-learning related neural activity. *BMC Neurosci.* *14*, P276.

- Fiala, J.C., Kirov, S.A., Feinberg, M.D., Petrak, L.J., George, P., Goddard, C.A., and Harris, K.M. (2003). Timing of neuronal and glial ultrastructure disruption during brain slice preparation and recovery in vitro. *J. Comp. Neurol.* *465*, 90–103.
- Fisher, D., Olasagasti, I., Tank, D.W., Aksay, E.R.F., and Goldman, M.S. (2013). A modeling framework for deriving the structural and functional architecture of a short-term memory microcircuit. *Neuron* *79*, 987–1000.
- Fowler, M.A., Sidiropoulou, K., Ozkan, E.D., Phillips, C.W., and Cooper, D.C. (2007). Corticolimbic expression of TRPC4 and TRPC5 channels in the rodent brain. *PLoS One* *2*, e573.
- Fransén, E., Tahvildari, B., Egorov, A. V, Hasselmo, M.E., and Alonso, A.A. (2006). Mechanism of graded persistent cellular activity of entorhinal cortex layer v neurons. *Neuron* *49*, 735–746.
- Fujisawa, S., Amarasingham, A., Harrison, M.T., and Buzsáki, G. (2008). Behavior-dependent short-term assembly dynamics in the medial prefrontal cortex. *Nat. Neurosci.* *11*, 823–833.
- Funahashi, S., and Inoue, M. (2000). Neuronal interactions related to working memory processes in the primate prefrontal cortex revealed by cross-correlation analysis. *Cereb. Cortex* *10*, 535.
- Funahashi, S., Bruce, C.J., and Goldman-Rakic, P.S. (1989). Mnemonic coding of visual space in the monkey's dorsolateral prefrontal cortex. *J. Neurophysiol.* *61*, 331–349.
- Galloway, E.M., Woo, N.H., and Lu, B. (2008). Persistent neural activity in the prefrontal cortex: a mechanism by which BDNF regulates working memory? *Prog. Brain Res.* *169*, 251–266.
- Gazzaley, A., and Nobre, A.C. (2012). Top-down modulation: bridging selective attention and working memory. *Trends Cogn. Sci.* *16*, 129–135.
- Gee, S., Ellwood, I., Patel, T., Luongo, F., Deisseroth, K., and Sohal, V.S. (2012). Synaptic activity unmasks dopamine D2 receptor modulation of a specific class of layer V pyramidal neurons in prefrontal cortex. *J. Neurosci.* *32*, 4959–4971.
- Gidon, A., and Segev, I. (2012). Principles governing the operation of synaptic inhibition in dendrites. *Neuron* *75*, 330–341.
- Goldman, M.S. (2003). Robust Persistent Neural Activity in a Model Integrator with Multiple Hysteretic Dendrites per Neuron. *Cereb. Cortex* *13*, 1185–1195.
- Goldman-Rakic, P.S. (1995). Cellular basis of working memory. *Neuron* *14*, 477–485.
- Goldman-Rakic, P.S., Muly, E.C., and Williams, G. V (2000). D(1) receptors in prefrontal cells and circuits. *Brain Res. Brain Res. Rev.* *31*, 295–301.
- Gollo, L.L., Kinouchi, O., and Copelli, M. (2009). Active dendrites enhance neuronal dynamic range. *PLoS Comput. Biol.* *5*, e1000402.
- Gómez González, J.F., Mel, B.W., and Poirazi, P. (2011). Distinguishing Linear vs. Non-Linear Integration in CA1 Radial Oblique Dendrites: It's about Time. *Front. Comput. Neurosci.* *5*, 44.
- González-Burgos, G., and Barrionuevo, G. (2001). Voltage-gated sodium channels shape subthreshold EPSPs in layer 5 pyramidal neurons from rat prefrontal cortex. *J. Neurophysiol.* *86*, 1671–1684.

González-Burgos, G., Krimer, L.S., Povysheva, N. V, Barrionuevo, G., and Lewis, D. a (2005). Functional properties of fast spiking interneurons and their synaptic connections with pyramidal cells in primate dorsolateral prefrontal cortex. *J. Neurophysiol.* *93*, 942–953.

Gorelova, N.A., and Yang, C.R. (2000). Dopamine D1/D5 receptor activation modulates a persistent sodium current in rat prefrontal cortical neurons in vitro. *J. Neurophysiol.* *84*, 75–87.

Grillner, S., Markram, H., De Schutter, E., Silberberg, G., and LeBeau, F.E.N. (2005). Microcircuits in action—from CPGs to neocortex. *Trends Neurosci.* *28*, 525–533.

Grobin, A.C., Heenan, E.J., Lieberman, J.A., and Morrow, A.L. (2003). Perinatal Neurosteroid Levels Influence GABAergic Interneuron Localization in Adult Rat Prefrontal Cortex. *J. Neurosci.* *23*, 1832–1839.

Gundersen, V., Shupliakov, O., Brodin, L., Ottersen, O., and Storm-Mathisen, J. (1995). Quantification of excitatory amino acid uptake at intact glutamatergic synapses by immunocytochemistry of exogenous D-aspartate. *J. Neurosci.* *15*, 4417–4428.

Gutkin, B.S., Laing, C.R., Colby, C.L., Chow, C.C., and Ermentrout, G.B. (2001). Turning on and off with excitation: the role of spike-timing asynchrony and synchrony in sustained neural activity. *J. Comput. Neurosci.* *11*, 121–134.

Haeusler, S., and Maass, W. (2007). A statistical analysis of information-processing properties of lamina-specific cortical microcircuit models. *Cereb. Cortex* *17*, 149–162.

Haeusler, S., Schuch, K., and Maass, W. (2009). Motif distribution, dynamical properties, and computational performance of two data-based cortical microcircuit templates. *J. Physiol. Paris* *103*, 73–87.

Hagenston, A.M., Fitzpatrick, J.S., and Yeckel, M.F. (2008). MGluR-mediated calcium waves that invade the soma regulate firing in layer V medial prefrontal cortical pyramidal neurons. *Cereb. Cortex* *18*, 407–423.

Haider, B., Duque, A., Hasenstaub, A.R., and McCormick, D.A. (2006). Neocortical network activity in vivo is generated through a dynamic balance of excitation and inhibition. *J. Neurosci.* *26*, 4535–4545.

Haj-Dahmane, S., and Andrade, R. (1998). Ionic mechanism of the slow afterdepolarization induced by muscarinic receptor activation in rat prefrontal cortex. *J. Neurophysiol.* *80*, 1197–1210.

Hammond, C., and Crépel, F. (1992). Evidence for a Slowly Inactivating K⁺ Current in Prefrontal Cortical Cells. *Eur. J. Neurosci.* *4*, 1087–1092.

Harlow, J.M. (1868). Recovery from the passage of an iron bar through the head. *Publ Massachusetts Med Soc* *2*, 327–347.

Harris, K.D. (2005). Neural signatures of cell assembly organization. *Nat. Rev. Neurosci.* *6*, 399–407.

Hay, E., Schürmann, F., Markram, H., and Segev, I. (2013). Preserving axosomatic spiking features despite diverse dendritic morphology. *J. Neurophysiol.* *109*, 2972–2981.

Hines, M.L., and Carnevale, N.T. (2001). NEURON: a tool for neuroscientists. *Neuroscientist* *7*, 123–135.

- Hofer, S.B., Ko, H., Pichler, B., Vogelstein, J., Ros, H., Zeng, H., Lein, E., Lesica, N. a, and Mrsic-Flogel, T.D. (2011). Differential connectivity and response dynamics of excitatory and inhibitory neurons in visual cortex. *Nat. Neurosci.* *14*, 1045–1052.
- Homayoun, H., and Moghaddam, B. (2007). NMDA receptor hypofunction produces opposite effects on prefrontal cortex interneurons and pyramidal neurons. *J. Neurosci.* *27*, 11496–11500.
- Jadi, M., Polsky, A., Schiller, J., and Mel, B.W. (2012). Location-dependent effects of inhibition on local spiking in pyramidal neuron dendrites. *PLoS Comput. Biol.* *8*, e1002550.
- Jaffe, D.B., and Carnevale, N.T. (1999). Passive normalization of synaptic integration influenced by dendritic architecture. *J. Neurophysiol.* *82*, 3268–3285.
- Kalmbach, B.E., Chitwood, R. a., Dembrow, N.C., and Johnston, D. (2013). Dendritic Generation of mGluR-Mediated Slow Afterdepolarization in Layer 5 Neurons of Prefrontal Cortex. *J. Neurosci.* *33*, 13518–13532.
- Katz, Y., Menon, V., Nicholson, D. a, Geinisman, Y., Kath, W.L., and Spruston, N. (2009). Synapse distribution suggests a two-stage model of dendritic integration in CA1 pyramidal neurons. *Neuron* *63*, 171–177.
- Kawaguchi, Y., and Kubota, Y. (1993). Correlation of physiological subgroupings of nonpyramidal cells with parvalbumin- and calbindinD28k-immunoreactive neurons in layer V of rat frontal cortex. *J. Neurophysiol.* *70*, 387–396.
- Knable, M.B., and Weinberger, D.R. (1997). Dopamine, the prefrontal cortex and schizophrenia. *J. Psychopharmacol.* *11*, 123–131.
- Ko, H., Hofer, S.B., Pichler, B., Buchanan, K. a, Sjöström, P.J., and Mrsic-Flogel, T.D. (2011). Functional specificity of local synaptic connections in neocortical networks. *Nature* *473*, 87–91.
- Ko, H., Cossell, L., Baragli, C., Antolik, J., Clopath, C., Hofer, S.B., and Mrsic-Flogel, T.D. (2013). The emergence of functional microcircuits in visual cortex. *Nature* *496*, 96–100.
- Komendantov, A.O., and Ascoli, G.A. (2009). Dendritic excitability and neuronal morphology as determinants of synaptic efficacy. *J. Neurophysiol.* *101*, 1847–1866.
- Komiyama, T., Sato, T.R., O'Connor, D.H., Zhang, Y.-X., Huber, D., Hooks, B.M., Gabbito, M., and Svoboda, K. (2010). Learning-related fine-scale specificity imaged in motor cortex circuits of behaving mice. *Nature* *464*, 1182–1186.
- Korngreen, A., and Sakmann, B. (2000). Voltage-gated K⁺ channels in layer 5 neocortical pyramidal neurones from young rats: subtypes and gradients. *J. Physiol.* *525*, 621–639.
- Kreuz, T., Chicharro, D., Greschner, M., and Andrzejak, R.G. (2011). Time-resolved and time-scale adaptive measures of spike train synchrony. *J. Neurosci. Methods* *195*, 92–106.
- Krichmar, J.L., Nasuto, S.J., Scorcioni, R., Washington, S.D., and Ascoli, G.A. (2002). Effects of dendritic morphology on CA3 pyramidal cell electrophysiology: a simulation study. *Brain Res.* *941*, 11–28.
- Kuenzi, F.M., Fitzjohn, S.M., Morton, R.A., Collingridge, G.L., and Seabrook, G.R. (2000). Reduced long-term potentiation in hippocampal slices prepared using sucrose-based artificial cerebrospinal fluid. *J. Neurosci. Methods* *100*, 117–122.

- Kumar, A., Vlachos, I., Aertsen, A., and Boucsein, C. (2013). Challenges of understanding brain function by selective modulation of neuronal subpopulations. *Trends Neurosci.* 1–8.
- Kuroda, M., Yokofujita, J., and Murakami, K. (1998). An ultrastructural study of the neural circuit between the prefrontal cortex and the mediodorsal nucleus of the thalamus. *Prog. Neurobiol.* 54, 417–458.
- Kvitsiani, D., Ranade, S., Hangya, B., Taniguchi, H., Huang, J.Z., and Kepecs, A. (2013). Distinct behavioural and network correlates of two interneuron types in prefrontal cortex. *Nature.*
- De la Pena, E., and Geijo-Barrientos, E. (1996). Laminar Localization, Morphology, and Physiological Properties of Pyramidal Neurons that Have the Low-Threshold Calcium Current in the Guinea-Pig Medial Frontal Cortex. *J. Neurosci.* 16, 5301–5311.
- Lapish, C.C., Durstewitz, D., Chandler, L.J., and Seamans, J.K. (2008). Successful choice behavior is associated with distinct and coherent network states in anterior cingulate cortex. *Proc. Natl. Acad. Sci. U. S. A.* 105, 11963–11968.
- Larkum, M.E., and Nevian, T. (2008). Synaptic clustering by dendritic signalling mechanisms. *Curr. Opin. Neurobiol.* 18, 321–331.
- Larkum, M.E., Nevian, T., Sandler, M., Polsky, A., and Schiller, J. (2009). Synaptic integration in tuft dendrites of layer 5 pyramidal neurons: a new unifying principle. *Science* 325, 756–760.
- Lau, P.-M., and Bi, G.-Q. (2005). Synaptic mechanisms of persistent reverberatory activity in neuronal networks. *Proc. Natl. Acad. Sci. U. S. A.* 102, 10333–10338.
- Lavzin, M., Rapoport, S., Polsky, A., Garion, L., and Schiller, J. (2012). Nonlinear dendritic processing determines angular tuning of barrel cortex neurons in vivo. *Nature* 490, 5–9.
- Lewis, D. a, and González-Burgos, G. (2006). Pathophysiologically based treatment interventions in schizophrenia. *Nat. Med.* 12, 1016–1022.
- Lim, S., and Goldman, M.S. (2013). Balanced cortical microcircuitry for maintaining information in working memory. *Nat. Neurosci.* 16, 1306–1314.
- Litwin-Kumar, A., and Doiron, B. (2012). Slow dynamics and high variability in balanced cortical networks with clustered connections. *Nat. Neurosci.* 15, 1498–1505.
- Loewenstein, Y., and Sompolinsky, H. (2003). Temporal integration by calcium dynamics in a model neuron. *Nat. Neurosci.* 6, 961–967.
- Longordo, F., To, M.-S., Ikeda, K., and Stuart, G.J. (2013). Sublinear integration underlies binocular processing in primary visual cortex. *Nat. Neurosci.* 16, 714–723.
- Van der Loos, H., Glaser, E.M., and others (1972). Autapses in neocortex cerebri: synapses between a pyramidal cell's axon and its own dendrites. *Brain Res.* 48, 355.
- Lorenzon, N.M., and Foehring, R.C. (1995). Characterization of pharmacologically identified voltage-gated calcium channel currents in acutely isolated rat neocortical neurons. II. Postnatal development. *J. Neurophysiol.* 73, 1443–1451.
- Losonczy, A., and Magee, J.C. (2006). Integrative properties of radial oblique dendrites in hippocampal CA1 pyramidal neurons. *Neuron* 50, 291–307.

- Lübke, J., Markram, H., Frotscher, M., and Sakmann, B. (1996). Frequency and dendritic distribution of autapses established by layer 5 pyramidal neurons in the developing rat neocortex: comparison with synaptic innervation of adjacent neurons of the same class. *J. Neurosci.* *16*, 3209–3218.
- Luczak, A., Barthó, P., Marguet, S.L., Buzsáki, G., and Harris, K.D. (2007). Sequential structure of neocortical spontaneous activity in vivo. *Proc. Natl. Acad. Sci. U. S. A.* *104*, 347–352.
- Mainen, Z.F., and Sejnowski, T.J. (1996). Influence of dendritic structure on firing pattern in model neocortical neurons. *Nature* *382*, 363–366.
- Major, G., Polsky, A., Denk, W., Schiller, J., and Tank, D.W. (2008). Spatiotemporally graded NMDA spike/plateau potentials in basal dendrites of neocortical pyramidal neurons. *J. Neurophysiol.* *99*, 2584–2601.
- Major, G., Larkum, M.E., and Schiller, J. (2013). Active properties of neocortical pyramidal neuron dendrites. *Annu. Rev. Neurosci.* *36*, 1–24.
- Mann, E.O., Kohl, M.M., and Paulsen, O. (2009). Distinct roles of GABA(A) and GABA(B) receptors in balancing and terminating persistent cortical activity. *J. Neurosci.* *29*, 7513–7518.
- Markram, H. (1997). A network of tufted layer 5 pyramidal neurons. *Cereb. Cortex* *7*, 523–533.
- Markram, H., Lübke, J., Frotscher, M., Roth, A., and Sakmann, B. (1997). Physiology and anatomy of synaptic connections between thick tufted pyramidal neurones in the developing rat neocortex. *J. Physiol.* *500 (Pt 2)*, 409–440.
- Markram, H., Toledo-Rodriguez, M., Wang, Y., Gupta, A., Silberberg, G., and Wu, C. (2004). Interneurons of the neocortical inhibitory system. *Nat. Rev. Neurosci.* *5*, 793–807.
- McCormick, D. a (2003). Persistent Cortical Activity: Mechanisms of Generation and Effects on Neuronal Excitability. *Cereb. Cortex* *13*, 1219–1231.
- McCulloch, W.S., and Pitts, W. (1943). A logical calculus of the ideas immanent in nervous activity. *Bull. Math. Biophys.* *5*, 115–133.
- Metz, A.E., Jarsky, T., Martina, M., and Spruston, N. (2005). R-type calcium channels contribute to afterdepolarization and bursting in hippocampal CA1 pyramidal neurons. *J. Neurosci.* *25*, 5763–5773.
- Migliore, M., and Shepherd, G.M. (2002). Emerging rules for the distributions of active dendritic conductances. *Nat. Rev. Neurosci.* *3*, 362–370.
- Miller, E.K. (2000). The prefrontal cortex and cognitive control. *Nat. Rev. Neurosci.* *1*, 59–65.
- Miller, E.K., Erickson, C. a, and Desimone, R. (1996). Neural mechanisms of visual working memory in prefrontal cortex of the macaque. *J. Neurosci.* *16*, 5154–5167.
- Miller, E.K., Freedman, D.J., and Wallis, J.D. (2002). The prefrontal cortex: categories, concepts and cognition. *Philos. Trans. R. Soc. Lond. B. Biol. Sci.* *357*, 1123–1136.
- Milojkovic, B. a, Zhou, W.-L.W.-L., and Antic, S.D. (2007). Voltage and calcium transients in basal dendrites of the rat prefrontal cortex. *J. Physiol.* *585*, 447–468.
- Molnár, Z., and Cheung, A.F.P. (2006). Towards the classification of subpopulations of layer V pyramidal projection neurons. *Neurosci. Res.* *55*, 105–115.

- Morishima, M., and Kawaguchi, Y. (2006). Recurrent connection patterns of corticostriatal pyramidal cells in frontal cortex. *J. Neurosci.* *26*, 4394–4405.
- Morishima, M., Morita, K., Kubota, Y., and Kawaguchi, Y. (2011). Highly differentiated projection-specific cortical subnetworks. *J. Neurosci.* *31*, 10380–10391.
- Murayama, M., Pérez-Garci, E., Nevian, T., Bock, T., Senn, W., and Larkum, M.E. (2009). Dendritic encoding of sensory stimuli controlled by deep cortical interneurons. *Nature* *457*, 1137–1141.
- Murphy, B.K., and Miller, K.D. (2003). Multiplicative Gain Changes Are Induced by Excitation or Inhibition Alone. *J. Neurosci.* *23*, 10040–10051.
- Myme, C.I.O., Sugino, K., Turrigiano, G.G., and Nelson, S.B. (2003). The NMDA-to-AMPA ratio at synapses onto layer 2/3 pyramidal neurons is conserved across prefrontal and visual cortices. *J. Neurophysiol.* *90*, 771–779.
- Nasif, F.J., Sidiropoulou, K., Hu, X.-T., and White, F.J. (2005). Repeated cocaine administration increases membrane excitability of pyramidal neurons in the rat medial prefrontal cortex. *Pharmacol. Exp. Ther.* *312*, 1305–1313.
- Nevian, T., Larkum, M.E., Polsky, A., and Schiller, J. (2007). Properties of basal dendrites of layer 5 pyramidal neurons: a direct patch-clamp recording study. *Nat. Neurosci.* *10*, 206–214.
- Oikonomou, K.D., Short, S.M., Rich, M.T., and Antic, S.D. (2012). Extrasynaptic glutamate receptor activation as cellular bases for dynamic range compression in pyramidal neurons. *Front. Physiol.* *3*, 334.
- Oswald, A.-M.M., Doiron, B., Rinzel, J., and Reyes, A.D. (2009). Spatial profile and differential recruitment of GABAB modulate oscillatory activity in auditory cortex. *J. Neurosci.* *29*, 10321–10334.
- Otsuka, T., and Kawaguchi, Y. (2008). Firing-pattern-dependent specificity of cortical excitatory feed-forward subnetworks. *J. Neurosci.* *28*, 11186–11195.
- Oviedo, H. V, and Reyes, A.D. (2005). Variation of input-output properties along the somatodendritic axis of pyramidal neurons. *J. Neurosci.* *25*, 4985–4995.
- Oviedo, H. V, and Reyes, A.D. (2012). Integration of subthreshold and suprathreshold excitatory barrages along the somatodendritic axis of pyramidal neurons. *PLoS One* *7*, e33831.
- Papoutsis, A., Kastellakis, G., Psarrou, M., Anastasakis, S., and Poirazi, P. (2013). Coding and decoding with dendrites. *J. Physiol. Paris*.
- Parekh, R., and Ascoli, G.A. (2013). Neuronal morphology goes digital: a research hub for cellular and system neuroscience. *Neuron* *77*, 1017–1038.
- Perin, R., Berger, T.K., and Markram, H. (2011). A synaptic organizing principle for cortical neuronal groups. *Proc. Natl. Acad. Sci. U. S. A.* *108*, 5419–5424.
- Petanjek, Z., Judas, M., Kostovic, I., and Uylings, H.B.M. (2007). Lifespan Alterations of Basal Dendritic Trees of Pyramidal Neurons in the Human Prefrontal Cortex: A Layer-Specific Pattern. *Cereb. Cortex* *18*, 915–929.
- Peteanu, L., Mao, T., Sternson, S.M., and Svoboda, K. (2009). The subcellular organization of neocortical excitatory connections. *Nature* *457*, 1142–1145.

- Petrides, M. (2005). Lateral prefrontal cortex: architectonic and functional organization. *Philos. Trans. R. Soc. Lond. B. Biol. Sci.* *360*, 781–795.
- Peyrache, A., Khamassi, M., Benchenane, K., Wiener, S.I., and Battaglia, F.P. (2009). Replay of rule-learning related neural patterns in the prefrontal cortex during sleep. *Nat. Neurosci.* *12*, 919–926.
- Pissadaki, E.K., Sidiropoulou, K., Reczko, M., and Poirazi, P. (2010). Encoding of spatio-temporal input characteristics by a CA1 pyramidal neuron model. *PLoS Comput. Biol.* *6*, e1001038.
- Poirazi, P., and Mel, B.W. (2001). Impact of active dendrites and structural plasticity on the memory capacity of neural tissue. *Neuron* *29*, 779–796.
- Poirazi, P., Brannon, T., and Mel, B.W. (2003a). Arithmetic of subthreshold synaptic summation in a model CA1 pyramidal cell. *Neuron* *37*, 977–987.
- Poirazi, P., Brannon, T., and Mel, B.W. (2003b). Pyramidal neuron as two-layer neural network. *Neuron* *37*, 989–999.
- Polsky, A., Mel, B.W., and Schiller, J. (2004). Computational subunits in thin dendrites of pyramidal cells. *Nat. Neurosci.* *7*, 621–627.
- Polsky, A., Mel, B.W., and Schiller, J. (2009). Encoding and decoding bursts by NMDA spikes in basal dendrites of layer 5 pyramidal neurons. *J. Neurosci.* *29*, 11891–11903.
- Rall, W. (1967). Distinguishing theoretical synaptic potentials computed for different soma-dendritic distributions of synaptic input. *J. Neurophysiol.* *30*, 1138–1168.
- Ramaswamy, S., Hill, S.L., King, J.G., Schürmann, F., Wang, Y., and Markram, H. (2012). Intrinsic morphological diversity of thick-tufted layer 5 pyramidal neurons ensures robust and invariant properties of in silico synaptic connections. *J. Physiol.* *590*, 737–752.
- Rao, S.G., Williams, G. V, and Goldman-Rakic, P.S. (1999). Isodirectional tuning of adjacent interneurons and pyramidal cells during working memory: evidence for microcolumnar organization in PFC. *J. Neurophysiol.* *81*, 1903–1916.
- Ratiu, P., Talos, I.-F., Haker, S., Lieberman, D., and Everett, P. (2004). The tale of Phineas Gage, digitally remastered. *J. Neurotrauma* *21*, 637–643.
- Reimann, M.W., Anastassiou, C.A., Perin, R., Hill, S.L., Markram, H., and Koch, C. (2013). A Biophysically Detailed Model of Neocortical Local Field Potentials Predicts the Critical Role of Active Membrane Currents. *Neuron* *79*, 375–390.
- Rinzel, J., and Rall, W. (1974). Transient response in a dendritic neuron model for current injected at one branch. *Biophys. J.* *14*, 759–790.
- Romo, R., Brody, C.D., Hernández, a, and Lemus, L. (1999). Neuronal correlates of parametric working memory in the prefrontal cortex. *Nature* *399*, 470–473.
- Russell, T.A., Rubia, K., Bullmore, E.T., Soni, W., Suckling, J., Brammer, M.J., Simmons, A., Williams, S.C., and Sharma, T. (2000). Exploring the social brain in schizophrenia: left prefrontal underactivation during mental state attribution. *Am. J. Psychiatry* *157*, 2040–2042.
- Sanchez-Vives, M. V, and McCormick, D. a (2000). Cellular and network mechanisms of rhythmic recurrent activity in neocortex. *Nat. Neurosci.* *3*, 1027–1034.

- Sanders, H., Berends, M., Major, G., Goldman, M.S., and Lisman, J.E. (2013). NMDA and GABAB (KIR) conductances: the “perfect couple” for bistability. *J. Neurosci.* *33*, 424–429.
- Sarid, L., Bruno, R., Sakmann, B., Segev, I., and Feldmeyer, D. (2007). Modeling a layer 4-to-layer 2/3 module of a single column in rat neocortex: interweaving in vitro and in vivo experimental observations. *Proc. Natl. Acad. Sci. U. S. A.* *104*, 16353–16358.
- Sato, T.R., Gray, N.W., Mainen, Z.F., and Svoboda, K. (2007). The functional microarchitecture of the mouse barrel cortex. *PLoS Biol.* *5*, e189.
- Schaefer, A.T., Larkum, M.E., Sakmann, B., and Roth, A. (2003). Coincidence detection in pyramidal neurons is tuned by their dendritic branching pattern. *J. Neurophysiol.* *89*, 3143–3154.
- Schaefer, A.T., Helmstaedter, M., Schmitt, A.C., Bar-Yehuda, D., Almog, M., Ben-Porat, H., Sakmann, B., and Korngreen, A. (2007). Dendritic voltage-gated K⁺ conductance gradient in pyramidal neurones of neocortical layer 5B from rats. *J. Physiol.* *579*, 737–752.
- Schneider, C.J., Bezaire, M., and Soltesz, I. (2012). Toward a full-scale computational model of the rat dentate gyrus. *Front. Neural Circuits* *6*, 83.
- De Schutter, E., Ekeberg, O., Kotaleski, J.H., Achard, P., and Lansner, A. (2005). Biophysically detailed modelling of microcircuits and beyond. *Trends Neurosci.* *28*, 562–569.
- Seamans, J.K. (2003). Synaptic Basis of Persistent Activity in Prefrontal Cortex In Vivo and in Organotypic Cultures. *Cereb. Cortex* *13*, 1242–1250.
- Seamans, J.K., and Yang, C.R. (2004). The principal features and mechanisms of dopamine modulation in the prefrontal cortex. *Prog. Neurobiol.* *74*, 1–58.
- Seamans, J.K., Durstewitz, D., Christie, B.R., Stevens, C.F., and Sejnowski, T.J. (2001). Dopamine D1/D5 receptor modulation of excitatory synaptic inputs to layer V prefrontal cortex neurons. *Proc. Natl. Acad. Sci. U. S. A.* *98*, 301–306.
- Seamans, J.K., Lapish, C.C., and Durstewitz, D. (2008). Comparing the prefrontal cortex of rats and primates: insights from electrophysiology. *Neurotox. Res.* *14*, 249–262.
- Segev, I., and London, M. (2000). Untangling dendrites with quantitative models. *Science* *290*, 744–750.
- Seung, H.S. (2009). Reading the book of memory: sparse sampling versus dense mapping of connectomes. *Neuron* *62*, 17–29.
- Shafi, M., Zhou, Y., Quintana, J., Chow, C., Fuster, J.M., and Bodner, M. (2007). Variability in neuronal activity in primate cortex during working memory tasks. *Neuroscience* *146*, 1082–1108.
- Shu, Y., Hasenstaub, A.R., and McCormick, D. a (2003). Turning on and off recurrent balanced cortical activity. *Nature* *423*, 288–293.
- Sidiropoulou, K., and Poirazi, P. (2012). Predictive Features of Persistent Activity Emergence in Regular Spiking and Intrinsic Bursting Model Neurons. *PLoS Comput. Biol.* *8*, e1002489.
- Sidiropoulou, K., Lu, F.-M., Fowler, M.A., Xiao, R., Phillips, C., Ozkan, E.D., Zhu, M.X., White, F.J., and Cooper, D.C. (2009). Dopamine modulates an mGluR5-mediated depolarization underlying prefrontal persistent activity. *Nat. Neurosci.* *12*, 190–199.

- Silver, R.A. (2010). Neuronal arithmetic. *Nat. Rev. Neurosci.* *11*, 474–489.
- Sivyer, B., and Williams, S.R. (2013). Direction selectivity is computed by active dendritic integration in retinal ganglion cells. *Nat. Neurosci.* 1–10.
- Smith, S.L., Smith, I.T., Branco, T., and Häusser, M. (2013). Dendritic spikes enhance stimulus selectivity in cortical neurons in vivo. *Nature* *503*, 115–120.
- Song, S., Sjöström, P.J., Reigl, M., Nelson, S., and Chklovskii, D.B. (2005). Highly nonrandom features of synaptic connectivity in local cortical circuits. *PLoS Biol.* *3*, e68.
- Spruston, N. (2008). Pyramidal neurons: dendritic structure and synaptic integration. *Nat. Rev. Neurosci.* *9*, 206–221.
- Squire, L.R., Berg, D., Bloom, F.E., Lac, S. Du, and Ghosh, A. (2012). *Fundamental neuroscience* (Chicago: Academic Press).
- Sterratt, D., Graham, B., Gillies, A., and Willshaw, D. (2011). *Principles of Computational Modelling in Neuroscience* (Cambridge University Press).
- Stiefel, K.M., and Sejnowski, T.J. (2007). Mapping function onto neuronal morphology. *J. Neurophysiol.* *98*, 513–526.
- Stuart, G.J., and Sakmann, B. (1994). Active propagation of somatic action potentials into neocortical pyramidal cell dendrites. *Nature* *367*, 69–72.
- Sun, X., Gu, X.Q., and Haddad, G.G. (2003). Calcium influx via L- and N-type calcium channels activates a transient large-conductance Ca²⁺-activated K⁺ current in mouse neocortical pyramidal neurons. *J. Neurosci.* *23*, 3639–3648.
- Tahvildari, B., Fransén, E., Alonso, A.A., Hasselmo, M.E., and Franse, E. (2007). Switching between “On” and “Off” states of persistent activity in lateral entorhinal layer III neurons. *Hippocampus* *17*, 257–263.
- Takahashi, H., and Magee, J.C. (2009). Pathway interactions and synaptic plasticity in the dendritic tuft regions of CA1 pyramidal neurons. *Neuron* *62*, 102–111.
- Tamás, G., Buhl, E.H., and Somogyi, P. (1997a). Fast IPSPs elicited via multiple synaptic release sites by different types of GABAergic neurone in the cat visual cortex. *J. Physiol.* *500* (Pt 3, 715–738.
- Tamás, G., Buhl, E.H., and Somogyi, P. (1997b). Massive autaptic self-innervation of GABAergic neurons in cat visual cortex. *J. Neurosci.* *17*, 6352–6364.
- Tegnér, J., Compte, A., and Wang, X.-J. (2002). The dynamical stability of reverberatory neural circuits. *Biol. Cybern.* *87*, 471–481.
- Thomson, A.M., and Destexhe, A. (1999). Dual intracellular recordings and computational models of slow inhibitory postsynaptic potentials in rat neocortical and hippocampal slices. *Neuroscience* *92*, 1193–1215.
- Thomson, A.M., and Deuchars, J. (1997). Synaptic interactions in neocortical local circuits: dual intracellular recordings in vitro. *Cereb. Cortex* *7*, 510.

- Thomson, A.M., and Lamy, C. (2007). Functional maps of neocortical local circuitry. *Front. Neurosci.* *1*, 19–42.
- Thomson, A.M., West, D.C.C., Hahn, J., and Deuchars, J. (1996). Single axon IPSPs elicited in pyramidal cells by three classes of interneurons in slices of rat neocortex. *J. Physiol.* *496* (Pt 1, 81–102.
- Thuault, S.J., Malleret, G., Constantinople, C.M., Nicholls, R., Chen, I., Zhu, J., Panteleyev, A., Vronskaya, S., Nolan, M.F., Bruno, R., et al. (2013). Prefrontal Cortex HCN1 Channels Enable Intrinsic Persistent Neural Firing and Executive Memory Function. *J. Neurosci.* *33*, 13583–13599.
- Thurley, K., Senn, W., and Lüscher, H.-R. (2008). Dopamine increases the gain of the input-output response of rat prefrontal pyramidal neurons. *J. Neurophysiol.* *99*, 2985–2997.
- Trachtenberg, J.T., Chen, B.E., Knott, G.W., Feng, G., Sanes, J.R., Welker, E., and Svoboda, K. (2002). Long-term in vivo imaging of experience-dependent synaptic plasticity in adult cortex. *Nature* *420*, 788–794.
- Tseng, K.Y., and O'Donnell, P. (2005). Post-pubertal emergence of prefrontal cortical up states induced by D1-NMDA co-activation. *Cereb. Cortex* *15*, 49–57.
- Tsiola, A., Hamzei-Sichani, F., Peterlin, Z., and Yuste, R. (2003). Quantitative morphologic classification of layer 5 neurons from mouse primary visual cortex. *J. Comp. Neurol.* *461*, 415–428.
- Tziridis, K., Dicke, P.W., and Thier, P. (2009). The role of the monkey dorsal pontine nuclei in goal-directed eye and hand movements. *J. Neurosci.* *29*, 6154–6166.
- Vetter, P., Roth, A., and Häusser, M. (2001). Propagation of action potentials in dendrites depends on dendritic morphology. *J. Neurophysiol.* *85*, 926–937.
- Wang, X.-J. (1999). Synaptic basis of cortical persistent activity: the importance of NMDA receptors to working memory. *J. Neurosci.* *19*, 9587–9603.
- Wang, X.-J. (2001). Synaptic reverberation underlying mnemonic persistent activity. *Trends Neurosci.* *24*, 455–463.
- Wang, H.-X., and Gao, W.-J. (2009). Cell type-specific development of NMDA receptors in the interneurons of rat prefrontal cortex. *Neuropsychopharmacology* *34*, 2028–2040.
- Wang, J., and O'Donnell, P. (2001). D(1) dopamine receptors potentiate nmda-mediated excitability increase in layer V prefrontal cortical pyramidal neurons. *Cereb. Cortex* *11*, 452–462.
- Wang, H., Stradtman, G.G.G., Wang, X.-J., and Gao, W.-J.J. (2008). A specialized NMDA receptor function in layer 5 recurrent microcircuitry of the adult rat prefrontal cortex, supplement. *Proc. Natl. Acad. Sci. U. S. A.* *105*, 16791.
- Wang, M., Ramos, B.P., Paspalas, C.D., Shu, Y., Simen, A., Duque, A., Vijayraghavan, S., Brennan, A., Dudley, A., Nou, E., et al. (2007). Alpha2A-adrenoceptors strengthen working memory networks by inhibiting cAMP-HCN channel signaling in prefrontal cortex. *Cell* *129*, 397–410.
- Wang, M., Yang, Y., Wang, C.-J., Gamo, N.J.J., Jin, L.E.E., Mazer, J.A. a, Morrison, J.H.H., Wang, X.-J., and Arnsten, A.F.T. (2013). NMDA Receptors Subserve Persistent Neuronal Firing during Working Memory in Dorsolateral Prefrontal Cortex. *Neuron* *77*, 736–749.

- Wang, Y., Markram, H., Goodman, P.H., Berger, T.K., Ma, J., and Goldman-Rakic, P.S. (2006). Heterogeneity in the pyramidal network of the medial prefrontal cortex. *Nat. Neurosci.* *9*, 534–542.
- Watanabe, Y., and Funahashi, S. (2004). Neuronal activity throughout the primate mediodorsal nucleus of the thalamus during oculomotor delayed-responses. I. Cue-, delay-, and response-period activity. *J. Neurophysiol.* *92*, 1738–1755.
- Weaver, C.M., and Wearne, S.L. (2008). Neuronal firing sensitivity to morphologic and active membrane parameters. *PLoS Comput. Biol.* *4*, e11.
- Wei, D.S., Mei, Y. a, Bagal, A., Kao, J.P., Thompson, S.M., and Tang, C.M. (2001). Compartmentalized and binary behavior of terminal dendrites in hippocampal pyramidal neurons. *Science* *293*, 2272–2275.
- Wilgus, J., and Wilgus, B. (2009). Face to face with Phineas Gage. *J. Hist. Neurosci.* *18*, 340–345.
- Van Wingerden, M., Vinck, M., Tijms, V., Ferreira, I.R.S., Jonker, A.J., and Pennartz, C.M.A. (2012). NMDA receptors control cue-outcome selectivity and plasticity of orbitofrontal firing patterns during associative stimulus-reward learning. *Neuron* *76*, 813–825.
- Winograd, M., Destexhe, A., and Sanchez-Vives, M. V (2008). Hyperpolarization-activated graded persistent activity in the prefrontal cortex. *Proc. Natl. Acad. Sci. U. S. A.* *105*, 7298–7303.
- Woo, R.-S., Li, X.-M., Tao, Y., Carpenter-Hyland, E., Huang, Y.Z., Weber, J., Neiswender, H., Dong, X.-P., Wu, J., Gassmann, M., et al. (2007). Neuregulin-1 enhances depolarization-induced GABA release. *Neuron* *54*, 599–610.
- Woodward, J.J., and Pava, M.J. (2009). Effects of ethanol on persistent activity and up-States in excitatory and inhibitory neurons in prefrontal cortex. *Alcohol. Clin. Exp. Res.* *33*, 2134–2140.
- Xu, N., Harnett, M.T., Williams, S.R., Huber, D., O'Connor, D.H., Svoboda, K., and Magee, J.C. (2012). Nonlinear dendritic integration of sensory and motor input during an active sensing task. *Nature* *492*, 247–251.
- Yamada, M., Pita, M.D.C.R., Iijima, T., and Tsutsui, K.-I. (2010). Rule-dependent anticipatory activity in prefrontal neurons. *Neurosci. Res.* *67*, 162–171.
- Yang, C.R., Seamans, J.K., and Gorelova, N. (1996). Electrophysiological and morphological properties of layers V-VI principal pyramidal cells in rat prefrontal cortex in vitro. *J. Neurosci.* *16*, 1904–1921.
- Yassin, L., Benedetti, B.L., Jouhanneau, J.-S., Wen, J. a, Poulet, J.F. a, and Barth, A.L. (2010). An embedded subnetwork of highly active neurons in the neocortex. *Neuron* *68*, 1043–1050.
- Yoshimura, Y., and Callaway, E.M. (2005). Fine-scale specificity of cortical networks depends on inhibitory cell type and connectivity. *Nat. Neurosci.* *8*, 1552–1559.
- Yoshimura, Y., Dantzker, J.L.M., and Callaway, E.M. (2005). Excitatory cortical neurons form fine-scale functional networks. *Nature* *433*, 868–873.
- Young, C.E., and Yang, C.R. (2004). Dopamine D1/D5 receptor modulates state-dependent switching of soma-dendritic Ca²⁺ potentials via differential protein kinase A and C activation in rat prefrontal cortical neurons. *J. Neurosci.* *24*, 8–23.

- Yu, Y.-C., Bultje, R.S., Wang, X., and Shi, S.-H. (2009). Specific synapses develop preferentially among sister excitatory neurons in the neocortex. *Nature* *458*, 501–504.
- Yu, Y.-C., He, S., Chen, S., Fu, Y., Brown, K.N., Yao, X.-H., Ma, J., Gao, K.P., Sosinsky, G.E., Huang, K., et al. (2012). Preferential electrical coupling regulates neocortical lineage-dependent microcircuit assembly. *Nature* *486*, 113–117.
- Zador, A.M., Agmon-Snir, H., and Segev, I. (1995). The morphoelectrotonic transform: a graphical approach to dendritic function. *J. Neurosci.* *15*, 1669–1682.
- Zhang, W., and Linden, D.J. (2003). The other side of the engram: experience-driven changes in neuronal intrinsic excitability. *Nat. Rev. Neurosci.* *4*, 885–900.
- Zhang, Z., Reboreda, A., Alonso, A., Barker, P. a, and Séguéla, P. (2011). TRPC channels underlie cholinergic plateau potentials and persistent activity in entorhinal cortex. *Hippocampus* *21*, 386–397.
- Zhang, Z., Cordeiro Matos, S., Jegó, S., Adamantidis, A., and Séguéla, P. (2013). Norepinephrine Drives Persistent Activity in Prefrontal Cortex via Synergistic $\alpha 1$ and $\alpha 2$ Adrenoceptors. *PLoS One* *8*, e66122.
- Zheng, P., Zhang, X.-X., Bunney, B.S., and Shi, W.-X. (1999). Opposite modulation of cortical N-methyl-d-aspartate receptor-mediated responses by low and high concentrations of dopamine. *Neuroscience* *91*, 527–535.
- Zikopoulos, B., and Barbas, H. (2007). Parallel driving and modulatory pathways link the prefrontal cortex and thalamus. *PLoS One* *2*, e848.

10 Appendix

10.1 Tables

10.1.1 Structure of model cells with simplified morphology

	Length (μm)	Diameter (μm)
Pyramidal cell		
Soma	75	10.14
Basal dendrite	150	1
Proximal apical dendrite	400	3.4
Distal apical dendrite	400	2.6
Axon	113.22	1.1
Inhibitory interneuron		
Soma	53	42
Axon	113.22	0.7

10.1.2 Passive properties of simplified pyramidal cells and interneurons.

	$C_M, \mu\text{F}/\text{cm}^2$	$R_A, \text{ohm}/\text{cm}$	$R_M, \text{k}\Omega \text{ cm}^2$
Pyramidal cell			
Soma	1.2	100	16
Basal dendrite	2	100	5.9
Proximal apical dendrite	1.2	150	5.9
Distal apical dendrite	1.2	150	5.9
Axon	1.2	150	12
Inhibitory interneuron			
Soma	1.2	150	15
Axon	1.2	150	15

10.1.3 Active ionic properties of simplified pyramidal neurons

Mechanisms	Soma	Axon	Basal Dendrites	Proximal Apical dendrites	Distal Apical dendrites
Fast sodium, S/cm^2	0.1809	0.18	0.0018	0.005	0.0036
Delayed rectifier K^+, S/cm^2	0.0216	0.0054	0.0054	2.16e-5	5.4e-6
Persistent sodium, S/cm^2	0.18e-5	0	1.8e-5	5.4e-5	1.8e-4
A-type K^+, S/cm^2	7e-4	0	7e-4	7e-5	7e-5
D-type K^+, S/cm^2	1.026e-3	0	6e-4	1.2e-3	1.2e-3

N-type calcium, S/cm ²	2e-5	0	6e-5	6e-5	1e-3
T-type calcium, S/cm ²	6e-6	0	0	6e-5	6e-6
CaR, S/cm ²	3e-5	0	0	9e-6	1.5e-3
L-type calcium, S/cm ²	3e-5	0	0	1.9e-4	3.6e-6
sAHP, S/cm ²	1.4e-1	0	0	2.75e-3	2.75e-5
fAHP, S/cm ²	2.2e-3	0	0	2.2e-5	2.2e-6
H-current, S/cm ²	7.2e-6	0	9e-6	1.4e-5	9e-5
dADP current, S/cm ²	0	0	0	0	0
Calcium diffusion model	Yes	No	Yes	Yes	Yes
E _{Na} , mV	+55	+55	+55	+55	+55
E _K , mV	-80	-80	-80	-80	-80
E _{Ca} , mV	+140	-	+140	+140	+140
E _h , mV	-10	-	-10	-10	-10
E _L , mV	-65	-65	-65	-65	-65

10.1.4 Distributions of active and passive conductances of the pyramidal neurons with detailed morphology (adapted from (Sidiropoulou, Poirazi, 2012)).

Mechanisms	Soma	Axon	Basal Dendrites	Apical Dendrites
R _m (KΩ*cm ²)	30	30	Uniform: 24 or sigmoidally decreased up to half of the somatic conductance: 30+(15-30)/(1.0+ exp (10-distance/5))	Sigmoidally decreased up to half of the somatic conductance: 30 + (15-30)/(1.0+ exp (300-distance/50))
R _a (Ω*cm)	100	100	100	50
C _m (μf/cm ²)	1.2	1.2	2	1.2
Fast sodium, S/cm ²	0.155	0.31	0.0031	0.0062
Delayed rectifier K ⁺ , S/cm ²	0.045	0.045	0.00405	0.000045
Persistent sodium, S/cm ²	0.6e-5	0	0.6e-5	If distance from the soma <200μm: 0.6e-5

					If distance from the soma >200μm: 3e-5 *(<distance>/200)
A-type S/cm²	K⁺,	9e-4	0	Uniform: 31.5e-4 or If distance from the soma <50μm: 18e-4 If distance from the soma >50μm: 45e-4	If distance from the soma <100μm: 9e-4 If distance from the soma >100μm but <300μm: 9e-5*(300/<distance>) If distance from the soma >300μm: 9e-5
D-type S/cm²	K⁺,	5.28e-3	0	0	If distance from the soma <100μm: 5.28e-3 If distance from the soma >100μm but <300μm: 5.28e-4*(300/<distance>) If distance from the soma >300μm: 5.28e-4
N-type calcium, S/cm²		0.3e-4	0	Uniform: 1.95e-6 or If distance from the soma <50μm: 1e-6 If distance from the soma >50μm: 3e-6	If distance from the soma <200μm: 1e-6 If distance from the soma >200μm: 0.96e-4*(<distance>/200)
T-type calcium, S/cm²		1e-4	0	1e-5	If distance from the soma <200μm: 1e-4 If distance from the soma >200μm: 1e-4*(<distance>/200)
R-type calcium, S/cm²		37.5e-5	0	0	If distance from the soma <200μm: 18.75e-5 If distance from the soma >200μm: 37.5e-5*(<distance>/200)
L-type calcium, S/cm²		3e-4	0	0	If distance from the soma <200μm: 3e-4 If distance from the soma >200μm: 3e-4*(30/<distance>)
sAHP, S/cm²		1.25e-2	0	0	If distance from the soma <200μm: 1.25e-3

				If distance from the soma >200 μ m: 1.25e-6
fAHP, S/cm ²	3e-5	0	0	If distance from the soma <200 μ m: 15e-7 If distance from the soma >200 μ m: 3e-8
H-current, S/cm ²	9.36e-6	0	9.36e-6	Increases sigmoidally up to 10x the somatic conductance using the following equation: $9.36e-6 + (93.6e-6 - 9.36e-6) / (1.0 + \exp(300 - \text{distance} / 50))$
dADP current, S/cm ²	0	0	0	0
Calcium diffusion model	Yes	No	Yes	Yes

10.1.5 Active ionic properties of inhibitory interneurons

Mechanisms	Soma	Axon
Sodium conductance, S/cm ²	0.225	0.54
Delayed rectifier, S/cm ²	0.018	0.018
D-type K ⁺ , S/cm ²	7.25e-5	0
E _{Na} , mV	+55	+55
E _K , mV	-80	-80
E _L , mV	-70	-70

10.1.6 Synaptic parameters

	AMPA	NMDA	GABA _A	GABA _B
Pyramidal cell				
Conductance, nS	0.00019 (basal) 0.00024 (apical)	0.25 (basal) 0.22 (apical)	6.9e-4	1.05e-4
Reversal potential, mV	0	0	-80	-80
Rise time, ms	0.6*	4.3	1.5	9.8
Fall time, ms	4.3*	93	14	72
Inhibitory interneuron				

Conductance, nS	7.5e-4	3.2e-4	5.1e-4	-
Reversal potential, mV	0	0	-80	-
Rise time, ms	0.3*	0.5*	3	-
Fall time, ms	5.5*	66.3*	24	-

*Data adapted from voltage-clamp recordings

10.1.7 Summary of synaptic connections in the microcircuit.

Type of connection	Location	# of synapses	Reference
Thalamocortical (incoming)	Proximal dendrite	90	(Kuroda M <i>et al.</i> , 1998)
Pyramidal recurrent	Basal dendrite	5	(Markram <i>et al.</i> , 1997)
Pyramidal-to-interneuron	Soma	2	(Buhl <i>et al.</i> , 1997)
Autapses in pyramidal neurons	Basal dendrite	1	(Lübke <i>et al.</i> , 1996; Tamás <i>et al.</i> , 1997b)
Interneuron-to-pyramidal	Soma	4	(Tamás <i>et al.</i> , 1997a)
Autapses in the interneuron	Soma	12 synaptic contacts producing ~350pA	(Tamás <i>et al.</i> , 1997b; Bacci <i>et al.</i> , 2003)

10.1.8 Mean \pm std of the morphological features between SIG and SUB

	Diameter (μ m)	Length (μ m)	EL	MEP	Path diameter (μ m)	Path length (μ m)	Branch order
SIG	0.78 \pm 0.25	73.53 \pm 53.68	0.27 \pm 0.42	1.64 \pm 1	3.87 \pm 0.72	126.74 \pm 55.65	3.14 \pm 1.15
SUB	1.71 \pm 0.74	25.1 \pm 20.74	1.34 \pm 3.61	2.22 \pm 1.18	5.38 \pm 1.03	38.64 \pm 23.87	1.82 \pm 0.88

10.1.9 Classification results of the morphological features.

Feature	Accuracy	Sensitivity	Specificity	Threshold
Path Length	0.87±0.02	0.82±0.04	0.91±0.03	76.45 μm
Diameter	0.85±0.02	0.95±0.02	0.75±0.04	1.19 μm
Mean diameter	0.78±0.04	0.88±0.05	0.69±0.04	4.66 μm
Length	0.74±0.03	0.55±0.05	0.92±0.02	54.63 μm
Branch Order	0.76±0.03	0.71±0.04	0.8±0.03	3
EL	0.62±0.03	0.97±0.02	0.26±0.05	1.14
MEP	0.63±0.08	0.91±0.05	0.35±0.21	2.21

10.1.10 Mean ± std of the predictive morphological features between SIG and SUB dendrites from the 9 case neurons.

	Path length (μm)	Diameter (μm)	Branch order
SIG	133.2±55.51	0.67±0.2	2.71±1.02
SUB	43.33± 26.38	1.53±0.71	1.68± 0.82

10.2 Mathematical formalism

10.2.1 Pyramidal cell

The somatic (s), axonic (a), basal (bd) and apical (ad) dendritic compartments obey the following current balance equations:

$$C_m \frac{dV_s}{dt} = I_l + I_{Na_f} + I_{Na_P} + I_{K_{dr}} + I_D + I_A + I_{SAHP} + I_{fAHP} + I_{CaL} + I_{CaN} + I_{CaR} + I_{CaT} + I_h + I_{dADP} + I_{syn} \quad (1)$$

$$C_m \frac{dV_{bd}}{dt} = I_l + I_{Na_f} + I_{Na_P} + I_{K_{dr}} + I_D + I_A + I_{CaN} + I_h + I_{dADP} + I_{syn} \quad (2)$$

$$C_m \frac{dV_{ad}}{dt} = I_l + I_{Na_f} + I_{Na_P} + I_{K_{dr}} + I_D + I_A + I_{SAHP} + I_{fAHP} + I_{CaL} + I_{CaN} + I_{CaR} + I_{CaT} + I_h + I_{dADP} + I_{syn} \quad (3)$$

$$C_m \frac{dV_a}{dt} = I_l + I_{Na_f} + I_{K_{dr}} \quad (4)$$

where I_l is the leak current, I_{Na_f} is the fast sodium current, I_{Na_P} is the persistent sodium current, $I_{K_{dr}}$ is the delayed rectifier K^+ current, I_D and I_A are the D- and A-type K^+ currents, respectively, I_{SAHP} and I_{fAHP} are the slow and fast after-hyperpolarizing (AHP) currents, I_{CaL} , I_{CaN} , I_{CaT} and I_{CaR} are the L-, N-, T- and R-type calcium currents, I_h is the h-current, I_{dADP} is the CAN current.

10.2.1.1 The leak current

$$I_l = g_l * (V - E_l) \quad (5)$$

where for pyramidal neurons $E_l = -65$ mV.

10.2.1.2 The fast sodium channel (Durstewitz & Gabriel, 2007)

$$I_{Na_f} = g_{Na(fast)} * (V - E_{rev}) \quad (6)$$

$$g_{Na(fast)} = g * m^3 * h$$

$$\frac{dm}{dt} = \frac{m_\infty - m}{t_m}$$

$$m_{\infty} = \frac{ma}{ma + mb}$$

$$ma = \frac{-0.2816 * (v + 28)}{-1 + e^{\frac{-v+28}{9.3}}}$$

$$mb = \frac{0.2464 * (v + 1)}{-1 + e^{\frac{v+1}{6}}}$$

$$t_m = \frac{1}{ma + mb}$$

$$\frac{dh}{dt} = \frac{h_{\infty} - h}{t_h}$$

$$h_{\infty} = \frac{ha}{ha + hb}$$

$$ha = \frac{0.098}{e^{\frac{v+23.1}{20}}}$$

$$hb = \frac{1.4}{1 + e^{\frac{-(v+25.1)}{10}}}$$

$$t_h = \frac{1}{ha + hb}$$

where $E_{rev}=0$ mV.

10.2.1.3 The persistent sodium channel (Durstewitz & Gabriel, 2007)

$$I_{NaP} = g_{NaP} * (V - E_{rev}) \tag{7}$$

$$g_{NaP} = g * m * h$$

$$ma = \frac{-0.2816 * (v + 12)}{-1 + e^{\frac{-v+12}{9.3}}}$$

$$mb = \frac{0.2464 * (v - 15)}{-1 + e^{\frac{v-15}{6}}}$$

$$ha = 2.8e^{-5} * e^{\frac{-(v+42.8477)}{4.0248}}$$

$$hb = \frac{0.02}{1 + e^{\frac{-(v-413.9284)}{148.2589}}}$$

where $E_{rev} = 0$ mV and dm/dt , m_{∞} , t_m , dh/dt , h_{∞} , t_h as for fast sodium current.

10.2.1.4 The delayed rectifier potassium current (Durstewitz and Gabriel, 2007)

$$I_{Kdr} = g_{Kdr} * (V - E_{rev}) \quad (8)$$

$$g_{Kdr} = gmax * n^4$$

$$\frac{dn}{dt} = \frac{n_{\infty} - n}{t}$$

$$n_{\infty} = \frac{na}{na + nb}$$

$$t = \frac{1}{na + nb}$$

$$na = \frac{-0.018*(v-13)}{-1 + e^{\frac{-(v+13)}{25}}}$$

$$nb = \frac{0.00544 * (v - 23)}{-1 + e^{\frac{(v-23)}{12}}}$$

where $E_{rev} = 0$ mV.

10.2.1.5 The fast inactivating potassium current (Poirazi, Brannon, & Mel, 2003)

$$I_A = gmax * n * l * (V - E_K) \quad (9)$$

$$\frac{dn}{dt} = \frac{n_{\infty} - n}{tn}$$

$$\frac{dl}{dt} = \frac{l_{\infty} - l}{tl}$$

$$n_{\infty} = \frac{1}{1 + \alpha_n}$$

$$l_{\infty} = \frac{1}{1 + \alpha_l}$$

$$tn = \frac{betn}{qt * 0.1 * (1 + \alpha_n)}$$

$$betn = e^{\frac{0.001 * \left(-1.8 - \frac{1}{\frac{(v+40)}{1+e^{\frac{v}{5}}}} \right) * 0.39 * (v+1) * 9.648e4}{8.315 * (273.16 + celsius)}}$$

$$q_t = 5^{\frac{celsius - 24}{10}}$$

$$a_n = e^{\frac{0.001 * \left(-1.8 - \frac{1}{\frac{(v+40)}{1+e^{\frac{v}{5}}}} \right) * (v+1) * 9.648e4}{8.315 * (273.16 + celsius)}}$$

$$t_l = \frac{0.26}{v + 50}$$

$$a_l = e^{\frac{0.001 * 3 * (v+1) * 9.648e4}{8.315 * (273.16 + celsius)}}$$

10.2.1.6 L-type calcium current (Poirazi et al., 2003)

$$I_{Ca(L)} = g * (m^2 * h^2 + s^2 * 8) * (V - E_{Ca}) \quad (10)$$

$$\frac{dm}{dt} = \frac{m_{\infty} - m}{t_m}$$

$$m_{\infty} = \frac{1}{1 + a}$$

$$a = e^{\frac{0.001 * -4.6 * (v+1) * 9.648e4}{8.315 * (273.16 + celsius)}}$$

$$\frac{ds}{dt} = \frac{s_{\infty} - s}{t_s}$$

$$s_{\infty} = \frac{\alpha}{1 + \alpha}$$

$$\alpha = \left(\frac{[Ca^{+2}]_i}{b} \right)^2$$

$$t_s = 180 + \frac{1}{[Ca^{+2}]_i + 0.01}$$

$$h = \frac{0.025}{0.025 + [Ca^{+2}]_i}$$

where $t_m=1.5$ (ms).

10.2.1.7 N-type Calcium current (Poirazi et al., 2003)

$$I_{Ca(N)} = g * m^2 * h^2 * h_2 * (V - E_{Ca}) \quad (11)$$

$$\frac{dm}{dt} = \frac{m_{\infty} - m}{t_m}$$

$$m_{\infty} = \frac{1}{1 + a}$$

$$a = e^{\frac{0.001 * -3.4 * (v+21) * 9.648e4}{8.315 * (273.16 + celsius)}}$$

$$\frac{dh}{dt} = \frac{h_{\infty} - h}{t_h}$$

$$h_{\infty} = \frac{1}{1 + b}$$

$$b = e^{\frac{0.001*2*(v+40)*9.648e4}{8.315*(273.16+celsius)}}$$

$$h2 = \frac{0.025}{0.025 + [Ca^{+2}]_i}$$

where $t_m = 1.5$ ms and $t_h = 75$ ms and dm/dt , m_∞ as for L-type calcium current.

10.2.1.8 R-type calcium current (Poirazi et al., 2003)

$$I_{Ca(R)} = g * m^3 * h(V - E_{Ca}) \quad (12)$$

$$E_{CaR} = 1 \frac{e^3 * R * (celsius + 273.15)}{2 * Faraday} * \log \left(\frac{[Ca^{+2}]_o}{[Ca^{+2}]_i} \right)$$

$$m_\infty = \frac{1}{1 + e^{\frac{-(v+43.5)}{3}}}$$

$$h_\infty = \frac{1}{1 + e^{v+50}}$$

where $t_m = 70$ ms and $t_h = 20$ ms and dm/dt , dh/dt as for N-type calcium current.

10.2.1.9 Low threshold activated calcium current (Poirazi et al., 2003)

$$I_{Ca(R)} = g * m^2 * h * (V - E_{Ca}) \quad (13)$$

$$m_\infty = \frac{1}{1 + a}$$

$$a = e^{\frac{0.001*-3*(v+36)*9.648e4}{8.315*(273.16+celsius)}}$$

$$h_\infty = \frac{1}{1 + b}$$

$$b = e^{\frac{0.001*5.2*(v+68)*9.648e4}{8.315*(273.16+celsius)}}$$

where $t_m = 1.5$ ms, $t_h = 10$ ms and dm/dt , dh/dt as for N-type calcium current.

10.2.1.10 The fast calcium dependent potassium current (I_{fAHP}) (Shao et al., 1999)

$$I_{fAHP} = g * O * (V - E_K) \quad (14)$$

The channel has three states: active (O), non active (C) and inactivated (I). The transition from C to O is calcium dependent. The transition from O to I is voltage dependent and is responsible for the presence of the fast afterhyperpolarization potential. The transition from I to C is voltage dependent and slow as well.

$$\begin{aligned} C &\leftrightarrow O (K_3, K_4) \\ O &\leftrightarrow I (K_1, 0) \\ I &\leftrightarrow C (K_2, 0) \\ C + O + I &= 1 \end{aligned}$$

where K_1 , K_2 , K_4 are described by function a_2 and K_3 by function a_1 and correspond to the transition rates between open (O), close (C) and inactivated (I) states:

$$a_1 = \frac{1}{t_{min} + \frac{1}{\frac{1}{(t_{max} - t_{min})} + e^{\frac{(v-v_{half})}{K}}}} * 1e8 * ([Ca^{+2}]_i)^3$$

$$a_2 = \frac{1}{t_{min} + \frac{e^{-(v-v_{half})}}{K}}$$

where

	(ms)	(ms)	(mV)	K (mV)
K1	0.1	-	-10	1.0
K2	0.1	-	-120	-10.0
K3	0.001	1.0	-20	7.0
K4	0.2	-	-44	-5.0

and $[Ca^{+2}]_i$ is the internal calcium concentration (mM).

10.2.1.11 *The slow calcium dependent potassium channel I_{SAHP} (Poirazi et al., 2003)*

$$I_{SAHP} = g * m^2 * (V - E_{Ca}) \quad (15)$$

$$m_{\infty} = \frac{a}{a + 1}$$

$$a = \frac{[Ca^{+2}]_i}{0.008}$$

$$t_m = \frac{0.008}{[Ca^{+2}]_i + 0.008}$$

where $[Ca^{+2}]_i$ is the internal calcium concentration (mM) and dm/dt as for N-type calcium current.

10.2.1.12 *Hyperpolarization Activated Current I_h (Poirazi et al., 2003)*

$$I_h = g * n * (V - E_h) \quad (16)$$

$$\frac{dn}{dt} = \frac{n_{\infty} - n}{t_n}$$

$$n_{\infty} = 1 - \frac{1}{1 + e^{\frac{(-90-v)}{10}}}$$

$$t_n = 2 * \left(\frac{1}{e^{\frac{(v+145)}{-17.5}} + e^{\frac{v+16.8}{16.5}}} + 10 \right)$$

else when $v > -10$ $t_n = 1$ (ms). The reversal potential, $E_h = -10$ mV.

10.2.1.13 *Slow inactivating potassium current (I_D) (Durstewitz & Gabriel, 2007)*

$$I_D = g * a * b * (V - E_K) \quad (17)$$

$$\frac{da}{dt} = \frac{a_\infty - a}{t_a}$$

$$\frac{db}{dt} = \frac{b_\infty - b}{t_b}$$

$$a_\infty = \frac{1}{1 + e^{\frac{(v+34)}{6.5}}}$$

$$b_\infty = \frac{1}{1 + e^{\frac{(v+65)}{6.6}}}$$

$$t_b = 200 + \frac{3200}{1 + e^{\frac{-(v+63.6)}{4}}}$$

where $t_a=10$ ms.

10.2.1.14 *The dADP (CAN) mechanism (Sidiropoulou & Poirazi, 2012)*

$$I_{n(CAN)} = g * m^2 * (V - E_n) \quad (18)$$

$$I_{Na} = 0.7 * I_{n(CAN)}$$

$$m_\infty = \frac{\alpha}{\alpha + \beta}$$

$$t_m = \frac{1}{\frac{\alpha + \beta}{\tau_{adj}}}$$

$$\alpha = \beta * \left(\frac{[Ca^{+2}]_i}{cac} \right)^2$$

$$t_{adj} = 3^{\frac{celsius-22}{10}}$$

where beta = 0.0001 1/ms and cac = 0.0004 mM and dm/dt as for N-type calcium current.

10.2.2 Inhibitory interneuron

The somatic (s) and axonic (a) compartments obey the following current balance equations:

$$C_m \frac{dV_s}{dt} = I_l + I_{Naf} + I_{Kdr} + I_D + I_{syn} \quad (19)$$

$$C_m \frac{dV_a}{dt} = I_l + I_{Naf} + I_{Kdr} \quad (20)$$

where I_l is the leak current, I_{Naf} is the fast sodium current, I_{Kdr} is the delayed rectifier K^+ current and I_D is the D-type K^+ current.

10.2.2.1 The leak current

$$I_l = g_l * (V - E_l) \quad (21)$$

where $E_l = -70mV$.

10.2.2.2 The fast sodium channel (Durstewitz & Gabriel, 2007)

$$I_{Naf} = g_{Na(fast)} * (V - E_{rev}) \quad (22)$$

$$g_{Na(fast)} = g * m^3 * h$$

$$\frac{dm}{dt} = \frac{m_{\infty} - m}{t_m}$$

$$m_{\infty} = \frac{ma}{ma + mb}$$

$$ma = \frac{-0.2816 * (v + 28)}{-1 + e^{\frac{-v+28}{9.3}}}$$

$$mb = \frac{0.2464 * (v + 1)}{-1 + e^{\frac{v+1}{6}}}$$

$$t_m = \frac{1}{ma + mb}$$

$$\frac{dh}{dt} = \frac{h_\infty - h}{t_h}$$

$$h_\infty = \frac{ha}{ha + hb}$$

$$ha = \frac{0.098}{e^{\frac{v+23.1}{20}}}$$

$$hb = \frac{1.4}{1 + e^{\frac{-(v+25.1)}{10}}}$$

$$t_h = \frac{1}{ha + hb}$$

where $E_{rev}=0$ mV.

10.2.2.3 The delayed rectifier potassium current (Durstewitz and Gabriel, 2007)

$$I_{Kdr} = g_{Kdr} * (V - E_{rev}) \quad (23)$$

$$g_{Kdr} = g_{max} * n^4$$

$$\frac{dn}{dt} = \frac{n_\infty - n}{t}$$

$$n_\infty = \frac{na}{na + nb}$$

$$t = \frac{1}{na + nb}$$

$$na = \frac{-0.018 * (v - 13)}{-1 + e^{\frac{-(v+13)}{25}}}$$

$$nb = \frac{0.00544 * (v - 23)}{-1 + e^{\frac{(v-23)}{12}}}$$

where $E_{rev} = 0$ mV.

10.2.2.4 Slow inactivating potassium current (I_D) (Durstewitz & Gabriel, 2007)

$$I_D = g * a * b * (V - E_K) \quad (24)$$

$$\frac{da}{dt} = \frac{a_\infty - a}{t_a}$$

$$\frac{db}{dt} = \frac{b_\infty - b}{t_b}$$

$$a_\infty = \frac{1}{1 + e^{\frac{(v+34)}{6.5}}}$$

$$b_\infty = \frac{1}{1 + e^{\frac{(v+65)}{6.6}}}$$

$$t_b = 200 + \frac{3200}{1 + e^{\frac{-(v+63.6)}{4}}}$$

where $t_a = 10$ ms.

10.2.3 Synaptic currents

10.2.3.1 NMDA receptor (pyramidal neurons) (Polsky, Mel, & Schiller, 2009)

$$I_{nmda} = g \times (V - E_{rev}) \quad (25)$$

$$i[Ca^{+2}] = \frac{inmda}{10}$$

$$g = \frac{A - B}{1 + n * e^{-gamma*v}}$$

$$\frac{dA}{dt} = \frac{-A}{tau1}$$

$$\frac{dB}{dt} = \frac{-B}{tau2}$$

where $E_{rev} = 0$ mV, $tau1 = 90$ ms, $tau2 = 5$ ms, $gamma = 0.08$ mV⁻¹, $n = 0.25$ mM⁻¹.

Note that the conductance of the NMDA is multiplied by the term $1/(1 + n * e^{-gamma*v})$ that give a sigmoidal voltage-dependence (including the Mg⁺² blocking) (Polsky et al., 2009).

10.2.3.2 NMDA receptor (interneurons) (Destexhe, Mainen, & Sejnowski, 1994)

$$I_{nmda} = g \times (V - E_{rev}) \quad (26)$$

$$ica = \frac{7 * Inmda}{10}$$

$$g = (R_{on} + R_{off}) * B$$

$$\frac{dR_{on}}{dt} = \frac{R_{inf} - R_{on}}{R\tau}$$

$$\frac{dR_{off}}{dt} = -\beta * R_{off}$$

$$R_{inf} = \frac{Cmax * \alpha}{Cmax * \alpha + \beta}$$

$$R\tau = \frac{1}{a * Cmax + \beta}$$

$$B = \frac{1}{1 + \frac{e^{-0.072v} * [Mg^{+2}]}{3.57}}$$

where $Mg^{+2} = 1$ mM, $Cmax = 1$ mM, $\alpha = 4$ ms⁻¹mM⁻¹, $\beta = 0.015$ ms⁻¹, and $E_{rev} = 0$ mV.

10.2.3.3 AMPA receptor (Destexhe et al., 1994)

$$I_{AMPA} = g \times (V - E_{rev}) \quad (27)$$

$$g = R_{on} + R_{off}$$

$$\frac{dR_{on}}{dt} = \frac{R_{inf} - R_{on}}{R\tau}$$

$$\frac{dR_{off}}{dt} = -\beta * R_{off}$$

$$R_{inf} = \frac{Cmax * \alpha}{Cmax * \alpha + \beta}$$

$$R\tau = \frac{1}{a * Cmax + \beta}$$

where for pyramidal neurons $E_{rev} = 0$ mV, $\alpha = 10$ ms⁻¹, $\beta = 0.15$ ms⁻¹, $C_{max} = 1$ mM. For inhibitory interneurons $E_{rev} = 0$ mV, $\alpha = 10$ ms⁻¹, $\beta = 0.18$ ms⁻¹, and $C_{max} = 1$ mM.

10.2.3.4 GABA_A receptor (Destexhe et al., 1994)

$$I_{GABAA} = g \times (V - E_{rev}) \quad (28)$$

$$g = R_{on} + R_{off}$$

$$\frac{dR_{on}}{dt} = \frac{R_{inf} - R_{on}}{R\tau}$$

$$\frac{dR_{off}}{dt} = -\beta * R_{off}$$

$$R_{inf} = \frac{C_{max} * \alpha}{C_{max} * \alpha + \beta}$$

$$R\tau = \frac{1}{a * C_{max} + \beta}$$

where for pyramidal neurons $E_{rev} = -80$ mV, $\alpha = 5$ ms⁻¹, $\beta = 0.18$ ms⁻¹, and $C_{max} = 1$ mM.

For inhibitory interneurons $E_{rev} = -80$ mV, $\alpha = 5$ ms⁻¹, $\beta = 0.2$ ms⁻¹, $C_{max} = 1$ mM.

10.2.3.5 GABA_B receptor (Pissadaki, Sidiropoulou, Reczko, & Poirazi, 2010)

$$I_{GABAB} = g \times (V - E_{rev}) \quad (29)$$

$$g = R_{on} + R_{off}$$

$$\frac{dR_{on}}{dt} = \frac{R_{inf} - R_{on}}{R\tau}$$

$$\frac{dR_{off}}{dt} = -\beta * R_{off}$$

$$R_{inf} = \frac{C_{max} * \alpha}{C_{max} * \alpha + \beta}$$

$$R\tau = \frac{1}{a * C_{max} + \beta}$$

where $E_{rev} = -80$ mV, $\alpha = 0.001$ ms⁻¹, $\beta = 0.0047$ ms⁻¹, and $C_{max} = 10$ mM.

References

Destexhe, A., Mainen, Z. F., & Sejnowski, T. J. (1994). Synthesis of models for excitable membranes, synaptic transmission and neuromodulation using a common kinetic formalism. *Journal of computational neuroscience*, 1(3), 195–230.

Durstewitz, D., & Gabriel, T. (2007). Dynamical basis of irregular spiking in NMDA-driven prefrontal cortex neurons. *Cerebral cortex*, 17(4), 894–908. doi:10.1093/cercor/bhk04

Pissadaki, E. K., Sidiropoulou, K., Reczko, M., & Poirazi, P. (2010). Encoding of spatio-temporal input characteristics by a CA1 pyramidal neuron model. (L. J. Graham, Ed.) *PLoS computational biology*, 6(12), e1001038. doi:10.1371/journal.pcbi.1001038

Poirazi, P., Brannon, T., & Mel, B. W. (2003). Online Supplement : About the Model 1 Building the Model. *Neuron*, 37(2).

Polsky, A., Mel, B. W., & Schiller, J. (2009). Encoding and decoding bursts by NMDA spikes in basal dendrites of layer 5 pyramidal neurons. *The Journal of Neuroscience*, 29(38), 11891–903. doi:10.1523/JNEUROSCI.5250-08.2009

Shao, L. R., Halvorsrud, R., Borg-Graham, L., & Storm, J. F. (1999). The role of BK-type Ca²⁺-dependent K⁺ channels in spike broadening during repetitive firing in rat hippocampal pyramidal cells. *The Journal of physiology*, 521 Pt 1, 135–46.

Sidiropoulou, K., & Poirazi, P. (2012). Predictive Features of Persistent Activity Emergence in Regular Spiking and Intrinsic Bursting Model Neurons. (A. Morrison, Ed.) *PLoS Computational Biology*, 8(4), e1002489. doi:10.1371/journal.pcbi.1002489

Athanasia Papoutsi

Date of Birth: 05/02/82

E-mail: papoutsi@imbb.forth.gr, athpapoutsi@gmail.gr

Education

PhD Candidate in Neuroscience March 2009–December 2013
“Modeling approaches for analyzing the properties of persistent activity in the prefrontal cortex”.

Computational Biology Lab (CBL), Institute of Molecular Biology and Biotechnology (IMBB), Foundation for Research and Technology Hellas (FORTH), Affiliated with the Department of Biology, University of Crete (UOC).

Supervisor: P. Poirazi, Research Associate Professor.

Advisory committee: Prof. G. Chalepakis, Dr. P. Poirazi, Prof. I. Segev.

Masters in the Brain and Mind Sciences December 2006–December 2008

Interdepartmental Graduate Programme, Faculty of Medicine, UOC.

Grade: 9.06/10, classification: Excellent (Distinction).

Ptychion (BSc) in Biology September 2000-July 2005

Faculty of Biology, National and Kapodistrian University of Athens (UOA).

Grade: 6.82/10, classification: Very Good.

The Moraitis School, Athens

September 1993 - July 1999

Graduation GPA: 18.1/20

Research experience

Research Assistant, CBL, IMBB, FORTH

September 2008-March 2009

Lab Rotation in Systems Physiology

March 2008-September 2008

“Study of time-varying force pulses”.

Systems Physiology and Computational Neuroscience Laboratory, Faculty of Medicine, UOC.

Skills: neuronal recording (electromyography), analysis of neurophysiological signals, development of several programs in MATLAB for signal processing.

Supervisor: C. Christakos, Associate Professor of Physiology.

Lab Rotation in Computational Neuroscience

September 2007-March 2008

“The role of cellular and synaptic mechanisms during persistent activity in a model neuron”.

CBL, IMBB, FORTH.

Programming Skills: Neuron Simulation Environment, Igor program, Matlab.

Supervisor: P. Poirazi, Research Associate Professor.

Graduation Thesis in Molecular Neuroscience

July 2004-July 2005

“Study of the protective effect of neurosteroids in neuron cell cultures”

Department of Animal and Human Physiology, Faculty of Biology, UOA.

Biological techniques: Cell culture, differentiation, RT-PCR, Western-blot analysis, DNA laddering.

Supervisor: P. Papazafiri, Assistant Professor. Grade: 10/10

Publications

Papoutsis A., Psarrou M., Kastellakis G., Poirazi P. '*Morphology dictates integration mode and shapes function*', to be submitted.

Papoutsis A., Sidiropoulou K., Poirazi P. "*Dendritic nonlinearities reduce size requirements and mediate ON and OFF states of persistent activity in a PFC microcircuit model*", Submitted in Plos Computational Biology.

Konstantoudaki X., **Papoutsis A.**, Chalkiadaki K., Poirazi P., Sidiropoulou K. "*Modulatory effects of inhibition on persistent activity in a cortical microcircuit model*", Frontiers in Neural Circuits (2014).

Papoutsis A., Sidiropoulou K., Cutsuridis V., Poirazi P. "*Induction and modulation of persistent activity in a layer V PFC microcircuit model*", Frontiers in Neural Circuits (2013).

Papoutsis A., Kastellakis G., Psarrou M., Anastasakis S. and Poirazi P. "*Coding and Decoding with Dendrites*", Journal of Physiology-Paris (2013).

Papoutsis A., Sidiropoulou K., Poirazi P. "*Memory Beyond Synaptic Plasticity: The Role of Intrinsic Neuronal Excitability*", Book Chapter in Memory Mechanisms in Health and Disease: Mechanistic Basis of Memory, World Scientific Pub Co Inc., (2012).

Conference papers / Oral Presentations

Petrantonakis P., **Papoutsis A.**, Poirazi P., "*Towards Predicting Persistent Activity of Neurons by Statistical and Fractal Dimension-Based Features*", 2013 International Joint Conference on Neural Networks.

Krioneriti D., **Papoutsis A.**, Poirazi P., "*Mechanisms underlying the emergence of Up and Down states in a model PFC microcircuit*", selected oral presentation, CNS 2011, Stockholm, 23-28 July 2011. doi:10.1186/1471-2202-12-S1-O7

Posters

Peer reviewed poster presentations

Papoutsis A., Petrantonakis P. and Poirazi P., "*Dendritic nonlinearities enable PFC microcircuits to serve as predictive modules of persistent activity*", CNS (2013), Paris.

Psarrou M., **Papoutsis A.**, and Poirazi P., "*Influence of dendritic morphology on single neuron arithmetic*", AREADNE (2012), Research in Encoding and Decoding of Neural Ensembles, pp 80, Santorini.

Krioneriti, D, **Papoutsis, A.** and Poirazi, P, "*Mechanisms underlying the emergence of Up and Down states and their transition to persistent firing in a model PFC microcircuit*", EMBO Conference, "The Assembly and Function of Neuronal Circuits", Ascona (2011), Switzerland.

Papoutsis A., Sidiropoulou K. and Poirazi P., "*Microcircuits in the prefrontal cortex: In silico investigation of their role in the emergence, maintenance and termination of persistent activity*", AREADNE (2010), Research in Encoding and Decoding of Neural Ensembles, pp 89, Santorini.

Sidiropoulou K., **Papoutsi A.**, Poirazi P., “*Information coding via persistent activity in layer V prefrontal cortical neuron models*”, EMBO Conference: “The Assembly and Function of Neuronal Circuits”, Ascona (2009), Switzerland.

Konstantoudaki X., Sidiropoulou K., **Papoutsi A.** and Poirazi P. “*The role of distinct interneuron cell types in initiation and maintenance of persistent activity in a prefrontal cortical microcircuit model*”. *Frontiers in Behavioral Neuroscience* (2009). Conference Abstract: 41st European Brain and Behaviour Society Meeting. doi: 10.3389/conf.neuro.08.2009.09.198

Papoutsi A., Sidiropoulou K., Poirazi P. “*Mechanisms underlying persistent activity in a model PFC microcircuit*”, *CNS* (2009), Berlin, BMC Neuroscience 2009. doi: 10.1186/1471-2202-10-S1-P42

Poster Presentations

Papoutsi A., Georgopoulou D., Poirazi P. “*Single-neuron integration of background activity generates prolonged depolarizations in a PFC model cell*”, FENS (2012), Barcelona.

Sidiropoulou K., **Papoutsi A.**, Poirazi P., “*Encoding of persistent firing in a model of layer V prefrontal cortical neurons*”, Program No. 875.15. 2009 Neuroscience Meeting Planner. Chicago, IL: Society for Neuroscience (2009). Online.

Papoutsi A., Sidiropoulou K. and Poirazi P., “*Cellular and synaptic mechanisms underlying persistent activity in a model PFC microcircuit*”, 22nd Conference of the Hellenic Society for Neuroscience (2008), pp149.

Sidiropoulou K., **Papoutsi A.** and Poirazi P., “*Biophysical mechanisms involved in initiating and maintaining persistent activity in a PFC pyramidal model neuron*”, AREADNE (2008), Research in Encoding and Decoding of Neural Ensembles, pp 89.

Papoutsi A., Sidiropoulou K. and Poirazi P., “*The role of cellular and synaptic mechanisms during persistent activity in a model neuron*”, 21st Conference of the Hellenic Society for Neuroscience (2007), pp184-185, Thessaloniki.

Xilouri M., **Papoutsi A.** and Papazafiri P., “*Expression and function of the GABAA receptor during differentiation of P19-N neurons*”, 27th Scientific Conference of the Hellenic Society for Biological Sciences (2005), pp 277-278, Nafplio.

Awards / Scholarships

- Scholarship, IMBB, FORTH (ERC grant: “dEMORY”, January 2013-until now).
- Scholarship, IMBB, FORTH (NSRF grant: “Synergasia”, October 2011-December 2012).
- Scholarship, IMBB, FORTH (FP-7 grant: HP-SEE ‘High-Performance Computing Infrastructure for South East Europe’s Research Communities, September 2010-September 2011).
- Scholarship, IMBB, FORTH, (September 2009-September 2010).
- “*Theodor-Theochari Cozzika Award*”. Young Greek Neuroscientist Award for the poster presentation during the 22nd conference of Hellenic Society for Neuroscience, for attendance of the EBBS Conference (October 2008).
- “*Maria-Michail Manassaki Scholarship*”, UOC (October 2007 - September 2008).
- “*Maria-Michail Manassaki Scholarship*”, UOC (October 2006 - September 2007).
- *Onassis Foundation Travel Award*, The 2007 Lectures in Biology: Channels and Channelopathies, The Onassis Foundation Science Lecture Series, Heraklion (June 2007).

- Hellenic Mathematical Society Award, 56th National Mathematical Competition (January 1996).
- Greek Ministry of Education Award, for exceptional performance (June 1994).

Teaching Experience

Teacher of Biology

“Epilogi” Preparatory School, Heraklion, Crete (September 2008-until now).

Student supervision

Undergraduate students:

Dimitra Georgopoulou “*Impact of basal dendrites in the emergence of Up and Down states*”, Practical training, May 2011-June 2011.

Masters students:

Daphne Krioneriti. Thesis title: “*Modeling up and down states in a PFC microcircuit*”, May 2010-June 2011.

Maria Psarrou. Thesis title: “*Role of dendritic morphology and ionic mechanisms on bursting activity in pyramidal neurons*”, March 2010 - March 2011.

Additional Skills

Languages:

English (Fluent – Proficiency)

French (Very Good - Certificat)

Italian (Conversational - attended a 2 years course).

Programming Skills:

MATLAB, NEURON, IgorPro, Python.

Software Skills:

MS office including PowerPoint, Photoshop and Illustrator.

Positions of Responsibility and Interests

Professional memberships:

Hellenic Union of Bioscience (PEV).

Hellenic Union for Neuroscience (HSN).

Federation of European Neuroscience Societies (FENS).

Interests:

Traveling, swimming.

Completed “Coursera” courses: Game theory, Learn to Program: the fundamentals.